DEVELOPMENT OF WIRELESS SENSOR NETWORK TECHNOLOGY FOR SOIL PROPERTY MONITORING

By

ZHEN LI

Bachelor of Tele-communication Engineering

South China Agricultural University

Guangzhou, Guangdong, China

2004

Submitted to the Faculty of the
Graduate College of the
Oklahoma State University
in partial fulfillment of
the requirements for
the Degree of
MASTER OF SCIENCE
July, 2009

DEVELOPMENT OF WIRELESS SENSOR

NETWORK TECHNOLOGY FOR SOIL PROPERTY

MONITORING

Thesis Approved:

Dr. Ning Wang

Thesis Adviser

Dr. John Solie

Dr. Randy Taylor

Dr. Paul Weckler

Dr. A. Gordon Emslie

Dean of the Graduate College

ACKNOWLEDGMENTS

I would like to express my gratitude to my advisor, Dr. Ning Wang for her continuous support and guidance during the past two years. Dr Wang's expertise, understanding, and patience added considerably to my graduate experience. I appreciate her vast knowledge and skill in many areas, and her assistance in writing this thesis. I would also like to thank other members of my committee, Dr. John Solie, Dr. Randy Tayler, and Dr. Paul Weckler for the assistance they provided at all levels of the research project.

I would like to express my gratitude to Drs. Hailin Zhang and Chad Godsey for their support and assistance during sensor selection, installation and calibration. Very special thanks will give to Aaron Franzen, Haixia Li, Peyman Taher, Kevin Stunkle, Arunv Kumar, and Yeyin Shi, who have helped during system construction and field tests. I would also like to thank everyone in the Biosystems and Agricultural Engineering Department, without their help, the project and my course study could not be completed.

I would like to express my gratitude to my advisor in China, Dr. Tiansheng Hong, for his continuous help and support over these years. Without his help, this thesis could not have come to an end as smoothly. Also, I would like to express my gratitude to Nancy Rogers for her assistant to the living and studying related affairs.

I would like to acknowledge the financial support from the National Science Foundation (CNS-0709329).

Finally, I would like to thank my parents and relatives for their great supporting during my study and living in the United States.

TABLE OF CONTENTS

LIST OF TABLES

LIST OF FIGURES

NOMENCLATURE

Chapter 1

RF	Radio frequency
MEMS	Micro-Electro-Mechanical Systems
WSN	Wireless sensor network
DAQ	Data acquisition
RAM	Random Access Memory
ROM	Read only Memory
GUI	Graphical user interface
LAN	Local Area Network
UWSN	Under-water wireless sensor network
SMS	Short Message Service
WSAN	Wireless sensor and actuator network

Chapter 2

WSN	Wireless sensor network
SMC	Soil Moisture Content
R	Resister
Cs	Stray capacitance
C	Medium capacitance
G	Energy loss due to relaxation and ionic conductivity

V_{inp}	Supply voltage
V_{oup}	EC-5 sensor analog reading
w	Gravimetric SMC
M_w	Mass of water in a sample
M_s	Total mass of a sample
θ	Volumetric SMC
V_w	Volume of water in a sample
V_t	Total volume
V_s	Volume of solids in a sample
V_a	Volume of air in a sample
θ_i	Volumetric water content at the *i*th level
$V_{water,i}$	Volume of water at the *i*th level
CMOS	Complementary Metal-Oxide-Semiconductor
Sc	Scale of the sensor
Std_v	Standard deviation of volumetric water content
Std_s	Standard deviation of sensor output

Chapter 3

HSSN	Hybrid soil sensor network
LWSN	Local wireless sensor network
LCCN	Long-distance cellular communication network
GPRS	General Packet Radio Service
SMC	Soil Moisture Content
TDR	Time domain reflectrometry tensiometer

EC_a	Apparent soil electrical conductivity
ER	Electrical resistivity
EM	Electromagnetic conduction
TIR	Thermal infrared
AVHRR	Advanced Very High Resolution Receiver
MODIS	Moderate Resolution Imaging Spectroradiometer
RF	Radio Frequency
DAQ	Data acquisition
QoS	Quality of service
LRWPAN	Low-rate Wireless Personal Area Network
SMS	Short Message Service
LRCCN	Long Range Cellular Communication Network
DSSS	Direct-sequence spread-spectrum
QPSK	Quadratic phase shift keying
VWC	Volumetric water content
EC	Bulk electrical conductivity
σ_{raw}	Raw electrical conductivity value from EC-TE
T	Real temperature
T_1	Transmitted temperature reading
Ex	Excitation
PDU	Protocol data unit
ACK	Acknowledgement
ORM	Object-relational mapping

POJO	Plain old java objects
DAO	Data access object
CRUD	Create, read, update and delete
Raw	Received sensor reading from EC-TE
θ	Volumetric water content
$N_{R,pdr}$	Packet delivery rate
Nt	Number of packet transmitted
Nr	Number of packet received
$N_{R,val}$	Valid data rate
Nv	Number of valid packets
$N_{R,err}$	Data error rate
Ne	Number of packets with error

Chapter 4

QoS	Quality of service
PRR	Packet Reception Rate
PL(d)	Path loss in a distance *d*
P_t	Transmitted power
P_r	Received power
P_{tm}	Transmitted power in *dBm*
P_{rm}	Received power in *dBm*
d	Separation distance
d_0	Received-power reference point
$PL(d_0)$	Path loss at the received-power reference point

f	Carrier frequency
T	Temperature
RH	Relative Humidity
h_p	Wheat canopy height
λ	Wave length of carrier wave
H_1	Threshold of crop canopy height for Rayleigh roughness
$r_{\max}$	Maximum radius for Fresnel zone clearance
H_2	Fresnel zone clearance tolerance
RBW	Resolution Band Width
DANL	Displayed Average Noise Level
PL_{fs}	Path-loss predicted using Free Space model
PL_{pe}	Path-loss predicted using Plane Earth model
h_{t}	Transmitter height
h_{r}	Receiver height
G_{t}	Transmitter gain
G_{r}	Receiver gain
PL_{ch}	Path-loss predicted using COST-Hata model
$\text{a}(h_{\text{T}})$	Sub-urban correction constant
$N_{R,packet}$	Packet Reception Rate
$N_{received}$	Number of packets received
$N_{transmitted}$	Number of packets transmitted
$\Delta\ N_{R,packet}$	Packet reception rate deviation
$T_{R,packet}$	Threshold of reliable communication

h_M	Mobile station height in COST-Hata model
h_T	Transmitter height in COST-Hata model
h_B	Receiver height in COST-Hata model
C	COST-Hata model constant

CHAPTER I

INTRODUCTION

1.1 Wireless Sensor Networks

Notable scientific revolutions have led to maturity in many industrial areas such as radio frequency (RF) technology, integrated circuits, smart sensors, and Micro-Electro-Mechanical Systems (MEMS) (Mahfuz et al., 2005). These latest progresses made it possible for the mass-production of low-cost, low-power, multi-functional micro sensor nodes which can interact with the environment through sensors, actuators and radios all packaged in tiny devices. Colloquially, these devices are called “motes” or “smart dust”. The disposable low cost for a mote enables deployment of potentially hundreds or even thousands of them. By using power consumption strategies, these motes can last for years.

As one of the latest and most promising technology, wireless sensor network (WSN) utilizes smart-dusts’ unsupervised organizing, configuring and healing abilities to form networks which have nearly unlimited installation flexibility, outstanding mobility, and reduced maintenance complexity (Wang et al., 2006). With these advantages, WSN has been extensively implemented in military and air defense applications(Li et al., 2002; Meesookho et al., 2002; Arora et al., 2004), health centric observations (Milenkovic et al., 2006; Otto et al., 2006), logistics and storage support (Knot, 2004), transportation

management, structural health monitoring (Wang et al., 2007; Li et al., 2007) and other commercial or industrial areas (Kim et al., 2007; Sibley et al., 2002).

By far, the WSN applications in agriculture and environment are still at the beginning stage. Each in-field scenario usually demands special system configurations (Wang et al., 2006). Recent successful exploring efforts have revealed great adaptability of using WSN for data collection and control of the local environment. This has been generating significantly increased implementations. This chapter aims to give a brief survey in (1) existing WSN platforms, and (2) current agricultural and environmental WSN applications.

1.2 Current Development of Wireless Sensor Network Technology

To develop a WSN, there are normally three concerns: hardware, operating system, and network communication. Hardware includes (1) motes distributed in a monitoring field to form a mesh network, each of which has limited on-board signal processing ability while equipped with sensors and signal conditioning circuits, and (2) sink or gateway bridging motes via RF and system terminal via Internet (Bogena et al, 2006). Operating systems are deeply tied to hardware and responsible for coordinating the function of various on-board components to finish the assigned tasks like data acquisition, transmission and storage (Gay et al., 2003). Network communication is based on sets of standard rules on top of hardware and operating system for reliable message transmission. Once networked, the motes should collaboratively catch the ambient events, process and restore data in a limited level, transmit or receive data/command packets between local motes and gateway, and carry out actuations autonomously based on pre-programmed situations or passively by received commands.

1.2.1 Hardware Platforms

Commercially available platforms

Commercially available hardware platforms have been utilized most frequently in the documented agricultural and environmental WSN applications. They are equipped with commonly used sensors and provide standardized interface for connecting other sensors and/or equipments. Therefore, few extra peripheral components are required to be developed by developers for establishing a complete WSN system. These products are better solutions when size and cost are not with the highest priority. Another advantage of using the commercial platforms is that they usually have larger user groups and more resource of technical support which makes the system development much easier. The state-of-the-art WSN platforms, as shown in Table 1-1, can be categorized into two different types based on node size and mote-to-DAQ board configurations.

(1) Generic configuration. Manufactures are offering generic products in the form of single motes, sensor interfaces and entire systems. Most of the platforms fall into the "mote & DAQ extension board" style in this category. A mote is usually a pocket size circuit board with kernel components including CPU, memory, and radio. DAQ extension boards are circuit boards with sensors, A/D converters, counters and digital GPIOs. A mote could be connected to different DAQ extension boards depending on system requirements through standardized interfaces. One of the leading manufacturers in this category is Crossbow Technology (San Jose, CA, USA). It offers nearly a complete product line including wireless motes (Mica2, MicaZ, IRIS and Imote2), data acquisition boards (MTS, MDA, ITS and IMB400), gateways (Stargate and MIB), networking software (XMesh, XServer), and completed systems (Crossbow, 2008). Other prevalent

motes include TinyNode184 and TinyNode584 from Shockfish SA (Lausanne, Switzerland), Tmote Mini and Tmote Sky from Moteiv (now Sentilla, San Francisco, CA, USA), BTnode rev3 from the BTnode project group (ETH Zurich, Switzerland), and eyesIFXv2.1 from the Infineon Technologies (Neubiberg, Bavaria, Germany).

(2) “Data Logger & Radio” configuration. The major obstacle for agricultural engineers to use the first type of platforms in system development is that it requires intensive system programming and profound electronic background. Usually, companies manufacturing platforms in the second type either have one data logger providing general interfaces for nearly all regular sensors and controllers or make different models, each of which is capable for certain fixed type of sensors and controllers. Though this configuration sacrifices system flexibility and cost efficiency and increases power consumption to some extent, it has benefits in less programming and fewer extra peripheral system constructions. Examples of this category include: CR1000+RF4xx combination from Campbell Scientific (Logan, UT, USA), V/SG/G/TC-Link wireless sensor nodes from MicroStrain (Williston, VT, USA), and Em50R from Decagon Devices (Pullman, WA, USA).

Table 1-1 Outlines of WSN hardware platforms

Platform	Company	CPU	Power	Memory	I/Os and Sensor Extension	Radio	Operating System
Generic Configuration							
Mica2	Crossbow Technology	Atmega 128	3.3V battery 15uA sleep 8mA active 35mA max	128kB ROM 512kB Flash 4kB EEPROM	Regular I/Os*, 51pin interface to MDA/MTS/ITS DAQ extension boards	CC1000	TinyOS 1.x/2.x
MicaZ	Crossbow Technology	Atmega 128	3.3V battery 15uA sleep 8mA active 25.4.4mA max	Same as Mica2	Same as Mica2	CC2420	TinyOS
IRIS	Crossbow Technology	Atmega 1281	3.3V battery 15uA sleep 8mA active 25mA max	4kB RAM 128kB ROM 512kB Flash 4kB EEPROM	Same as Mica2	RF230	TinyOS
Imote2	Crossbow Technology	Intel PXA 271	3.3V battery 390uA sleep 66mA Active	256kB SRAM 32MB SDRAM 32MB Flash	GPIO/SPI/UART/I^{2}S/USB/AC'97/Camera/IMB400 multimedia extension board	CC2420	Embedded Linux or Windows support
TinyNode584	Shockfish SA	MSP 430	3.3V battery 0.004mA sleep 62mA max	10kB RAM 512kB Flash	Regular I/Os, extension board for custom interface electronics	XE1205	TinyOS
TinyNode184	Shockfish SA	MSP430 F2417	0.002mA sleep 25mA max	10kB RAM 512kB Flash	Same as TinyNode584	SX1211	TinyOS
Tmote Sky	Moteiv	TI MSP 430	3.3V battery 5.1uA sleep 23mA max	10kB RAM 48kB Flash	Regular I/Os, on board light/temp/PAR sensor, no manufacture built extension board	CC2420	TinyOS
BTnode rev3	BT Node Project	Atmega 128L	9.9mW sleep 198mW max for Bluetooth	64+128kB SRAM 128kB Flash 4kB EEPROM	Regular I/Os, no manufacture built extension board	ZV4002 Bluetooth or CC1000	TinyOS or BTnut
eyesIFXv2.1	Infineon Technology	MSP430 F1611	36mW max	10kB RAM 48kB ROM 4MB Flash	Same as BTnode	TDA 5250	TinyOS
Data Logger & Radio Configuration							
CR1000+RF4xx	Campbell Scientific	Renesas H8S 2322 for CR 1000	12V battery 1.6mA sleep 102.6mA/175 mA max together	4MB SRAM CF card extension	16 Analog inputs, 3 Analog outputs, 8 digital I/Os, full/half bridges, counters	RF401 RF411 RF416	LoggerNet 3.x, PC400 1.2 or ShortCut 2.2
x-Link nodes	MicroStrain	Not documented	0.5mA sleep 25mA max	up to 1,000,1000 measurements	Fixed on board sensors depending on series "x"	2.4GHz, 16 nodes maximum	Precompiled system in VB/VC++/LabView
Em50R	Decagon Device	Not documented	5 AA batteries	1 MB Data storage space	4 Analog inputs, 1 serial input	900MHz or 2.4GHz	ECH$_2$O Utility and DataTrac

Specially configured platforms

Besides the commercially available, general purpose wireless sensor motes, other nodes are built in particular configurations for specific purposes such as higher data

processing ability, larger communication range, smaller sizes or fitting with special sensors. An example is the NTP experimental platform (Kuo et al., 2008) which combined three regular platforms as III Zigbee Advanced Platform, ITRI Sensor Platform and Tmote. Other examples of specially configured platforms can be found in Cui et al. (2004), Handziski et al. (2006), and Zhou et al. (2007).

To make even smaller WSN motes, most of the components on a circuit board e.g. microprocessor, Flash, RAM and radio can be integrated into a chip. EM250 (Ember, Boston, MA, USA) provides ZigBee System-on-Chip capability within a size of 7mm x 7mm (Ember, 2005). It has 128kB Flash, 4 12-bit sigma-delta ADC channels, and twice the wireless range of regular ZigBee SoCs. Another example is the JN51xx series wireless microcontrollers & modules from Jennic (Sheffield, UK) (Jennic 2006). As an example, the sensor node used for greenhouse monitoring by Zhou et al. (2007) which integrated a JN5121 IEEE 802.15.4 compliant wireless microcontroller, a SHT1x humidity & temperature sensor, a TSL2550 light sensor, a M25P10 1Mbit serial flash memory and an antenna into a single circuit board. It is more compact in size. Although some particularly configured platforms were initialized in other areas, their similarities with the generic configured platforms make them quite transferable to agricultural and environmental solutions.

1.2.2 Operating Systems for WSN

Most WSN hardware platforms share some inherent features as limited on-board or on-chip resources, severe memory constraint, and highly precious power source. These restrictions demand that the operating system running in the motes has to be both very small in footprint and event-driven. TinyOS (University of California, Berkeley, CA,

USA) is an open-source embedded operating system (OS) specially designed for mote level devices within wireless sensor networks. It was developed through a collaboration work between the University of California, Berkeley and Intel Research Institute. The developing group has grown to be an international consortium, the TinyOS Alliance, and making TinyOS the de-facto standard OS for WSN. The latest official version is TinyOS 2.1 released on August 2008 which supports most of the general WSN platforms. Some other user-tailored versions are available for specific hardware configurations.

It is very common that a vast amount of data are collected and stored in motes after intense sensing. However, the raw data is usually a mixture of useful information and noise. It will be a waste of power if all the collected data are transmitted without any pre-selection. Hence, a query processing system to extract data from in-site motes named TinyDB is specially designed for WSNs running under TinyOS. Users can install TinyDB in the form of TinyOS components into their programs to filtrate and extract sensor data from motes through a simple SQL-like interface without C code programming.

There are other documented small footprint and high efficiency OS for WSN applications. A state machine based operating system, namely SenOS, was proposed in Kim et al. (2005). It offers a number of benefits when compared to TinyOS as (1) wider code generation tools; (2) allowance of controlled concurrency and reactivity; and (3) higher program resume efficiency. A mote-class WSN operating system named SOS was proposed primarily to achieve dynamic reprogramming (Han et al., 2005). Dynamically loadable modules and a common kernel are nested to support dynamic addition, modification, and removal of network services. Other compact size WSN operating

systems include MANTIS (Bhatti et al., 2005), Nano-Qplus (Park et al., 2006) and BTnuts (The BTnode Project, 2007) etc.

For gateway-class or resource-rich nodes such as stargate, Imote, and PDAs, Linux and Windows CE are applied as operating systems for proprietary communication or digital data processing stacks implementations.

Currently, the prevails operating systems are mostly academic research platforms only providing back-bone functionality while leaving most of the system developing workloads to the application developers. For agricultural engineers with less software developing background, a possible solution is to package some pre-compiled operating system as firmware inside the nodes with limited configuration interfaces and provide computer-based graphical user interfaces (GUI) executable programs for easy mote accessing. Examples can be found as Crossbow's XMesh and XSniffer/MoteConfig. The XMesh is a software library based on TinyOS which runs on motes with pre-build multi-hop, ad-hoc, mesh networking protocols and limited sensor board access methods (Crossbow, 2004). The XSniffer/MoteConfig together can provide wired and wireless system configuration as well as mote data access. Although every solution claimed full supports to its own hardware, none of them is able to cross platforms from different manufacturers.

1.2.3 Communications for WSN

The major issue in WSN communications is to achieve successful transmission and reception of messages. Terms of message delay, error rates, packet loss rate, power cost of transmission can be specified as system Quality of Service (QoS). Different network topologies and protocols can be employed depending on QoS requirements.

Network topology

A WSN is composed of nodes which transmitting and receiving messages over communication links either wired or wireless. A topology decides which route a message can be delivered from a transmitter to a receiver. As shown in Figure 1-1, the most common network topologies utilized in agricultural and environmental applications include star, tree, mesh, and web. It is common that a WSN consists of several subnets using different topologies.

A WSN, namely Web-based monitoring system, was proposed by Fukatsu et al. (2006) for crop field monitoring. Modules of the system were connected to each other via wireless local area network (LAN, IEEE802.11b/g) using the web topology. It had advantages in high-speed data transmission and shared workloads in small scale networks. However, when more nodes were added to the network, the number of links would increase exponentially, thus made the routing problem computationally intractable.

In star or tree topologies, routing is simple since nodes only talk with their parents or children. Due to the fact that messages have to be transmitted through routers or gateway working as hub nodes which require greater message processing, routing and decision-making abilities than regular nodes, the hub node failure may lead to partial or total network destruction in both of the topologies. Examples of agricultural WSN deployments with star or tree topology can be found in Li et al. (2008), and Dinh et al. (2007).

Mesh networks may be the most suitable solution for agricultural WSN to achieve high QoS in every aspect. Identical nodes in these networks are allowed to communicate with their nearest neighbors. It is quite robust to individual node or link failures since

messages between nodes can be delivered though multiple routing paths. Moreover, mesh networks are quite scalable, thus make them good models for WSN distributed over large geographical regions.

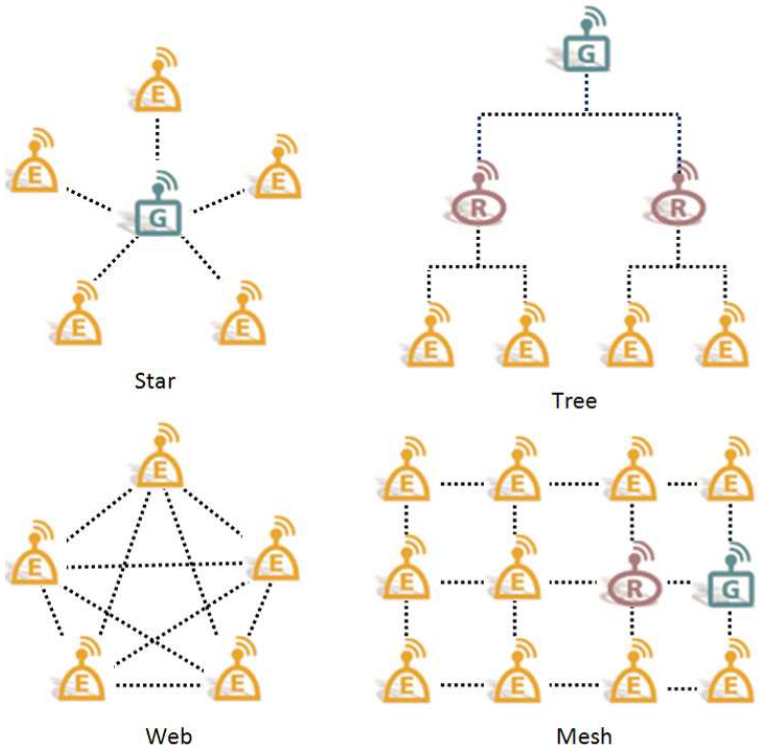

Figure 1-1 Common network topologies for agricultural and environmental WSNs

Communication protocols

For the short distance wireless communication between motes, ZigBee is probably the most popular protocol (Tolle et al., 2005; Hefeeda et al., 2007). It is supported by the association of ZigBee Alliance consist of companies and institutes working together for reliable, low-cost, and power-effective networking. ZigBee is derived from the IEEE 802.15.4 LRWPAN (Low-rate Wireless Personal Area Network) standards and has special definitions in the network and application layer upon the IEEE standards (Baronti et al., 2007). Other standards applied in WSN include WiFi (IEEE 802.11b), Bluetooth (IEEE 802.15.1). The cellular network service, e.g. GPRS (General Packet Radio Service)

and SMS (Short Message Service) plus the standard Internet Protocol (IP) are being used for site-to-user communications.

1.3 Obstacles and Solutions of WSN Technology in Agriculture and Environment Applications

Despite of the huge progress in WSN, it still lacks a generally accepted concept to define each application field. Thus, it is difficult to categorize deployments of wireless sensor network into agriculture and environment since they share a lot of similarities. The following survey will follow the categories of: (1) environmental monitoring, (2) herd and poultry management, and (3) precision agriculture applications.

1.3.1 Environmental Monitoring

WSNs can carry out un-supervised, real-time, short-interval, large-scale and dense sensing for eco-informatic monitoring. Once deployed, the nodes can continuously report observations for a long time without intensive human involvement. The successful implementations indicate that WSN is providing unparalleled opportunities to observe the physical world.

General purpose environmental monitoring systems

The Ohio State University demonstrated a WSN platform, the eXtreme Scale Mote (XSM), to detect and report rare, random, and ephemeral events of human activities over a $10km^2$ area (Dutta et al., 2005). The sensing suites supported were sound, magnetic field and passive infrared. Large-scale operation was achieved through a highly-integrated platform and human-in-the-loop operations were minimized.

An environmental monitoring system named éKo is marketed by Crossbow Technology (Crossbow, 2004). The system's wireless mesh network is based on

Crossbow's XMesh techniques. Each node runs the XMesh low-power ad-hoc mesh networking protocol either as sensor nodes or repeaters. The system supports a wide range of common sensors for environmental factor measurements such as soil moisture, salinity and ambient temperature.

Forestry observation and forest fire detection

Applications for forestry related observations have a major share in environmental monitoring. Tolle et al. (2005a) utilized a WSN to record surrounding micro-climate of a 70-meter tall redwood tree. The recorded variables include air temperature, relative humidity, and photosynthetically active solar radiation (PAR). The authors concluded that tiny differences in sensor positioning got magnified into large effects on the resulting data when sensors got small and the phenomenon got directional enough. Other similar applications can be found in (Tolle et al. 2005b; Selavo et al., 2007).

For early detection of forest fires, a WSN was developed based on the Fire Weather Index (FWI) system (Hefeeda et al., 2007). A distributed k-coverage algorithm was developed and tested to solve the coverage degrees for a given accuracy level in estimating different components of the FWI system.

Another WSN was reported in which the nodes were self-reprogrammable for accommodating to a forest fire's different acting stages. Mica2 motes were applied as sensor nodes in the system. By developing a new middleware paradigm called Agilla which treated programs running inside the nodes as composed mobile agents, in-network autonomous reprogramming is achieved by Agilla controlling agents to replace each other to enable nodes function accordingly during different stages of a forest fire (Fok et al., 2005).

Habitat monitoring

Wang et al. (2003) developed a habitat monitoring sensor network which could recognize and locate specific animal in real time. The target was classified based on acoustic spectrogram pattern matching and located based on Time Difference of Arrival (TDOA). For signal processing requirement, Pocket PCs were adopted rather than regular motes to serve as sensor nodes. Once an animal sound coming out, all the sensor nodes which detected the sound would cooperate to recognize and locate the animal.

An Internet-Sensor integration for habitat monitoring (INSIGHT) was developed by Demirbas et al. (2006). A web-server and an SQL database were maintained at the base station (a laptop) which could enable remote querying using website.

Water quality monitoring

A WSN system was presented by Han et al. (2008) for a real-time remote monitoring of sediment runoff at a low-water crossing. The optical soil sediment sensor was submerged into the water while the rest of the system was located on the bank. The in-site network followed the simple but reliable star topology. Data was firstly transmitted from sensor nodes to gateway using ZigBee and then from gateway to Internet server using GPRS service.

It is more challenging to build under water wireless sensor networks (UWSN) than the ground-based ones since radio communication does not transmit well inside water. However, aqueous environmental monitoring is important and meaningful since the largely unexplored water area covers nearly two-thirds of the earth's surface. For underwater monitoring, acoustic communications have to be employed to avoid the large latency, low bandwidth, and high error rate caused by regular radio waves. Cui et al.

(2006) categorized the UWSNs into two networking architectures as long-term, non-time-critical architecture and short-term, time-critical architecture Each has its own application areas. Accordingly, they presented a mobile UWSN configuration for each of the architectures. More detailed issues about limitations and potential solutions for UWSN can be found in Partan et al. (2007).

Other applications

Werner-Allen et al. (2005) carried out experiments using a wireless sensor network to monitor volcanic eruptions. Outdoor components within the network were: infrasound nodes, aggregator node, Global Positioning System (GPS) receiver node and FreeWave spread-spectrum modem. The infrasonic signal was collected by the infrasound nodes and the data was transmitted from the infrasound nodes to the aggregator, then to the FreeWave modem. A pair of the FreeWave modems was included for long distance communication. The GPS receiver node was used for providing accurate time-stamp to each of the infrasound nodes. Recorded Volcanic sound data was fed to the nodes for detection simulation. Results indicated that (1) detection accuracy was influenced by both the low-signal threshold and high-signal threshold, and (2) the packet loss rate varied due to weather conditions affecting radio transmission.

A hybrid sensor network was designed and evaluated for cane toad monitoring in Australia (Hu et al., 2009). Sound captured from sensor nodes distributed in the field was digitized and transmitted to base station. Resource-intensive tasks like fast Fourier transforms (FFT) and machine learning were carried out at base station to recognize vocalizations of up to ninth frog species.

1.3.2 Herd and Poultry Management

Livestock monitoring

Comprehensive and efficient monitoring of the animals is crucial for successful herd or poultry managements. An efficient monitoring can provide better understanding of animal behavior as well as early detections of individual or group potential health problems. The potential system platforms normally include GPS, RFID (Radio-frequency Identification) and WSN. However, practices indicated that GPS only and RFID systems are more vulnerable to system variability, energy consumption, costs and communication range (Butler et al., 2004; Ng et al., 2005). An RFID based cattle ear tag, namely the ZigBeef, claimed to have solved the dreaded short read-range problem by using the wand-based tag technology (ZigBeef, 2009). However, the information available from RFID tags is limited and the networks using this technology are constrained to peer-to-peer, single hop communications. The WSN technology is predominant in these aspects and thus can be a more suitable candidate.

A WSN system was established to study the lengths of time that cows spent near a water trough (Kwong et al., 2008). The sensor nodes in this study were packaged as a collar wore by the cows. These collars could record GPS data from a built-in receiver at pre-set temporal intervals and up-load the restored data whenever it entered a base-station's communication range. To increase the radio propagation paths and making the data on the collars more accessible, two specially designed antennas were placed on both sides of a cow's neck within a single collar. Field test results indicated that the antenna which had a line-of-sight communication to base station yielded higher received signal strength and a greater number of packets received than the one on the other side of a cow.

For outdoor deployment, a cattle management WSN system was demonstrated for monitoring cows' presence and pasture time in a strip of new grass (Nadimi et al., 2008). Besides mounting Zig-Bee based motes on the cows' neck, the authors applied a moving average window to improve packet delivery rate. The method could also reduce mote's power consumption. They found that the possibility for using a subset of the herd to indicate the total group was verified to make the whole system more economical and practical.

Wireless sensor network prototypes for single animal physiological monitoring were presented by Sousa Silva et al. (2005) and Lowe et al. (2007). The prototype introduced by Sousa Silva (2005) was named floating base sensor network (FBSN) for monitoring bovine brain electrical activities while the other one by Lowe (2007) was for logging unrestrained animal's physiological waveforms like ECG and EEG. System implementation results indicated that, (1) the radio range for telemetry operation was typically 10-20m in a commercial slaughter plant for poultry and up to 100m in open country; (2) the memory capacity allowed a maximum of 7 min data logging of two waves or 14 min data logging of one wave at a sampling rate of 1200 samples/s; and (3) the battery could last for 20h without replacement.

Poultry management

A WSN system was constructed for poultry management to continuously measure the deep body temperature (DBT) of broilers (Yang et al., 2007). In this study, each bird was implanted a temperature transmitter sending pulses at a position of 2cm deep into the abdominal cavity. The received pulses' period was calibrated to correlate with the bird and ambient temperature.

Rather than monitoring a single broiler, it is more practical to observe the environmental changes of the broiler-house. For this purpose, a sensor network based on a combination of a wireless LAN and mail delivery system was developed by Niimi et al. (2008). The sensor module, namely Mocro-Cube, was a board computer composed of several stackable boards including CPU board, LAN board, and special sensor board. A real monitoring system was constructed in a broiler house for environment monitoring. The authors addressed the system limitation of setting up an always-connected high-speed Internet.

In broiler houses, the electromagnetic environment is highly concentrated thus the normal radio propagation (path loss) rules won't apply. Darr et al. (2008) carried out experiments to build a model for predicting WSN signal strength in poultry layer facilities. They took the impacts of plastic enclosure, linear distance, cages and concrete floor into consideration. R^2 of the regressed Received Signal Strength Index (RSSI) prediction model was 0.86.

1.3.3 Precision Agriculture Applications

In-field data collection plays an important role in the precision agriculture. WSN deployments can support precision irrigation, variable-rate spraying, vineyard and greenhouse management, and provide field data to farmers for decision making or agriculturists for research purposes.

Precision irrigation and variable-rate treatment

WSN are finding more and more applications in precision irrigation and variable-rate pesticide, fertilizer, or herbicide treatments. However, most of them are still on the stage

of pure monitoring. The explorations which combined sensing and actuating are more valuable.

A site-specific irrigation/fertilization system was developed upon wireless valve controllers which could self-assemble into a mesh network and control the latching solenoid valves based on commands received from the field controller (Coates et al., 2007). The system could be potentially applied in orchards, greenhouses, landscapes and nurseries.

Kim et al. (2006) developed and tested a closed-loop automated irrigation system. The system had in-field sensing stations, an irrigation control station, a weather station and a base station. Sensing and weather stations cooperated to provide field status readings. The base station was responsible for irrigation scheduling and controlling sprinkler nozzles on a linear irrigation cart through the control station. The communication was totally wire-less between different stations using Bluetooth and the radio communication could reach up to 700m. Field conditions were successfully monitored by five in-field sensor stations every 10 seconds and transmitted to the base station every 15 minutes.

Another conceptual model with WSN involved for closed-loop site-specific irrigation was developed and field tested by King et al. (2005). The system performance was compared in parallel with a conventional uniform irrigation treatment to a potato crop field. Results showed that, with essentially equal water consumption, the tuber yield from under site-specific irrigation management was significantly greater by about 4% than the yield from uniform irrigation.

Vineyard and green house management

A large and dense WSN with 65 nodes distributed within an area of two acres was reported by Beckwith et al. (2004) for vineyard temperature measurement. The network's sensor locations were guided by the agricultural research interests rather than a purely mote centric perspective. For reliable communication, each packet was sent five times and limited to 8 hops. The motes sent temperature data in a five-minute interval which allowed researchers to explore a closer approximation to real-time monitoring. Besides the temperature data, telemetry data including battery performance, packet loss were also reported. The system data receiving rate was 77% on average.

For greenhouse management, a WSN prototype was presented by Liu et al. (2007) to measure the indoor temperature, light and soil moisture. Field data was sent back to the management center using the SMS (Short Message Service) communication based on GSM (Global System for Mobile communications) public mobile network. Monitored temperature readings from two nodes in different locations within a greenhouse indicated that the temperature in the central was more stable than near the window. By conducting radio propagation tests, the authors concluded that a proper antenna position was very important for reliable communication.

Another prototype was presented which could handle with both wireless sensing and actuating inside a greenhouse by Zhou et al. (2007). The network formed a star topology among which a coordinator was receiving sensed data from sensor nodes and sending commands to actuator nodes to control the electrical machines like heater, fan, and pump etc. The limitation of using star network in greenhouse management was solved by using ZigBee's multi-hop, mesh network architecture.

Supplying decision making and research

A WSN was developed by Washington State University to upgrade the network communication of a previously deployed Public Agricultural Weather System (PAWS) (Pierce et al., 2008). The network was divided into two parts as a regional WSN and an on-farm WSN. They had different node configurations and communication protocols. The regional WSN serves as a backbone network operating across farms, while the on-farm WSN focused on the temperature monitoring on the aim of frost protection decision making. Both WSN applications were successfully implemented in the intended applications. System data loss was 3.0, 3.5, and 7.0% for the best to the worst RSSI, respectively. The batteries could be charged most of a year by solar panels but still required replacements during winter months.

Another on-going project was presented by Panchard et al. (2006), to meet the information needs of the rural poor living in the semi-arid areas in India. Soil moisture was measured and related to yield map for field operation decision makings like seeding and irrigation. Their first prototyping system was developed in late 2004 – early 2005. System results were compared with measurements from CAOS (Center for Atmospheric and Oceanic Studies) as: results of temperature and humidity matched exactly, the pressure readings were consistently off by around 4 mbar and the soil moisture appeared to be noisy at 5%.

To understand the water and heat energy exchange between land surface and the atmosphere, a WSN with a soil temperature and moisture MEMS sensor was conducted by Jackson et al. (2008). MEMS sensor calibration was carried out and results indicated that the MEMS sensor exhibited rapid recovery time and good repeatability.

To provide a novel 3-D modular ambient field research system, a WSN is developed with nodes named NMRC25 (Bellis et al., 2005). Comparisons with other similar nodes like Mica2, Mica2Dot and Intel motes were carried out. Results indicated that the NMRC25 had higher digital signal processing abilities than regular WSN motes with its FPGA core unit, higher data transform rate through the VLSI 2.4GHz radio circuit, and shorter radio range.

1. 4 Research Gaps of WSN in Agricultural and Environmental Applications

In summary, the applications of wireless sensor network technology are spreading over every sub-area of agricultural and environmental activities. However, most of the implementations are still not mature. Few systems are ready-to-go for deployment. Besides interests of the common WSN research such as routing, coverage, energy saving and positioning, extra efforts have to be put into scientific aspects include: (1) building or verifying in-site radio propagation models for signal strength prediction; (2) averaging work load thus extending node life by pervasive computing; and (3) adding actuation abilities so that most of the present monitoring-only WSN could be upgraded to wireless sensor and actuator networks (WSAN).

1.5 Research Objectives

This research work for this thesis is part of a project granted by the National Science Foundation research project (CNS-0709329): “A Research and Education Infrastructure for Enabling Autonomic Sensor Grid Systems and Multidisciplinary Applications”. The main objectives include:

1) To design and develop a distributed data acquisition system based on hybrid wireless soil sensor network for unattended, real-time field-specific soil property monitoring;
2) To deploy the HWSSN system into the field and evaluate the system performance;
3) To find and analyze the major factors which affect in-field wireless path loss during wheat growing stages;
4) To evaluate applicability of existing, widely used path loss models for WSNs under wheat field conditions; and
5) To develop and verify multivariable radio path loss models for predicting in-field signal path loss during transmission under wheat field conditions.

1.6 Contributions

This thesis made a number of contributions on developing wireless sensor network technology for in-field agricultural applications, which included:

1) Conceptual design and experimental demonstration of two-generation wireless sensor network systems for soil property monitoring. (Li, Z. et al., 2008; Li, Z. et al., 2009(a)).
2) Statistical analysis on the influences of various impact factors to in-field radio wave propagation for low-power wireless sensor network applications. The impact factors include separation distance, antenna gain, plant canopy height, transmitter height, and receiver height (Li, Z. et al., 2009(b)).
3) New path loss models for predicting in-field radio propagation behaviors (Li, Z. et al., 2009(b)).

The researches carried out can potentially result in (1) better understanding of relationships between soil property changes along with plant growth and micro-climate situation; (2) controlling of variable rate fertilizer/pesticide operation or precision irrigation processes for lowering chemical and water consumption thus consequently preserving local environment; and (3) crop biomass quick measurement based on in-field RF signal attenuation patterns.

1.7 Thesis Outline

This thesis is a collection of papers that represent various steps taken to achieve a robust and remote monitoring system for supervising soil property parameters and to model in-field signal path loss of the system predicting communication performances.

Chapter 1 presents a survey of current wireless sensor network development and its environmental and agricultural applications. Examples of WSN implemented in forestry observation and forest fire detection, water management, herd and poultry management, precision agriculture and some other related areas are given. At the end of this chapter research gaps which need extra efforts on improving QoS of WSN in environmental and agricultural applications are discussed.

Chapter 2 presents the first generation of the monitoring system by introducing system networking topology, details of components selected and applied, soil moisture sensor calibration and data collected. Preliminary results stated that wireless sensor network could be successfully employed to monitor soil property.

Chapter 3 presents the second generation of the soil monitoring system. Compared to the first generation, more soil property parameters as soil electrical conductivity and near surface temperature were monitored. Data retrieving method has been upgraded from

manual field collection to automatic transmission through cellular GPRS service and Internet. The in-field WSN system was also upgraded for higher system reliability.

Chapter 4 covers: (1) the statistical analysis on the impact of various impact factors to in-field radio wave propagation. Box plots were used for excluding outliers within the sample spaces while paired sample t-tests were applied in the analysis of attenuation caused by separation distance, transmitter/receiver height, and plant height. (2) model development to evaluate and quantify in-field radio wave path loss introduced by impact factors and to predict received signal strength for the low-power WSN communications.

Chapter 5 states the conclusions of this thesis along with some recommendations for the future work.

References

Arora, A., P. Dutta, S. Bapat, V. Kulathumani, H. Zhang, V. Naik, V. Mittal, H. Cao, M. Demirbas, M. Gouda, Y. Choi, T. Herman, S. Kulkarni, U. Arumugam, M. Nesterenko, A. Vora, M. Miyashita. 2004. A line in the sand: a wireless sensor network for target detection, classification, and tracking. *Computer Networks*. 46(5): 605-634.

Baronti, P., P. Pillai, V. W. C. Chook, S. Chessa, A. Gotta, Y.F. Hu. 2007.Wireless sensor networks: A survey on the state of the art and 802.15.4 and ZigBee standards, Computer Communications. 30(7): 1655-1695.

Beckwith, R., C. Teibel, P. Bowen. 2004. Report from the field: results from an agricultural wireless sensor network. Local Computer Networks. In *Proc.* 29th Annual IEEE International Conference, 471-478.

Bellis, S.J., K. Delaney, B. O'Flynn, J.Barton, K.M. Razeeb, C.O'Mathuna. 2005. Development of field programmable modular wireless sensor network nodes for ambient systems. *Computer Communications.*28 (13): 1531-1544.

Bhatti, S., J. Carlson, H. Dai, J. Deng, J. rose, A. Sheth, B. Shucker, C. Gruenwald, A. Torgerson, R. Han. 2005. Mantis os: an embedded multithreaded operating system for wireless micro sensor platforms. ACM Kluwer Mobile Network Jounal, Special Issue on Wireless Sensor Networks.

Boegena, H., K. Schulz, H. Verrechken. 2006. Towards a network of Observatories in Terrestrial Environmental Research. *Advances in Geosciences*. 9:109-114.

Butler, Z. P. Corke, R. Peterson, D. Rus. 2004. Networked cows: virtual fences for controlling cows. In Proc. of ICRA, IEEE Conference on Robotics and Automation, 5: 4429-4436. New Orleans, LA.

Coates, R. W., M. J. Delwiche, R. Y. Evans, L. R. Oki, P. H. Brown. 2007. Site-Specific Water and Nutrient Application by Wireless Valve Controller Network. ASABE Paper No. 072247. Minneapolis, Minnesota, USA.

Crossbow Technology. 2004. XMesh User Mannual. Available at: http://www.xbow.com/Technology/MeshNetworking.aspx. Accessed 9 June 2009.

Crossbow Technology. 2008. IMB400 Datasheet. Available at: http://www.xbow.com/Products/Product_pdf_files/Wireless_pdf/Imote2_IMB400_Preliminary.pdf. Accessed 23 March 2009.

Cui, L., F. Wang, H.Y. Luo, H. L. Ju, T. P. Li. 2004. A Pervasive Sensor Node Architecture. *Network and Parallel computing.* 3222: 565-567.

Cui, J. H., J. J. Kong, M. Gerla, S. Zhou. 2006. The Challenges of Building Scalable Mobile Underwater Wireless Sensor Networks for Aquatic Applications. *IEEE Network, Special issue on Wireless Sensor Networking*. 20(3): 12-18.

Darr, M. J., L. Zhao. 2008. A Model for Predicting Signal Transmission Performance of Wireless Sensors in Poultry Layer Facilities. *Transactions of the ASABE.* 51(5): 1817-1827.

Demirbas, M., K. Y.Chow, C. S. Wan. 2006. INSIGHT: Internet-Sensor Integration for Habitat Monitoring, In *Proc.* of the 2006 International Symposium on World of Wireless, Mobile and Multimedia Networks: 553-558.

Dinh, T. L., W. Hu, P. Sikka, P. Corke, L. Overs, S. Brosnan. 2007. Design and Deployment of a Remote Robust Sensor Network: Experiences from an Outdoor Water Quality Monitoring Network. *Local Computer Networks*. 2007: 799-806.

Dutta, P., M. Grimmer, A. Arora, S. Bibyk, D. Culler. 2005. Design of a wireless sensor network platform for detecting rare, random, and ephemeral events. Information Processing In Sensor Networks. In *Proc.* of the 4th international symposium on Information processing in sensor networks. Article No. 70. Los Angeles, California, 2005.

Ember. 2005. EM250 data sheet. Available at: http://www.ember.com/pdf/120-0082-000_EM250_Datasheet.pdf. Accessed 23 March 2009.

Fok, C. L., G. C. Roman, C. Lu. 2005. Rapid Development and Flexible Development of Adaptive Wireless Sensor Network Applications. Distributed Computing Systems. In *Proc.* of 25th IEEE International Conference, 653-662.

Fukatsu, T., M. Hirafuji, T. Kiura. 2006. An agent system for operating Web-based sensor nodes via the Internet. *Journal of Robotics and Mechatronics*. 18(2): 186-194.

Gay, D., P. Levis, R.V. Behren, M. Welsh. 2003. The nesC Language: A Holistic Approach to Networked Embedded System. Available at: http://nescc.sourceforge.net/papers/nesc-pldi-2003.pdf. Accessed June 8 2009.

Han, C.C., R. Kumar, R. Shea, E. Kohler, M.B. Srivastava. 2005. A dynamic operating system for sensor nodes. In: MobiSys: 163-176.

Han, W., N. Q. Zhang, Y. L. Zhang. 2008. A two-layer wireless sensor network for remote sediment monitoring, ASABE Paper No. 084548, Providence, Rhode Island.

Handziski,V., A. Kopke, A. Willig, A. Wolisz. 2006. TWIST: a scalable and reconfigurable testbed for wireless indoor experiments with sensor networks. In *Proc.* of the 2nd international workshop on Multi-hop ad hoc networks: from theory to reality, SESSION: Sensor networks, 63-70. Florence, Italy.

Hefeeda, M. and M. Bagheri. 2007. Wireless Sensor Networks for Early Detection of Forest Fires. In MASS.

Hu, W., N. Bulusu, C. T. Chou, S. Jha, A. Taylor, V. N. Tran. 2009. Design and evaluation of a hybrid sensor network for cane toad monitoring. ACM Transactions on Sensor Networks (TOSN). 5(1): Article No. 4.

Jackson, T., K. Mansfield, M. Saafi, T. Colman, P. Romine. 2008. Measuring soil temperature and moisture using wireless MEMS sensors. Measurement. 41(4): 381-390.

Jennic. 2006. JN5139 datasheet. Available at: http://www.jennic.com/files/product_briefs/JN5139_PB_021008_v1.22.pdf. Accessed 24 March 2009.

Kim, S., S. Pakzad, D. Culler, J. Demmel, G. Genves, S. Glaser, M. Turon. 2007. Health monitoring of civil infrastructures using wireless sensor networks. In *Proc.* of the 6th international conference on Information processing in sensor networks, 254-263. Cambridge, Massachusetts, USA.

Kim, T.H. and S.Hong. 2005. State Machine based Operating System Architecture for Wireless Sensor Networks. In Parallel and Distributed Computing: Applications and Technologies. 3320: 803-806.

Kim, Y., R. G. Evans, W. iversen, F. J. Pierce2006. Instrumentation and Control for Wireless Sensor Network for Automated irrigation. ASABE Paper No. 061105. Portland, Oregon, USA.

King, B. A., R. W. Wall, L. R. Wall. 2005. Distributed Control and Data Acquisition System for Closed-Loop Site-Specific Irrigation Management with Center Pivots. *Applied Engineering in Agriculture.* 21(5): 871-878.

Knot, T. 2004. BP Frontiers Magazine. 9:6-10.

Kuo, S.P., C.Y. Lin, Y.F. Lee, et.al. 2008. The NTP Experimental Platform for Heterogeneous Wireless Sensor Networks. In *Proc.* of the 4th International Conference on Testbeds and research infrastructures for the development of networks & communities, Article No. 35. Innsbruck, Austria.

Kwong, K. H., H. G.Goh, C. Michie, I. Andonovic, B. Stephen, t. Mottram, D Ross. 2008. Wireless Sensor Networks for Beef and Dairy Herd Management. ASABE Paper No. 084587. Providence, Rhode Island, USA.

Li, D., K. D. Wong, Y. H. Hu, A. M. Sayeed. 2002. Detection, Classification and tracking of targets. *IEEE Signal Processing Mag.* 19: 17-29.

Li, M. U. H. Liu. 2007. Underground Structure Monitoring with Wireless Sensor Networks. In *Proc.* of the 6th international conference on Information processing in sensor networks, 69-78. Cambridge, Massachusetts, USA.

Li, Z., N. Wang, A. Franzen, X. Li. 2008. Development of a Wireless Sensor Network for Field Soil Moisture Monitoring. ASABE Paper No. 083835. Providence, Rhode Island, USA.

Li, Z., N. Wang, A. Franzen, P. Taher. 2009 (a). In-field Soil Property Monitoring using Hybrid Sensor Network. ASABE Paper No. 096191. Reno, NV, USA.

Li, Z., N. Wang. 2009 (b). Radio Wave Path Loss Model for Predicting In-site Signal Strength of Wireless Sensor Network in Wheat Field. Written for submission.

Liu, H., Z.J. Meng, S.H. Cui. 2007. A Wireless Sensor Network Prototype for Environmental Monitoring in Greenhouses. Wireless Communications, Networking and Mobile Computing. WiCom International Conference: 2344-2347.

Lowe, J. C., S. M. Abeyesinghe, T. G. M. Demmers, C. M. Wathes and D. E. F. McKeegan. 2007. A novel telemetric logging system for recording physiological signals in unrestrained animals. *Computers and Electronics in Agriculture.* 57(1): 74-79.

Mahfuz,M., K.Ahmed. 2005. A review of micro-nano-scale wireless sensor networks for environmental protection: prospects and challenges. *Sci. Technol. Adv. Mater.* 6 (3-4): 302-306.

Meesookho, C., S .Narayanan, C. Raghavendra. 2002. Collaborative classification applications in sensor networks. In *Proc.* Second IEEE Multichannel and Sensor array signal processing workshop, 370-374. Arlington, VA: IEEE.

Milenkovic, A. C. Otto, E. Jovanov. 2006. Wireless sensor networks for personal health monitoring: Issues and an implementation. Computer communications. 29: 2521-2533.

Nadimi, E. S., H. T. Sogaard, T. Bak, F. W. Oudshoorn. 2008. ZigBee-based wireless sensor networks for monitoring animal presence and pasture time in a strip of new grass. *Comput. Electron. Agric.* 61(2): 79-87.

Niimi, A., M. Wada, K. Ito, M. Toda, K. Hatanaka, O. Konishi. 2008. Broiler-house environment monitoring system using sensor network and mail delivery system. *Artificial Life and Robotics.* 13(1): 264-270.

Ng, M. L., K. S. Leong, D. M. Hall, P. H. Cole. 2005.A simple passive UHF RFID tag for livestock identification. In Proc. of IEEE International Symposium on Microwave, Antenna, Propagation and EMC Technologies for Wireless Communication, 67-70.

Otto, C., A. Milenkovic, C. Sanders, E. Jovanov. 2006. System Architecture of a Wireless Body Area Sensor Network for Ubiquitous Health Monitoring. *Journal of Mobile Multimedia.* 1(4):307-326.

Panchard, J., S. Rao, T. V. Prabhakar, H. S. Jamadagni, J. P. Hubaux. 2006. COMMON-Sense Net: Improved Water Management for Resource-Poor Farmers via Sensor

Networks, In *Proc.* Intern. Conference on Communication and Information Technologies and Development ICTD.

Park, S., J.W. Kim, K.Y. Shin, D. Kim. 2006. A Nano Operating System for Wireless Sensor Networks. Advanced Communication Technology. ICACT 2006. In *Proc.* The 8th International Conference, 1: 345-348.

Partan, J., J. Lurose, B. N. Levine. 2007. A survey of practical issues in underwater networks. ACM SIGMOBILE Mobile Computing and Communications Review. 11(4): 23-33.

Pierce, F. J., T. V. Elliott. 2008. Regional and on-farm wireless sensor networks for agricultural systems in Eastern Washington. Computers and Electronics in Agriculture. 61(1): 32-43.

Selavo, L., A. Wood, Q. Cao, et al. 2007. LUSTER: wireless sensor network for environmental research, Conference On Embedded Networked Sensor Systems. In *Proc.* of the 5th international conference on Embedded networked sensor systems, 103-116. Sydney, Australia.

Sibley, G. T., M. H. Rahini, G. S. Sukhatme, Robomote: A Tiny Mobile Robot Platform for Large-Scale Ad-hoc Sensor Networks. *Robotics and Automation*. 2: 1143-1148.

Sousa Silva, A. C., A. I. C.Arce, S. Souto, E. J. X. Costa. 2005. A wireless floating base sensor network for physiological responses of livestock. *Comput. Electron. Agric.*49(2): 246-254.

The BTnode Project. 2007. BTnode Programming – An Introduction to BTnut Applications. Available at:

http://www.btnode.ethz.ch/pub/uploads/Documentation/btnodetutorial_1.6.pdf. Accessed 9 June 2009.

Tolle, G., J. Polastre, R. Szewczyk, D. Culler, N. Tuner, K. Tu, S. Burgess. 2005. A Macroscope in the Redwoods. In *Proc.* Sensys '05, 51-63. San Diego, Califonia, USA.

Tolle, G., D. Culler. 2005. Design of an application-cooperative management system for wireless sensor networks. Wireless Sensor Networks. 2005. In *Proc.* of the Second European Workshop, 121-132.

Wang, H. B., J. Elson, L. Girod, D. Estrin, Y. Kung. 2003. Target classification and localization in habitat monitoring. *Acoustics, Speech, and Signal Processing*. 4: 6-10.

Wang, N., N.Q. Zhang, M.H. Wang. 2006. Wireless sensors in agriculture and food industry-Recent development and future perspective. *Computers and electronics in agriculture.* 50: 1-14.

Wang, Y., J. Lynch, K. Law. 2007. A wireless structural health monitoring system with multithreaded sensing devices: design and validation. *Structure & Infrastructure Engineering: Maintrnance, Management, Life-Cycl.* 3(2): 103-120.

Werner-Allen, G., J. Johnson; M. Ruiz, J. Lees, M. Welsh. 2005. Monitoring volcanic eruptions with a wireless sensor network. Wireless Sensor Networks. In *Proc.* of the Second European Workshop: 108-120.

Yang, H. H., Y.H. Bae, W. Min. 2007. Implantable Wireless Sensor Network to Monitor the Deep Body Temperature of Boilers. Software Engineering Research, Management & Applications. In *Proc.* 5th ACIS International Conference, 513-517. SERA.

Zhou, Y. M. X. L. Yang, X. S. Guo, M. G. Zhou, L. R. Wang. 2007. A Design of Greenhouse Monitoring & Control System Based on ZigBee Wireless Sensor Network. Wireless Communications, Networking and Mobile Computing. 2007: 2563-2567.

ZIGBEEF. 2008. The Z2 RFID System. Available at: http://www.zigbeef.com/usda_id.html. Accessed 10 June 2009.

CHAPTER II

DEVELOPMENT OF A WIRELESS SENSOR NETWORK FOR FIELD SOIL MOISTURE MONITORING

Zhen Li[1,4], Ning Wang[1], Aaron Franzen[1], Arunkumar Venkateshwaran[2], Chad Godsey[3], Xiaolin Li[2]

1. Biosystems and Agricultural Engineering, Oklahoma State University, USA;

2. Computer Science, Oklahoma State University, USA;

3. Plant and Soil Science, Oklahoma State University, USA;

4. College of Engineering, South China Agricultural University, China.

Abstract

A wireless sensor network system (WSNS) was developed and tested which was able to continuously monitor soil moisture content in a wheat field. The system consisted of 12 wireless nodes with star-type, tiered network architecture. Out of 12 wireless nodes, ten were used as the sensor nodes, one as a central node which collected data from the sensor nodes according to a preset schedule, and one as a base node which was connected to a PC to retrieve, store, and present the data. Each sensor node included a mote, a signal conditioning board, and four soil sensors buried at different depths in a given sampling location. The signal conditioning circuit was designed to provide excitation for the

sensors, condition sensor signals, and monitor the power supply voltage. The central node had an onboard 1M flash which can store data from 40 soil moisture sensors for 21 days at a sampling rate of every two hours. The soil moisture sensors were calibrated with the soil samples collected from the experiment site at nine soil moisture levels, 0%, 5%, 10%, 15%, 20%, 25%, 30%, 35% and 40%. To implement the system in a wheat field, all sensor nodes and the central node are solar powered, housed in watertight plastic boxes, and mounted on posts. Primary results show that the WSNs performed well for field soil moisture monitoring.

Keywords: Wireless sensor network, soil moisture sensor, precision agriculture, soil variability, solar power

2.1 Introduction

In the past few years, fresh water supplies have become increasingly short. This phenomenon leads to serious conflicts between water requirements and water supply in many countries. Precision irrigation techniques offer the potential to alleviate this conflict by reducing agricultural water consumption without adversely affecting food production. In precision irrigation, soil moisture is one of the key variables to calculate crop water demand. It is also one of the important environmental factors in controlling water and heat energy exchange between land surface and atmosphere through evaporation and plant transpiration (Jackson et al., 2007). The amount of water contained in a unit mass or volume of soil and the energy state of water in the soil are important factors affecting the growth of plants and yields.

Recently, demand from precision irrigation applications has motivated a significant increase in the types of commercially available devices for soil moisture content (SMC)

measurement such as time-domain reflectometry (Huisman et al, 2001, 2002) and ground penetration radar (Lambot et al., 2006). A dielectric-based moisture sensor was evaluated under dynamic conditions by incorporating it into a nylon block that was attached to an instrumented tine (Liu et al., 1996). The results indicated the feasibility of this approach for real-time applications. This type of sensor has the advantages of low cost and very fast response. However, this moisture sensor not only responded to soil moisture but also to salinity, soil texture, and temperature (Andrade et al., 2001). Whalley (1991) incorporated a microwave attenuation−based moisture sensor into a tillage tool and found that the main limitation of this approach was that the sensor interacted only with a small volume of soil adjacent to the probe. The tensiometer makes measurements through water potential or tension. Norikazu (1996) applied this type of sensor to measure the relationship between water migration and the diurnal frost heaving. The sensors described above are either expensive or sensitive to variables other than soil moisture. Sensors with sensitivity to other parameters require signal compensation, adding significant cost such that they are too expensive for use in a large scale, networked measurement system. Capacitance probe sensors are a popular electro-magnetic method for estimating soil water content. The basic principle is to incorporate the soil into an oscillator circuit and measure the resonant frequency. Capacitance probes are relatively cheap, safe, easy to operate, energy effective and easily automated (Kelleners, et al., 2004).

Commonly, the commercially available sensors are used to measure SMC at a single location in a field. Data is collected by a technician using a portable data acquisition device or by a stationary data-logger with a preset sampling frequency. In order to sample SMC at multiple spots in a field, the technician needs to take the measurements one by

one at each pre-selected spot. Alternatively, a number of stationary data acquisition devices need to be set up at the pre-selected locations and collect and store the measurement data which will be downloaded during a technician's field visit.

In some situations, the SMC sensor can be installed on agricultural machinery. Real-time SMC data acquisition can be conducted during field operations. In this way, a large amount of data can be collected with a very high spatial sampling density. However, the intensity of machine usage is limited, thus the opportunities for temporal data collection are reduced (Camilli et al. 2007). In order to improve the understanding of soil moisture variability in the whole range of a field, it will be necessary to collect field data timely and spatially, even in real-time, without using agricultural machines or manual operations. This requires the SMC sensors applied to be cost-effective for large scale installation and provides an opportunity for applying networked data collection devices which can be distributed in a field, sample the SMC data regularly, and be available during the entire cropping season (Camilli et al. 2007).

Wireless sensor network (WSN) is one of the newest and most promising technologies for soil moisture monitoring. The networked SMC measurement system allows in-situ, timely measurements. It consists of multiple small sensor nodes, each of which has limited on-board signal processing ability and is equipped with one or more sensors and their signal conditioning circuits (Bogena et al., 2006). The communication between sensor nodes is short–distanced and normally based on radio frequency (RF) (Akyildiz et al., 2002; Cardell-Oliver et al., 2004; Wang et al., 2006; Wark et al., 2007). To implement a WSN in soil moisture monitoring, several factors have to be guaranteed, i.e. the sensor nodes must be energy efficient and insensitive to environmental influences,

each node must be as inexpensive as possible, and each node requires a stable, independent power supply.

The utmost objective of this study is to design and develop a wireless sensor network system for continuous, in-field multi-plot SMC monitoring. The specific objectives include:

1. To design and develop hardware for a networked soil moisture monitoring system;
2. To develop communication protocols and software for in-field SMC data acquisition and communication;
3. To establish an efficient power supply unit for field implementation of the WSN; and
4. To conduct field tests to evaluate the developed WSN qualitatively.

2.2 Methods and Materials

2.1.1 Experimental Site

The experiments were conducted on the Experimental Farm of Oklahoma State University, Stillwater, Oklahoma. An experimental field was prepared and evenly divided into 10 strips with a size of about 10 meters by 30 meters. The sensor nodes were installed at the edge of each strip. Each sensor node connected four SMC sensors which were installed 3m from the sensor nodes and at four depths underground (50.8, 152.4, 304.8 and 609.6*mm*). The central node was installed at one end of the strip located in the center of the testing field.

2.2.2 Soil Moisture Sensor Selection

The sensor applied in this study needed to be inexpensive and energy-efficient. Taking these requirements into consideration, a capacitance based soil moisture sensor, namely

the EC-5, (ECH2O probe, Model EC-5, Decagon Devices, Pullman, MA, USA), was selected due to its features of low-cost, energy efficiency, dependability, and ease-of-use.

The equivalent circuit diagram of the EC-5 probe is illustrated in Figure 2-1 (Bogena, et al, 2007). For each measurement, EC-5 required an excitation pulse with an amplitude of 2.5V and a duration of 10ms (Decagon, 2006). This allowed the sensor to warm up, stabilize, conduct measurements, and prepare the data for a data acquisition system. An oscillator which generated a repetitive square waveform with a characteristic frequency of 70MHz was used for capacitance measurements. The total capacitance the sensor measured was made up of the capacitance of the medium, C, and the capacitance due to stray electric fields, Cs. It was also a function of the dielectric permittivity of the material surrounding the probe. The output of the sensor was a voltage ranging 10-40% of the excitation and reacted accordingly to the SMC changes.

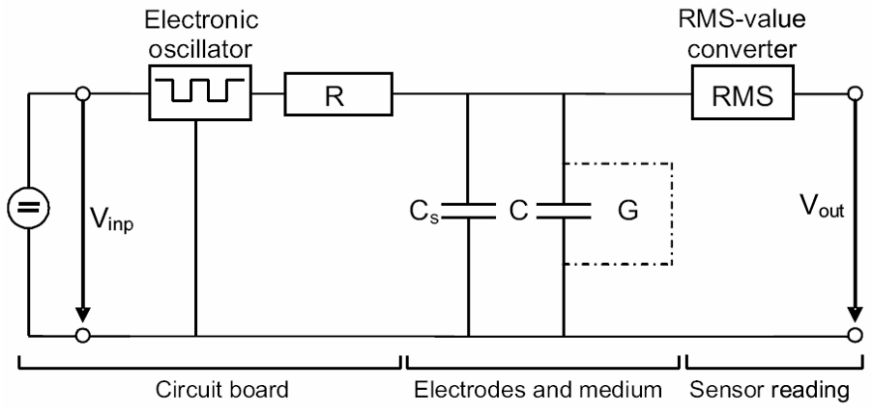

Figure 2-1 Equivalent circuit diagram of a capacitance sensor where R is a resister, C is the capacitance of the medium, Cs is the stray capacitance, G is the energy loss due to relaxation and ionic conductivity and V_{inp} and V_{out} are the supply and sensor reading voltage (Bogena, et al, 2007) .

2.2.3 Soil Moisture Content Sensor Calibration

Soil moisture content (SMC) is usually expressed on either a gravimetric (per-mass) or volumetric (per-volume) basis (Andrade-Sanchez et al, 2004). The fractional content of water in the soil can be expressed in terms of either mass or volume ratios as shown in Equation 2.1 and Equation 2.2:

$$w = M_w / M_s \qquad (2.1)$$

$$\theta = V_w / V_t = V_w / (V_s + V_w + V_a) \qquad (2.2)$$

Where w, the gravimetric SMC, is a ratio of the mass of water in a sample, M_w; to the total mass of the sample, M_s. θ, the volumetric SMC, is the ratio of the volume of water in a sample, V_w, to total volume, Vt. The latter is equal to the sum of the volumes of solids (V_s), water (V_w), and air (V_a).

The EC-5 probes were designed to measure the volumetric water content (VWC) in the soil. They are pre-calibrated by the manufacturer for most soil types. It was much less sensitive to variations in soil texture and electrical conductivity due to its high measurement frequency of 70MHz. However, to verify the SMC readings and the performance of the EC-5 sensor in the test field which had high clay content soil, a sensor calibration was conducted before they were deployed to the field in this study.

Soil samples were taken from three different locations in the test field (Figure 2-2). Location 1 and 3 were at the edge of the field and Location 2 was at the center of the field. Each soil sampling location was very close to the sensor nodes. At each sampling location, about 10 litter of soil was collected.

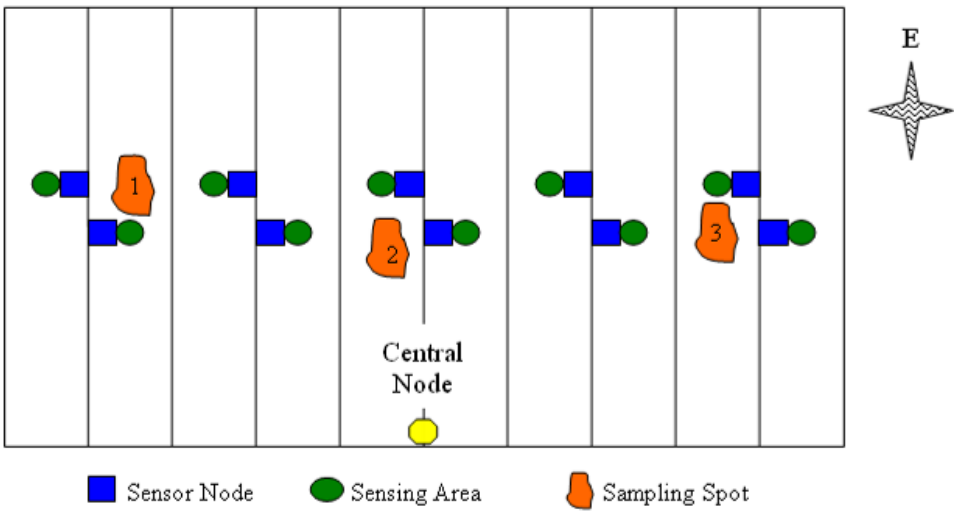

Figure 2-2 Soil sampling locations in the test field

The collected samples were first dried in a forced-air convection oven (Fisher Scientific, Waltham, MA, USA) at 105°C for more than 24 hours to obtain a 0% VWC. The dried soil samples were distributed into four containers to calibrate four SMC sensors simultaneously. Nine different soil moisture levels i.e. 0%, 5%, 10%, 15%, 20%, 25%, 35% and 40%, were created by adding water to the containers. The volume of water to be added in order to achieve specific moisture content was determined using Equation 2.3:

$$\theta_i = \left| \frac{V_{water,i}}{Vs} \right| \times 100\% \qquad i = 1, 2, \cdots, n \qquad (2.3)$$

Where θ_i was the targeted volumetric water content (%) at the ith level, $V_{water,i}$ is the volume of water (mL) to be added, and V_s was the volume of the dried matter of the samples (mL). It was assumed that both the volume of the air included in the soil and the changes in the total volume after water was added could be ignored. As a result, the total volume, V_t, equaled to the volume of soil V_s in the calibration. V_s was set to be 700mL.

During the calibration, the sensor outputs were collected every 5 seconds after water was added into the container. It took several hours for the added water to infiltrate into the soil and reach equilibrium. Every two hours the collected data was plotted with the horizontal axis representing the time stamps and vertical axis representing the sensor voltage output. A one-sample T-test was applied to each two-hour data set using SPSS (Version 15.0, SPSS Inc., Chicago, IL, USA). When a T-test performed on consecutive two-hour sets was within a certain alpha level, the soil was considered to have reached equilibrium. The averages of reading after the sensor reading stabilization were used to create the calibration equations.

Linear regression models were established using Excel (Version 2003, Microsoft, USA) to find the relationship between VWC within the soil and the sensor output. For each soil sample collected from the three locations in the experimental field, a linear regression model was established individually and compared. Another linear regression model was established based on an average of the data collected from the three locations. The regressed models were developed at a known reference temperature of 23°C and a stable power of 2.5 Volts from a DC power supply. They were also compared with those provided by the manufacturer.

2.2.4 Signal Conditioning Unit

As mentioned above, each EC-5 soil probe required an excitation voltage of 2.5V (10*mA*). An analog output channel of a microcontroller on the wireless senor node was used to generate the excitation signal. However, its driving capability (10*uA*) was not sufficient for the EC-5 sensor. A low power CMOS operational amplifier, LMC6484 (National Semiconductor, Santa Clara, CA, USA), was added which could work under a

positive voltage of 3.3V and had a driving ability of up to 30*mA*. In order to drive four SMC sensors, four followers were also added. All the inputs of the amplifiers were connected to a digital-to-analog channel of the microprocessor. The output of each follower was connected to the excitation input of an EC-5 sensor.

Power supply stability greatly affected SMC sensor performance (Bogena et al., 2007). Although the microcontroller could work within a wide power supply range from 2.7V to 3.6V, to generate stable excitation signals for the SMC sensors, current amplifiers needed to be powered by a voltage of at least 3.3V. A CMOS (Complementary Metal-Oxide-Semiconductor) voltage detector was added. The input of the detector was connected to the power supply pin of the signal conditioning board. If the supplying voltage to the amplifiers dropped below 3.3V, a signal would be issued to the external interrupt pin of the microcontroller to turn off SMC measurements until the supplying voltage returned to be above 3.3V. The circuitry of the signal conditioning board is shown in Figure 2-3.

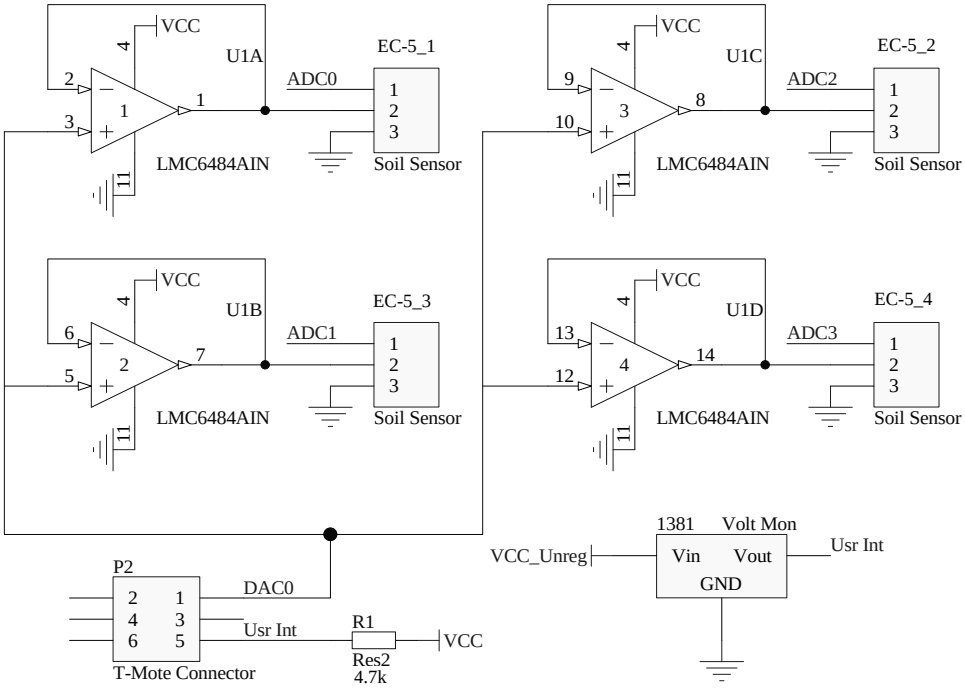

Figure 2-3 Design of the signal conditioning unit

2.2.5 Selection of WSN Development Environment

T-Mote Sky motes (Moteiv, San Francisco, CA, USA) were used to establish the field SMC wireless sensor network. Each mote was consisted of an MSP430 (Texas Instruments, TX, USA) microcontroller, analog-to-digital conversion, digital-to-analog conversion, and timing controls. An onboard Chipcon CC2420 RF communication chip (Texas Instruments, TX, USA) was available with a MAC-supported, 2.4GHz IEEE 802.15.4/ZigBee RF transceiver. An 8M flash memory was accessed through the high speed SPI interface of the microcontroller. All the wireless sensor nodes within the developed system were programmed and run under the open source embedded operating system, TinyOS 1.1 (University of California, Berkeley, CA, USA).

There were three types of nodes within the soil moisture monitoring system (Figure 2-4). A central node located on one edge of the testing area. Multiple sensor nodes (10 in

this study) were distributed in the field. A base node was connected to a laptop computer and used for downloading data from the central node or the sensor nodes in the field through RF transmission.

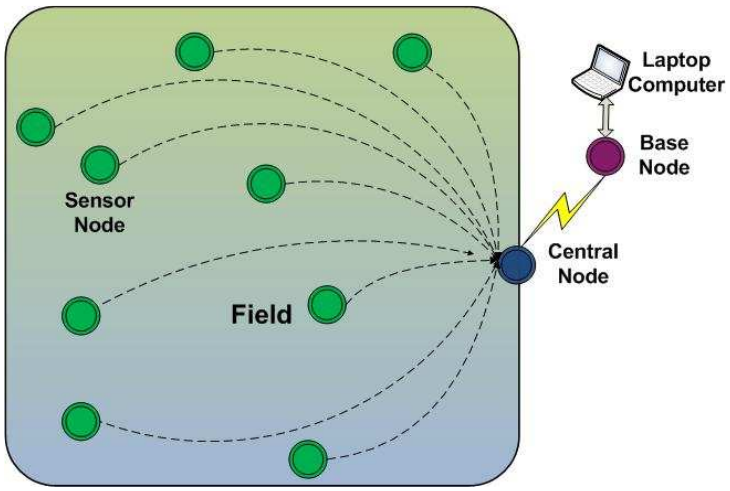

Figure 2-4 Network hierarchy of the system

2.2.6 SMC Sensor Installation

Each sensor node contained four EC-5 soil moisture sensors, a signal conditioning unit, a solar power supply unit and a T-mote-sky wireless sensor network mote. The moisture sensors were embedded in the soil at depths of 50.8, 152.4, 304.8 and 609.6*mm* (2, 6, 12, and 24 inches) as shown in Figure 2-5.

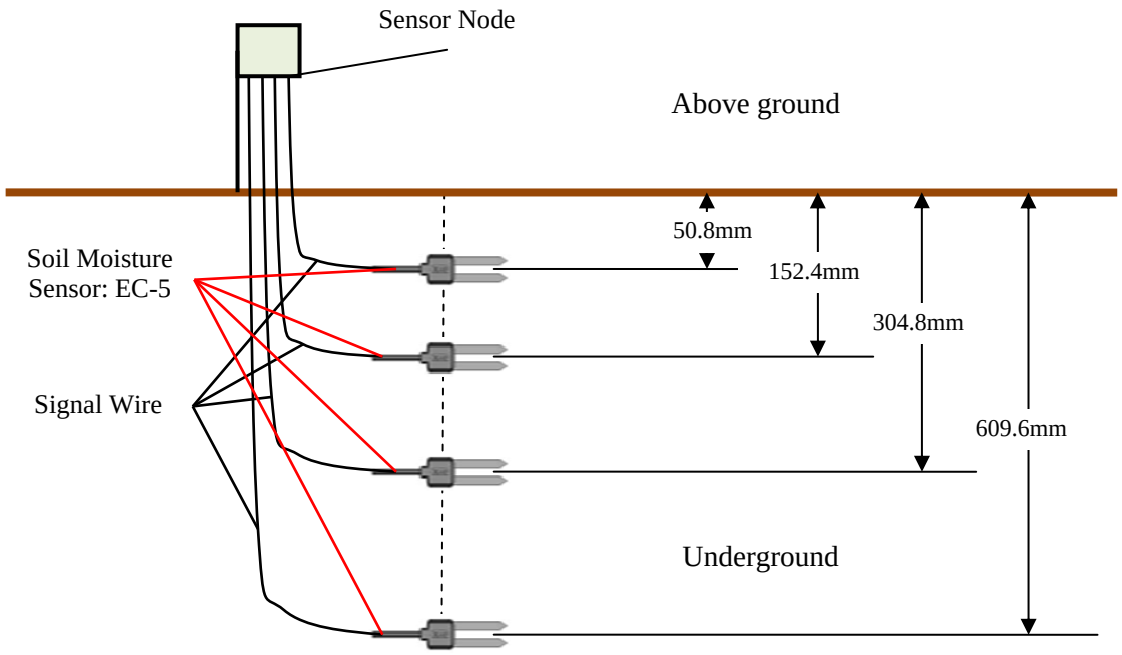

Figure 2-5 Field installation of the wireless sensor nodes

At a user-defined time interval (two hours in this study), each sensor node acquired the soil moisture sensor readings and stored them into an on-board flash memory. The sensor node wirelessly transmitted daily data to the central node for long-time data storage. The sensor node could store readings for 210 days from the four sensors with a sampling rate of every two hours. This was used as a data backup if central node has failure. At 21 day intervals, the base node was used to download data (wirelessly) from the central node. If the central node failed, data from each sensor node could be downloaded individually.

During preliminary field tests, plant biomass interfered with wireless transmission. Radio frequency signals were attenuated substantially by the crops, especially in the 2.4GHz range. To overcome this problem, all the sensor nodes in the field were mounted approximately 1.2m above ground while the central node was mounted about 1.5m above ground. The antenna of each sensor node was manually adjusted to face the central node.

2.2.7 Data Frame

Data transmission was carried out using a 104 byte TinyOS Wireless Transport Packet. The data were packed in a custom structure designed for the specific application. The packet definition and the explanation of each field inside the packet are given in Table 2-1.

Table 2-1 Field length and explanation within each data packet

Field Name	Length (bytes)	Explanation
Sensor 1	24	Soil moisture readings, 12 Readings/Day
Sensor 2	24	Soil moisture readings, 12 Readings/Day
Sensor 3	24	Soil moisture readings, 12 Readings/Day
Sensor 4	24	Soil moisture readings, 12 Readings/Day
Alarm	2	Alarm for low battery voltage
ID	2	Source ID; 0: Base Node; 1: Central Node; 2-65535: Sensor nodes
Target	2	Destination ID
Index	2	Sequential packet identifier

2.2.8 Power Supply Unit

Each wireless sensor node was powered with two 3.7V, 1300mAh lithium-ion batteries (Model: 18500, Tenergy Corporation, Sunnyvale, CA, USA), two 3.7V, 100mA solar panels (Model: MPT3.6-150, PowerFilm Solar, Ames, IA, USA), and a 3.3 V switching buck-boost regulator (Model: LTC3531-3.3, Linear Technology, Milpitas, CA, USA). The switching regulator accepted input voltages from 1.8V to 5.5V, and could source up to 200mA current. The resulting power supply provided a stable 3.3 V supply for the sensor node. The total storage capacity of 2600mAh was selected to allow the sensor nodes to operate for multiple days without sunlight. Figure 2-6 shows the circuit diagram for the power supply.

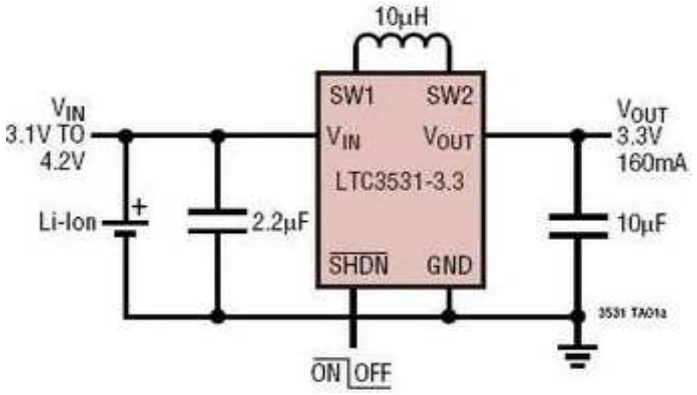

Figure 2-6 Power supply circuit diagram (Linear Technology, 2006)

2.3 Results and Discussion

2.3.1 VWC Sensor Calibration Result

One example of how valid data was decided is given using data collected from four sensors at VWC level of 25% using soil sample 1 (collected from sampling location 1, Figure 2-2). Standard deviation of each sensor's two-hour reading is given in Table 2-2:

Table 2-2 Standard deviation of each sensors reading at VWC level of 25% using soil sample 1

Time Stamp	Standard Deviation of sensor output (*m*V)			
	Sensor 1	Sensor 2	Sensor 3	Sensor 4
0:00:05 to 2:00:05	3.54	7.88	16.65	4.983
2:00:10 to 4:00:05	3.42	5.09	6.44	4.21
4:00:10 to 8:00:05	3.18	4.86	6.19	4.14
8:00:10 to 10:00:05	3.38	4.62	6.04	4.25

According to the specification of EC-5, its VWC measuring range is 0-100% while the output range is 10-40% of excitation voltage (250-1000mV at 2500mV excitation). The scale (Sc) of the sensor could be calculated as Equation 2.4:

$$Sc = \frac{100\%}{750mV} = 0.13\%/mV \qquad (2.4)$$

The standard deviation of the VWC reading could be calculated using Equation 2.5:

$$Std_v = Std_s \times Sc \qquad (2.5)$$

Where Std_v was the standard deviation of the VWC and Std_s was the standard deviation of each sensor's output. By applying the scale obtained from Equation 2.4 and the standard deviations of sensor output in Table 2-2, the standard deviation of VWC could be calculated and is shown in Table 2-3.

Table 2-3 Calculated standard deviation of VWC from each sensor at the level of 25% using soil sample 1

Time Stamp	Standard Deviation of VWC (%)			
	Sensor 1	Sensor 2	Sensor 3	Sensor 4
0:00:05 to 2:00:05	0.46	1.02	2.16	0.64
2:00:10 to 4:00:05	0.44	0.66	0.83	0.54
4:00:10 to 8:00:05	0.41	0.63	0.80	0.53
8:00:10 to 10:00:05	0.44	0.60	0.78	0.55

Table 2-3 indicates that within the first 2 hours, the VWC standard deviation of sensor 2 and sensor 3 and was 1.02% and 2.16%, respectively. After the first 2 hours, all of the standard deviations from 4 sensors' reading were less than 1.00% and it was assumed that water had evenly infiltrated within the soil. As a result, the valid data starting location was set to be 2 hour and 5 seconds after water was added within this calibration (25% VWC, soil sample 1).

Figure 2-7 presents the logged calibration data for one of the soil moisture levels from four soil moisture sensors. The red dotted line represents the dividing line (2:00:05) for invalid and valid data where consecutive, statistically equivalent two-hour sample sets occur as the sensor voltage outputs approach horizontality. Data before the dividing line

was considered to be invalid while data after the line was used for modeling the relationship between sensor output and moisture level.

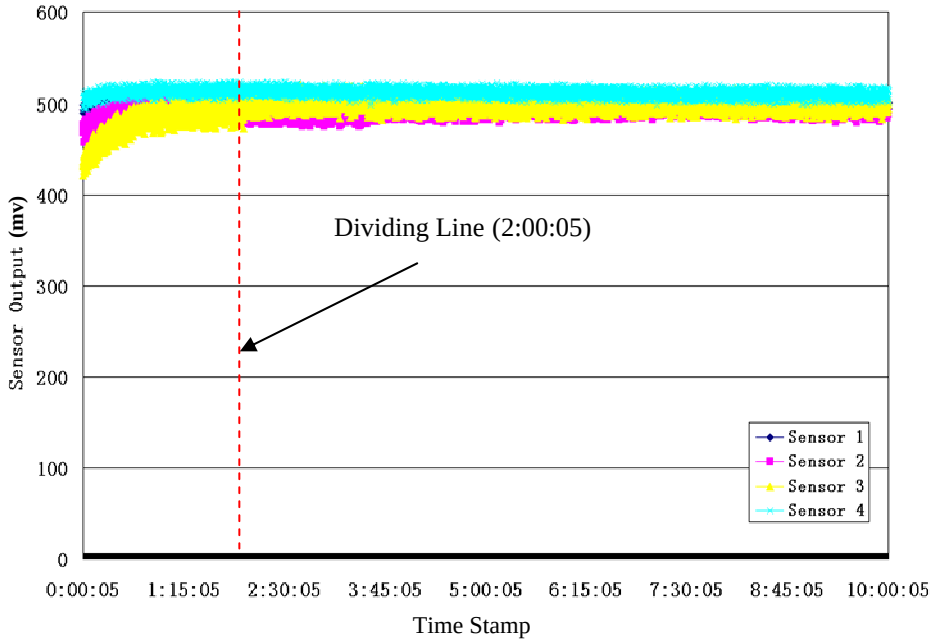

Figure 2-7 Selection of valid SMC data points in a reading sequence-sensor output curve

Linear regression was used to relate sensor outputs from different samples to soil moisture content. Regressed equations are in Equation 2.6-2.9 while Equation 2.10 was provided by the manufacturer.

Sample 1: $y = 0.1178x - 30.538$ (2.6)

Sample 2: $y = 0.1305x - 35.257$ (2.7)

Sample 3: $y = 0.1270x - 35.867$ (2.8)

Average: $y = 0.1250x - 33.710$ (2.9)

Manufacturer: $y = 0.1190x - 40.100$ (2.10)

Where x was the soil moisture sensor output in the unit of mV and y was the VWC with the unit of percentage (%). Coefficients of Determination (R^2) were 0.958, 0.967, 0.962 and 0.977 for three different types of soil and the average reading, respectively.

2.3.2 Field Test Results

Figure 2-8 shows in-field SMC data collected from the sensor node #9 in February, 2008. At the same time, volumetric rainfall of Stillwater, OK was measured and data was collected through a MESONET station (http://www.mesonet.org/) at Lake Carl Blackwell which was 262m away from the test field for comparisons of soil moisture collected from the system and water accumulation from the corresponding rainfall.

Figure 2-8 indicates that the reading from the system would change accordingly to the rainfall recorded by MESONET and then reflect the trend of soil moisture variability from sensor buried at 50.8*mm* underground varied significantly over rain time period, as the wheat crop water requirement and latent heat flux at this point in the growing season was minimal.

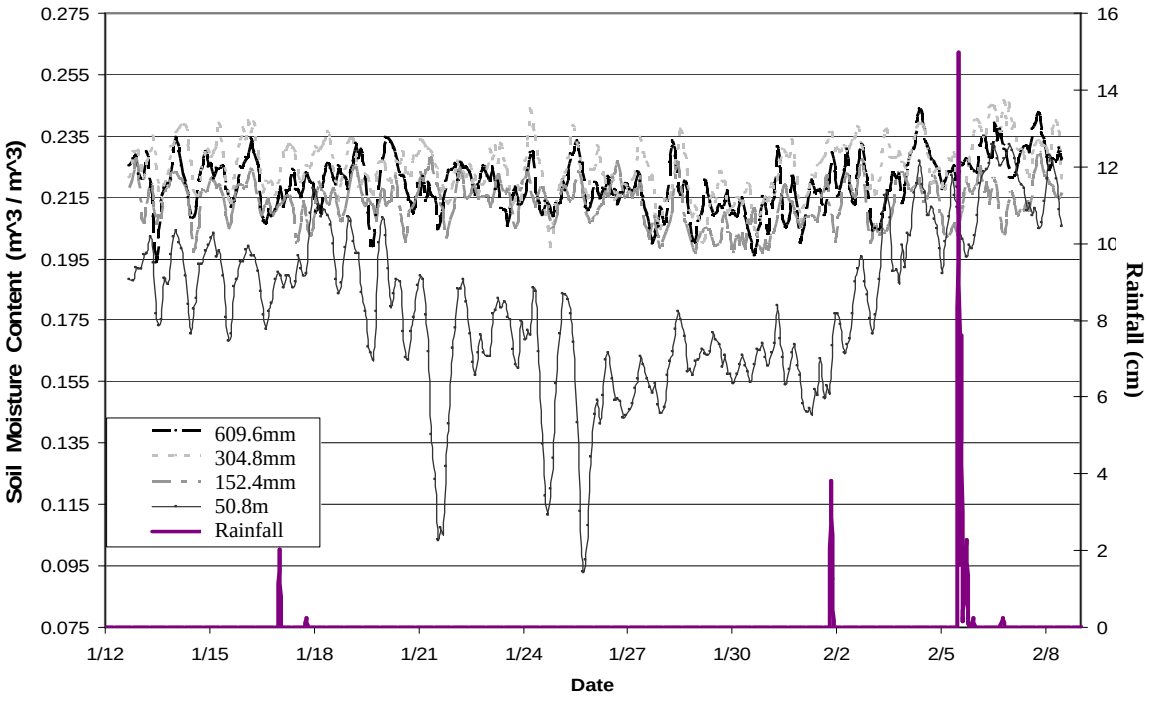

Figure 2-8 Soil moisture measurement results from one sensor node (Node 9) for January-February 2008

2.3.3 Discussion

1) SMC sensor. The EC-5 SMC sensor was well integrated into the development of the wireless sensor network. However, the quality of the excitation signal affected the performance which corresponds with the results from Bogena, et al, (2007). The addition of the supply voltage detection circuit could avoid the invalid SMC measurement.

The results of the sensor calibration show that a similar linear relationship between the SMC and sensor reading were found with that from the sensor manufacturer. However, the sensor performance could be sensitive to the temperature and soil conductivity. To achieve an accurate calibration curve, more detailed tests were needed before applying them to a field installation. Simple signal processing methods could also be recruited with a cautious consideration of energy consumption and resource requirement.

2) Data transmission. Throughout the development, the format of the communication data packet was modified with the consideration of not only including the data fields to be transferred, but also those for debugging the network communication. Due to complicated environment factors in the field, the data communications might be interrupted any time. To recover the network communication and the stored data, additional data fields were needed in the data packets. They could be used during the debugging of the network. During the test period of this study (November, 2007 – March, 2008), the crop height was well below the line of sight of sensor nodes. Further tests on network communication would be conducted when the crops were high enough to block the line-of-sight and affect the quality of communications.

3) Power supply. When developing a wireless sensor network, power supply unit was the one requiring relatively high cost. Hence, a cost-effective unit was needed. In this

study, the power consumption of the sensor nodes was carefully evaluated before they were deployed to the test field. The environment temperature changes and the charging time throughout a year were considered when selecting a solar charging battery system.

2.4 Conclusions

In this study, a WSN system for field soil moisture monitoring, including hardware and software, was developed. The hardware in the system included soil moisture sensors, their signal conditioning circuit, power supply units, and wireless sensor network modules. The system was installed in a crop field from November 2007 to September 2008. All the programs were written in NesC and running under TinyOS 1.1 environment.

The use of a commercially available soil moisture sensor, EC-5, took its advantages of low cost, low power consumption and ease of use. Calibrations were conducted before the sensors were deployed to the test field. Soil moisture sensor calibration using soil samples taken from the WSN deployment field resulted that, though soil samples from different strips close to each other in physical locations yielded similar relationships between soil moisture content and sensor output, the saturation levels for different soil samples were different. R^2 of the equations relating soil moisture content to sensor output though calibration were 0.958, 0.967, 0.962 and 0.977 for using soil obtained at three different in-field locations and using the averaged data, respectively. The results showed a good linear relationship between the sensor output and soil moisture level and a similar curve with the model provided by the manufacturer.

The soil moisture data at four depths and ten locations in the test field were collected. The data were compared to the rainfall reading from MESONET. In general, the reading

from the system would change accordingly to the rainfall recorded by MESONET and then reflect the trend of soil moisture variability.

Acknowledgements

The authors would like to acknowledge the support from the National Science Foundation CNS-0709329.

References

Akyildiz, I.F., Su, W., Sankarasubramaniam, Y., Cayirci, E., 2002. Wireless sensor networks: a survey. *Computer Networks.* 38: 393–422.

Andrade-Sanchez, P., Upadhyaya, S.K., Aguera-Vega, J. Jenkins, B.M., 2004. Evaluation of a Capacitance-based Soil Moisture Sensor for Real-time Applications. *Transactions of ASAE.* 47(4): 1281-1287.

Bogena H.R., Huisman J.A., Oberdorster C. and Vereecken H., 2007. Evaluation of a low-cost soil water content sensor for wireless network applications. *Journal of Hydrology.* 344(1-2): 32-42.

Boegena H., Schulz K., Verrechken H., 2006. Towards a network of Observatories in Terrestrial Environmental Research. *Advances in Geosciences.* 9:109-114.

Cardell-Oliver, R., Smettem, K., Kranz, M., Mayer, K. 2004. Field testing a wireless sensor network for reactive environmental monitoring [soil moisture measurement]. In *Proc.* of the Intelligent Sensors, Sensor Networks and Information Processing Conference.

Camilli A., Cugnasca C.E., Saraiva A.M., Hirakawa A.R., P. L. P., Correa. 2007. From wireless sensors to field mapping: Anatomy of an application for precision agriculture. *Computers and Electronics in Agriculture.* 58: 25-36.

Decagon Device. 2006. ECH2O Probe Operator's Manual, Version 5. Available at: http://www.decagon.com/pdfs/manuals/EC-20_EC-10_EC-5_v8.pdf. Accessed 14 June 2009.

Huisman, J.A., Sperl, C., Bouten, W. and J.M. Verstraten. 2001. Soil water content measurements at different scales: accuracy of time domain reflectometry and ground-penetrating radar. Journal of Hydrology. 245(1), 48-58.

Huisman, J.A., J.J.J.C. Snepvangers, W. Bouten, G.B.M. Heuvelink. 2002. Mapping spatial variation in surface soil water content: comparison of ground-penetrating radar and time domain reflectometry. *Journal of Hydrology.* 269(3), 194-207.

Jackson T., K. Mansfield, M. Saafi, T. Colman, P. Romine. 2007. Measuring soil temperature and moisture using wireless MEMS sensors. *Journal of Measurement.* 41(4):381-390.

Kelleners, T.J., R.W.O. Soppe, J.E. A yars , T.H. Skagg. 2004. Calibration of Capacitance Probe Sensors in a Saline Silty Clay Soil. *Soil Science Society of America Journal.* 68: 770-778.

Lambot, S., L. Weihermüller, J.A. Huisman, H. Vereecken, M. Vanclooster, E.C. Slob. 2006. Analysis of air-launched ground-penetrating radar techniques to measure the soil surface water content. Water Resource Research. 42: W11403. Available at: http://dx.doi.org/10.1029/2006WR005097. Accessed 12 June 2008.

Linear Technology. 2006. LTC3531/LTC3531-3.3/LTC3531-3 datasheet. Available at: http://cds.linear.com/docs/Datasheet/3531fb.pdf. Accessed 2 July 2009.

Liu, W., S.K. Upadahyaya, T. Kataoka, S. Shibusawa. 1996. Development of a texture/soil compaction sensor. In *Proc.* of the 3rd International Conference on Precision Agriculture, 617-630. Minneapolis, Minn, USA.

Norikazu, M. 1996. Soil moisture variability in relation to diurnal frost heaving on Japanese high mountain slopes. *Permafrost and Periglacial Process.* 7(2): 139-151.

Wang, N., N. Zhang, M. Wang. 2006. Wireless sensors in agriculture and food industry: recent developments and future perspective. *Computer and Electronics in Agriculture*. 50(1): 1–14.

Wark, T., P. Corke, P. Sikka, L. Klingbeil, Y. Guo, P. Crossman, P. Valencia, D. Swain, G. Bishop-Herley. 2007. Transforming Agriculture through Pervasive Wireless Sensor Networks. *Pervasive Computing.* 6(2): 50-57.

Whalley, W. R. 1991. Development and evaluation of a microwave soil moisture sensor for incorporation in a narrow cultivator tine. *Journal of Agricultural Engineering Research*. 50(1): 25−33.

CHAPTER III

IN-FIELD SOIL PROPERTY MONITORING USING HYBRID SENSOR NETWORK

Zhen Li[1,3], Ning Wang[1], Aaron Franzen[1], Peyman Taher[2]

1. Biosystems and Agricultural Engineering, Oklahoma State University, USA;

2. Computer Science, Oklahoma State University, USA;

3. College of Engineering, South China Agricultural University, China.

Abstract

A hybrid soil sensor network (HSSN) for in-situ, real-time soil property monitoring was developed and deployed to an experimental field. The HSSN included a local wireless sensor network (LWSN), formed by multiple sensor nodes installed at selected locations in the field to acquire readings from soil property sensors and transmit the data wirelessly to a data sink installed on the edge of the field; and a long-distance cellular communication network (LCCN). The field data were transmitted to a remote web server through General Packet Radio Service (GPRS) data transfer service provided by a commercial cellular provider. The data sink functioned as a gateway which received data from all sensor nodes; repacked the data, buffered the data according to cellular communication schedule, and transmitted the data packets to LCCN. A web server was

implemented on a PC to receive, store, process and display the real time field data. Data packets were transmitted based on an energy-aware self-organized routing algorithm. The completed HSSN has been in operation since it was deployed to the field in May 4th, 2009 and performed satisfactorily.

Keywords: Wireless Sensor Network; soil property; soil moisture;

3.1 Introduction

Soil property is the key influencing factor to crop growth and yield. The most commonly used parameters to define soil property include soil water-holding capacity, water content, bulk density, temperature, salinity, etc. Since soil is a complex medium, single parameter alone is not sufficient to describe the influences of the soil on crop growth and yield. Within these numerous parameters, soil moisture, apparent electrical conductivity, and near-surface temperature have been studied and used to describe and evaluate soil property.

Soil moisture content (SMC) is important in the water and energy interactions between land surface and atmosphere. Root-zone soil moisture is used to describe processes as basic vegetation transpiration and evaporation, surface runoff, and drainage. In-situ SMC measurement methods have been developed based on the large variations of dielectric constant between dry soil and water. The techniques include time domain reflectrometry tensiometers (TDR) (Huisman et al, 2001, 2002) and capacitive probes (Kelleners et al, 2004). *Apparent soil electrical conductivity (*EC_a*)* indicates the ability to conduct electrical current through soil profile. EC_a could be used to measure the solute concentration or salinity contained in soil pores. Since the EC_a is vulnerable to various factors that affecting plant growth such as clay content, temperature, organic compounds

and metals, it has been used as a quick, reliable, easy-to-take indicator of soil properties (Kitchen et al., 2003; Corwin and Lesch, 2005). EC_a can be measured from soil electrical resistivity (ER) (Lund et al, 1999) and soil electromagnetic conduction (EM) (Corwin and Lesch, 2005). TDR has also been used in measuring EC_a since the attenuation of the magnetic pulse amplitude is proportioned to the electrical conductivity (Dalton et al, 1984). Near-surface soil temperature reflects the integrated energy relationships from root-zone to plant canopy. It has confounded interactive effects on many soil and plant activities like nitrogen mineralization rate, soil water evaporation, under-ground CO_2 respiration, and solute saturation (Cassman and Munns, 1980; Davidson et al, 1998). Remote sensing of land surface emissivity by thermal infrared (TIR) using the Advanced Very High Resolution Radiometer (AVHRR) or Moderate Resolution Imaging Spectroradiometer (MODIS) can profile surface temperature in large areas (Wan and Li, 1997), while thermo-couples and thermistors can take ground truth readings with a fine resolution of 0.1 to 3m.

Decagon Devices Co. (Pullman, WA, USA) manufactures a series of low-power, soil-type-independent sensors which measure the soil properties based on capacitance/frequency domain technology (Campbell, 2002). The ECH2O-5 (EC-5) sensor is a capacitance-based, low-power soil moisture sensor and the ECH2O-TE (EC-TE) sensor is capable of measuring soil water content, electrical conductivity, and temperature at the same time.

Real-time and continuous monitoring of SMC, EC_a and near-surface soil temperature in remote and large areas, especially under harsh conditions, are advantageous for scientific activities in ecology, meteorology, agronomy and variable rate operations for

precision agriculture. However, in-field soil property information by far is largely acquired by periodic human survey through handheld, field-installed, or machine-mounted data loggers. Such monitoring methodologies depend greatly on the capability of machine and human labor involvements, thus, their temporal and spatial resolution are limited.

As a recent technology achievement, wireless sensor network (WSN) technology is a promising solution for large-scale, real-time, continuous environmental data acquisition (Beckwith et al, 2004; Liu et al, 2007). A WSN is composed of multiple low-cost, low-power, and multi-functional wireless sensor nodes distributed in a monitored field. The sensor nodes can form a communication network with various topologies through radio frequency (RF) communications. Each node has limited on-board signal processing ability and is equipped with sensors and signal conditioning circuits. Once networked, the sensor nodes can collaboratively measure the variations of field parameters, process and store data, transmit or receive data/command packets among local sensor nodes or between the sensor nodes and an in-field gateway, and carry out actuations autonomously based on pre-programmed situations or passively by received commands.

Recent exploring efforts have revealed great adaptability of using WSN for in-field data collection and control of the local environment. Monitored parameters ranged from temperature, humidity, rain fall, wind speed, and solar radiation within micro-climate to in-field soil properties like moisture, electrical conductivity, and near surface temperature as well as water quality such as sediment runoff and pollution concentration (Bellis et al, 2005; Fukatsu, et al, 2006; Panchard et al, 2006; Han et al, 2008; Pierce, et al, 2008). The WSN systems can be developed upon different hardware platforms consist of: (1)

Commercial available motes and data acquisition (DAQ) boards attached for sensor interfacing (Tolle, et al, 2005, Hefeeda and Bagheri, 2007), (2) data loggers with radio communication abilities or without this ability but connected to radio modules (Cortez and Sánchez, 2007), or (3) customized circuit boards with radio modules and necessary sensor interfacing integrated circuits (Valente et al, 2006; Stewart et al, 2007).

The goal of WSN communications is to achieve successful transmission and reception of data packets. Terms as message delay, error rates, packet loss rate, costs of transmission (power) are used to evaluate the Quality of Service (QoS) of a WSN system. To improve QoS, various network topologies and standards are employed. Most commonly, topologies utilized in agricultural applications include star, tree, mesh, web as well as their hybrids (Fukatsu, et al, 2006; Dinh, et al, 2007; Li, et al, 2008). Standardized protocols utilized include the ZigBee (IEEE 802.15.4) Low-rate Wireless Personal Area Network (LRWPAN), WiFi (IEEE 802.11b), and Bluetooth (IEEE 802.15.1).

The short range WSN is often not sufficient to meet the needs for a complete soil property monitoring system. In order to provide users an easy way to access field data, a long range data transmission network are commonly formed by long-range radio modems, e.g. the FreeWave (dataTaker, Chesterland, OH, USA), which supports a communication distance up to 15km (Wernet et al, 2005). To achieve data communications with a longer distance, GPRS, short message service (SMS), and Internet (IP) provided by cellular service providers are often used. The data transmitted are then stored in a database established on a web server in a remote personal computer for being accessed and queried by users through Internet. Further data analysis can also be implemented (Demibras et al, 2006; Han et al, 2008).

In this research, a two-tier hybrid wireless sensor network was developed to acquire field soil property data. The ultimate goal was to provide researchers and users real-time soil property data and allow the data to be accessed online from a dedicated website. The specific objectives of the research included:

1) To design and develop a distributed data acquisition system based on hybrid wireless soil sensor network (HWSSN) for unattended field-specific soil property monitoring;
2) To deploy the hybrid wireless sensor network into a crop field; and
3) To test the quality of service (QoS) of the developed HWSSN system under laboratory and field conditions, respectively.

3.2 Materials and Methods

Figure 3-1 depicts the architecture of the HWSSN developed in this research. The HWSSN includes two tiers as: (1) an in-field local wireless sensor network (LWSN), and (2) a long range cellular communication network (LRCN). In LWSN, a star-topology, single-hop networking cluster was formed including a central node and ten sensor nodes working together for collecting and transmitting soil parameter data. The physical locations of all the nodes were predefined before deployment and stayed stable unless a network reconfiguration was needed. At each location, a sensor node acquired soil property parameters including near-surface temperature, electrical conductivity, and soil moisture content at four underground depths of 50.8, 152.4, 304.8 and 609.6 mm every hour and wirelessly transmitted the data to the central node for temporary storage. The data stored in the central node would be uploaded to a gateway on request through

wireless communication and then propagate through the LRCN until it arrived at the web server.

The LRCN was formed by a gateway (Stargate, Crossbow Technology Inc., San Jose, CA, USA), a cellular modem, and a web server. The gateway was in sleeping mode most of the time. It waked up every hour and sent data upload requests to the central node. After receiving the request from the gateway, the central node transmitted the data stored in its buffer to the gateway. The gateway also initiated the cellular modem which would establish a communication with the web server though GPRS provided by a commercial cellular provider. All the data were then stored in a SQL database on the web server and could be accessed by users. The field property data were accessible and editable to authorized users by logging into the web server data base any time any where through Internet while the graphical data display and simple statistics were available to the public through Internet.

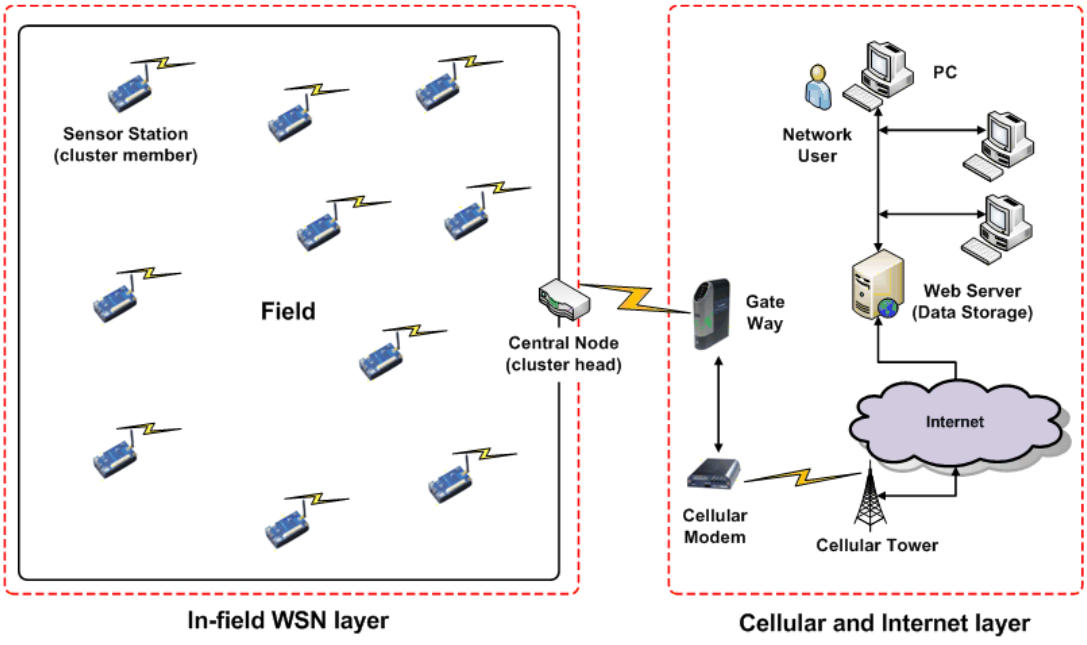

Figure 3-1 The architecture of the hybrid wireless soil sensor network

3.2.1 Hardware Design

Local wireless sensor network

The major tasks of LWSN included field data collection, temporary storage, and uploading to the central node. The current system replaced the previous in-field soil moisture monitoring system (Li et al, 2008) and was installed in an experimental field of Oklahoma State University in Stillwater, Oklahoma. Ten sensor nodes were deployed in between field strips. Five solar power stations were used. Each power station provided power to two sensor nodes. The central node was mounted on a pole and located at the center of the testing field.

1) Sensor Node. Figure 3-2 depicts the major components within a sensor node. IRIS motes (IRIS, Crossbow Technology Inc., San Jose, CA, USA) were used as the wireless control and communication unit. Each IRIS mote utilized a transceiver IC (AT86RF230, Atmel, San Jose, CA, USA) as the IEEE 802.15.4 compliant transceiver and its data transmit rate could reach 250kbps. The radio frequency ranged from 2405MHz to 2480MHz within the ISM (industrial, scientific and medical) band and could be divided to 16 programmable channels in 5MHz steps with 34dB or 36dB adjacent channel rejection. In this research, a TinyOS default RF frequency, channel 11 at 2405MHz was used. The system by far was the only user of 802.15.4 radio channels in the field and the risk of overlapping was minimized. The highest transmit power was +3.2*dBm*, and the receiver sensitivity was -101*dBm*. The modulation technique was DSSS/QPSK (direct-sequence spread-spectrum and quadratic phase shift keying). A ¼ wave dipole antenna with 0dBi gain was used.

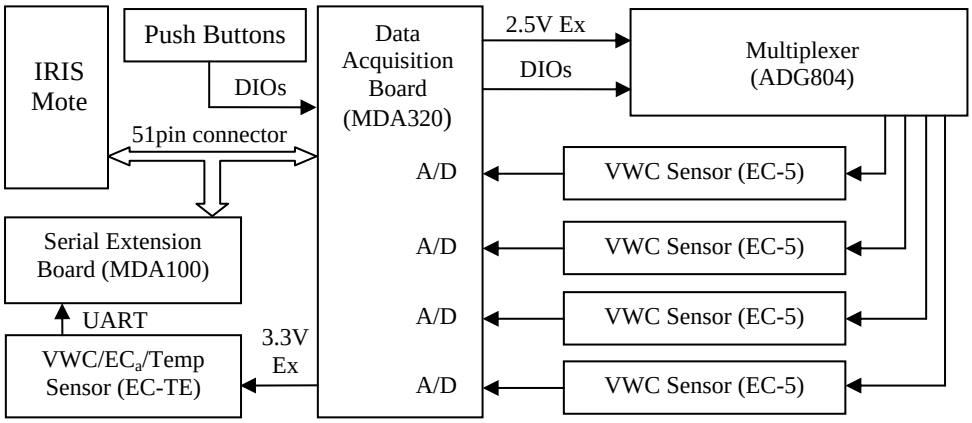

Figure 3-2 The block diagram of major components in a sensor node

Capacitance based soil moisture sensors, namely EC-5 (ECH2O probe, Model EC-5, Decagon Devices, Pullman, MA, USA) were applied for taking underground volumetric water content (VWC) . The total volume of influence (maximum possible measurement volume) of the EC-5 was approximately 181cm^3 (Figure 3-3a). EC-5 was calibrated based on local soil texture in the previous study (Li et al, 2008).

EC-TE sensors (Model ECH2O-TE, Decagon Devices, Pullman, MA, USA) were used to measure volumetric water content, temperature, and bulk electrical conductivity of soil and growing media (Figure 3-3b). The EC-TE sensor incorporated the same 70MHz oscillation circuit as EC-5 to determine the VWC. A thermistor in thermal contact with the probe prongs provides an average prong temperature, while the gold traces on the surface of the sensor form a four-probe electrical array (Wenner array) to measure electrical conductivity (Decagon Device, 2006). Once activated, the EC-TE sensor output a packet including three numerical data related to VWC, bulk electrical conductivity (EC), and temperature. The data packet was transmitted in an ASCII format with a dynamic length using 1200 baud serial communication to the IRIS mote. In the

data packet, the first numerical data was related to VWC readings which fell to a range from approximately 400 to 1300.

The raw electrical conductivity reading (σ_{raw}) from EC-TE was valid in the range from 0 to 1022 (Decagon Device, 2008). σ_{raw} could be converted to bulk electrical conductivities in dS/m using Equation 3.1. The EC reading was temperature corrected within the EC-TE probe.

$$EC = \begin{cases} \dfrac{\sigma_{raw}}{100} & \sigma_{raw} \le 700 \\ \dfrac{700 + 5(\sigma_{raw} - 700)}{100} & \sigma_{raw} > 700 \end{cases} \qquad (3.1)$$

Where EC was the bulk electrical conductivity in dS/m and σ_{raw} was the raw electrical conductivity reading received from an EC-TE probe.

The third data was corrected temperature reading T_1 in Celsius. The correction function is shown in Equation 3.2:

$$T_1 = 10 \times T + 400 \qquad (3.2)$$

Where T_1 is the transmitted temperature reading and T is the real temperature reading in $°C$ with one decimal place.

A multi-functional data acquisition board (MDA320, Crossbow Technology Inc., San Jose, CA, USA) was connected to the IRIS mote through a 51-pin extension connector (Figure 3-2). Four single-ended 0-2.5V analog input channels were used to read data from four EC-5 sensors. Three digital I/Os was used for enabling and selecting channels on the multiplexer while another two for responding to push buttons. MDA320 also provided 2.5V and 3.3V excitations to activate EC-5 and EC-TE sensors, respectively. All the on-going communication between IRIS and MDA320 went through I^2C interface.

Another DAQ board (MDA100, Crossbow Technology Inc., San Jose, CA, USA) was connected with the IRIS mote through the same 51-Pin connector to provide an UART interface to acquire data from the EC-TE sensor.

Together with the 2.5V excitation channel on MDA320, a multiplexer, ADG804 (Analog Device, Inc., Norwood, MA, USA) was used to power up the EC-5 sensors. The input of the multiplexer was connected to the MDA320's 2.5V excitation output. The output channels of the multiplexer were selected sequentially to excite one EC-5 sensor a time. The EC-TE was directly powered by the 3.3V excitation of MDA320.

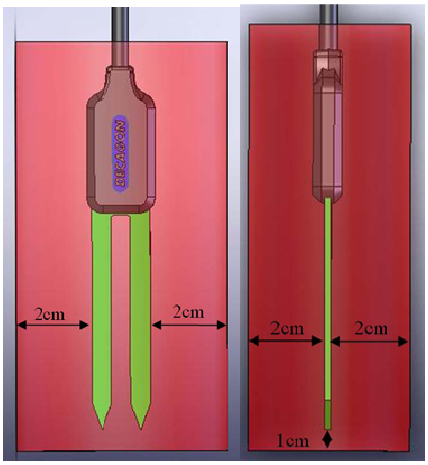

(a) EC-5 volume of influence

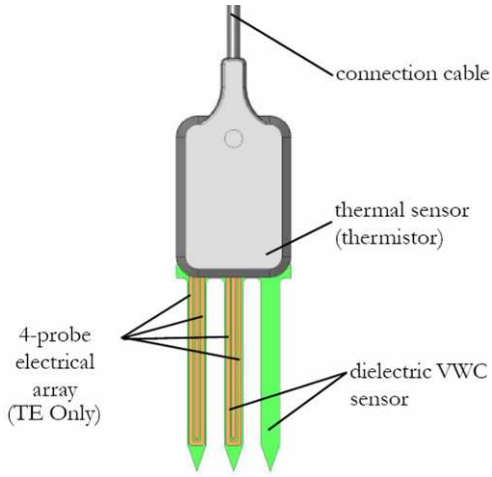

(b) Components on an EC-TE sensor

Figure 3-3 EC-5 sensor's volume of influence (a, Sakaki et al, 2008) and EC-TE configuration (b, Decagon Device, 2006)

Each sensor node was packaged in a weather-proof plastic container. Two sensor nodes were mounted 1.5 meter above ground on a steel pole installed at the edges of field strips. All antennas on sensor nodes were adjusted to face the central node and maintained for line-of-sight communications (Figure 3-4).

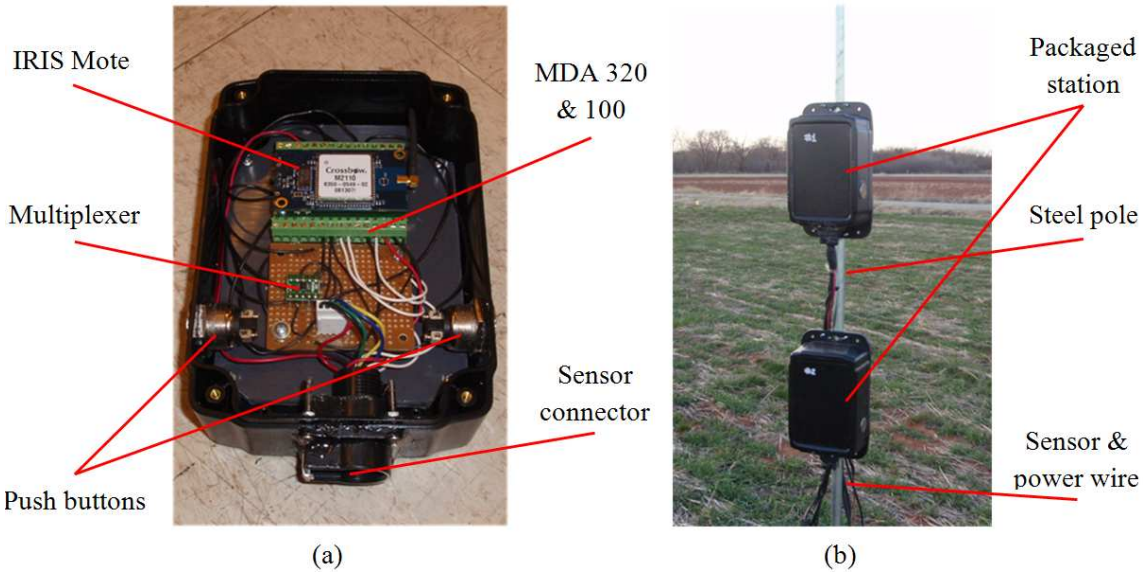

Figure 3-4 The package of sensor nodes (a) and installation (b)

Each sensor node was connected to four soil property sensors implanted at four different depths as 50.8, 152.4, 304.8 and 609.6mm underground (Figure 3-5). The lower three were all EC-5 sensors while the top one could be either EC-5 or EC-TE. Currently, five of the sensor nodes were using EC-5 while the other five were using EC-TE.

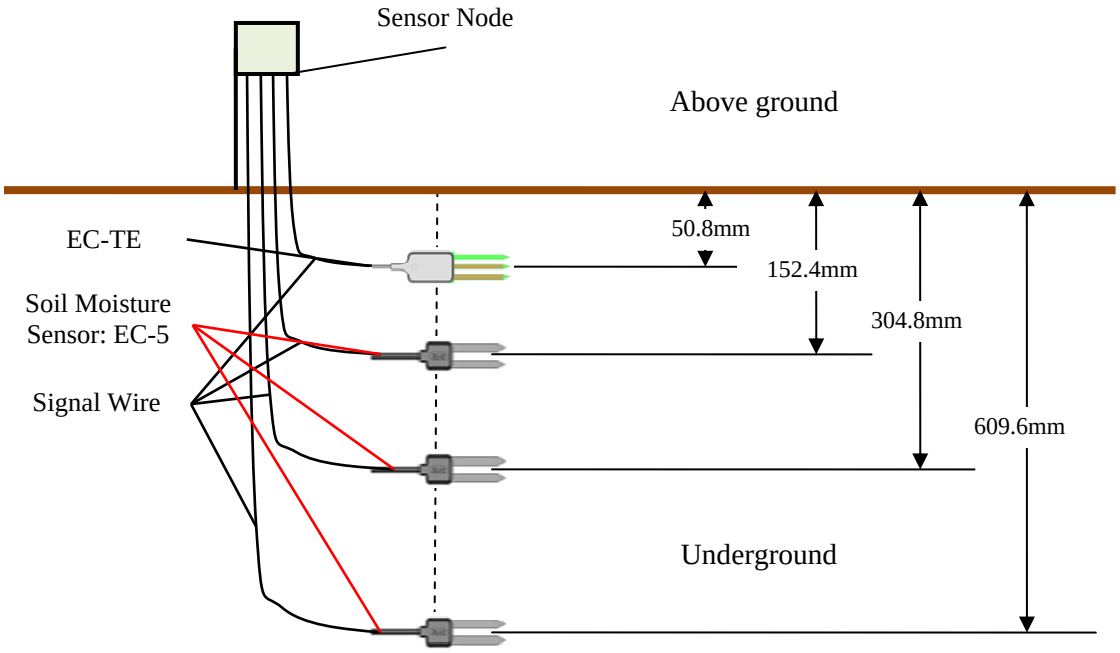

Figure 3-5 Sensor installation

Two pushbuttons were connected to two digital I/Os on the MDA320. One of the buttons, if pressed, would activate an immediate soil property sampling and data transmission. The other one would initiate a uploading of the restored data from a sensor node's local memory to a base node.

2) Central Node. The central node was formed by an IRIS mote with a 512kB flash for data storage. It was responsible for collecting and storing measurement data received from each sensor node and uploading the stored data to the gateway on request. The current address assignment was sufficient for restoring up to 210 day's data plus a ten-packet space for buffering incoming packets during data upload. Once a datum was uploaded, its space in the flash was cleared and refilled by a new datum.

3) Power Station. For each sensor node, power was primarily consumed by sensors, microprocessor on the IRIS mote and radio. The current power consumption and duration were calculated based on a one hour measurement loop. The current draws of major components were obtained from the datasheet of each component as shown in Table 3-1. The duration was controlled by program running inside the IRIS mote. In general, the power consumption was 26.4mW for one sensor node.

Table 3-1 Power consumption of each component within a sensor node

Part Name	Mote	EC-5	EC-TE	Radio
Current	8mA	10mA each	10mA	17mA
Duration	always	45 or 60ms	70 or 0ms	10ms

*the duration was based on a one hour measurement loop

Power stations were located on the edges of the field. Since there was no wired power available in the field, solar energy was considered the best solution for powering in-field

parts of the system. Each of the stations was composed of a 15W solar panel, a 12Ah rechargeable battery, and a 1A regulator (Figure 3-6).

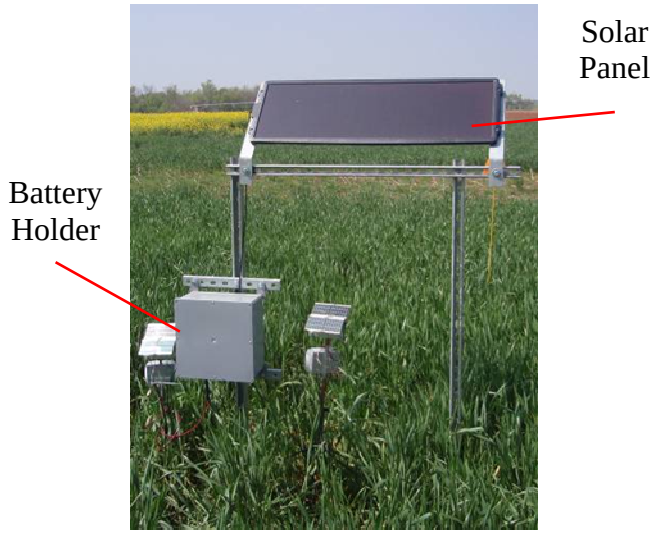

Figure 3-6 The power station

Long range communication networks

The LRCN consisted of a gateway, a cellular modem, and a remote web-server. The gateway was composed of a Stargate mother board (SPB400CB, Crossbow Technology Inc., San Jose, CA, USA), a Stargate communication extension daughter board (SDC400CA, Crossbow Technology Inc., San Jose, CA, USA), an IRIS mote serving as the base node, and a CF card. The gateway were packed together with a power supervisory controller, the central node, and a cellular modem (Model: MTCBA-G-G4, MultiTech, USA) in a weather proof box (Figure 3-7). For energy conservation purposes, the power supply to both the mother board and the cellular modem was turned off most of the day and on for a short period of time controlled by the power controller. Once powered up, the gateway sent three requests in series to the base node through a serial communication. The base node re-packaged the request using the TinyOS standard and forwarded the new request to the central node wirelessly. Upon receiving the request, the

central node started to upload buffered data to the gateway. Acknowledgement was sent by the gateway to the central node after a successful receipt of a data packet. Received packets then relayed to the cellular modem and transmitted to the web server through cellular communication network and the Internet. The data packets were also logged to the CF card on the Stargate for backup. Once data uploading was finished, the gateway informed the power controller to turn off power to the cellular modem and the mother board.

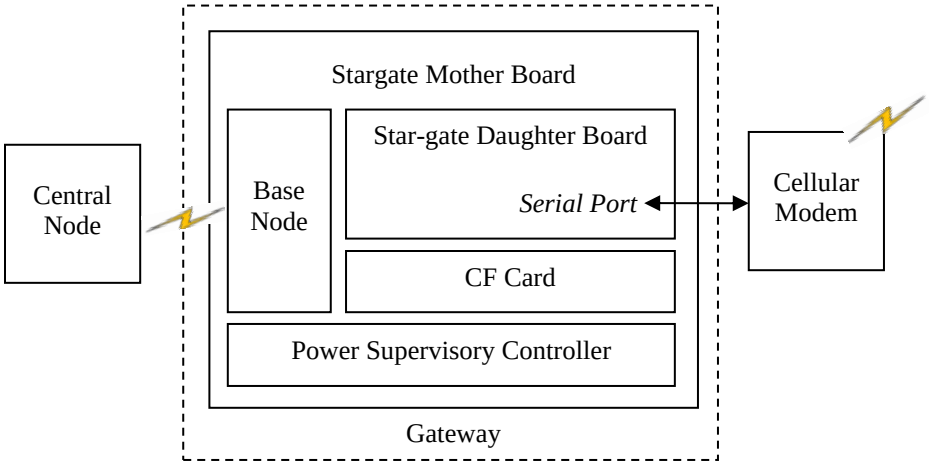

Figure 3-7 The major components of the LCRN

3.2.2 System Program Architecture

All the programs for wireless sensor network communications were implemented under the TinyOS 1.1 environment. In TinyOS development environments, components on IRIS motes and data acquisition extension boards were abstracted as “components” while well-defined “interfaces” were used to connect and define data flow between the “components”. A TinyOS application was implemented as a set of the component modules written in a C extension language, named NesC. The IRIS mote and two DAQs used in this research were fully supported by TinyOS.

Local wireless sensor networks

1) Sensor node program. The sensor node program was embedded in the IRIS mote and controlled the component activities of the IRIS mote, two DAQs, multiplexer, and radio transceiver. These activities included sampling soil property data every hour, storing data and transmitting the data wirelessly to the central node. The sensor node could respond to the requests either from the push buttons on the packaging box or some pre-defined commands received wirelessly from the central node or mobile base for immediate data upload. The sensor node program allowed autonomously type detection of the top sensor (EC-5 or EC-TE). If there was no EC-TE detected, it skipped the EC-TE measurement process and directly enters EC-5 measurement procedures. For power conserving purpose, the radio on the mote was disabled most of the time and enabled for a short period for data upload and command detection. Architecture of the sensor node program using TinyOS components is depicted in Figure 3-8.

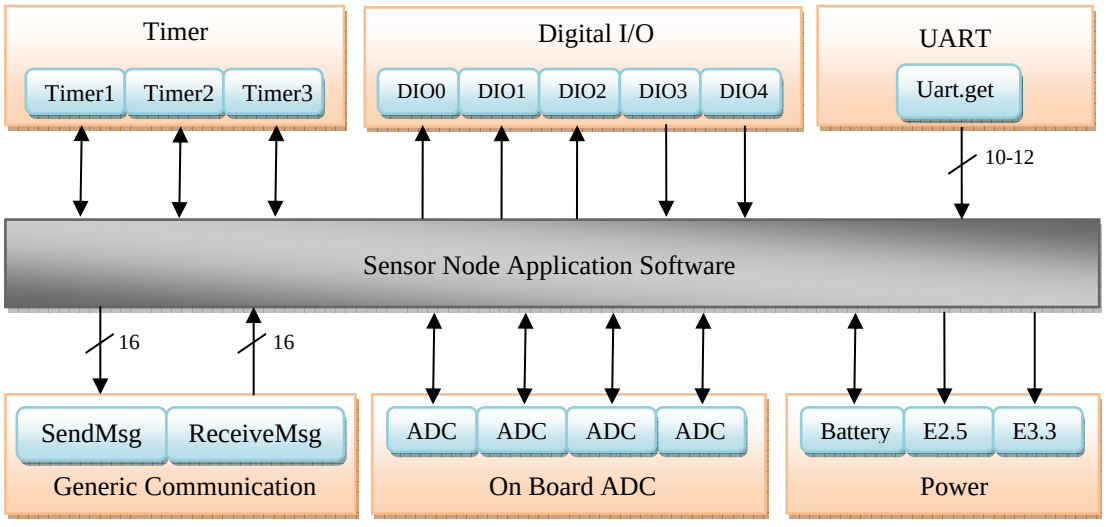

Figure 3-8 The program structure for the sensor nodes. The brown blocks were components while the blue blocks were interfaces provided within each component

The system running on a sensor node was coordinated by three timers as Timer1, Timer2 and Timer3. Timer1 was the main system timer running continuously and generating the “Timer1.fired” events repeatedly every one hour. Once the “Timer1.fired” event was passed to the system core, Timer2 as well as the 3.3V excitation were activated for a regular soil property measurement. Steps as multiplexer channel selection, excitation generation, data acquisition and wireless transmission were embedded into different slots of Timer2. Timer3 was independent from the regular measurement process but would be activated by the two push buttons. If the push button for taking one immediate measurement was pressed, Timer3 would be activated to run once lasting 50ms. When the “Timer3.fired” event was received by the system core along with the push button indicator telling which button was pressed in this situation, a measurement would be initiated exactly the same as the regular one. If the push button for uploading the restored 24 hour measurement data was pressed, Timer3 would be activated for nesting the steps as data reading, packaging, and sending within its slots. Figure 3-9 depicts steps and timing within each regular measurement procedure nested in Timer2 after the “Timer1.fired” event was received by the system core.

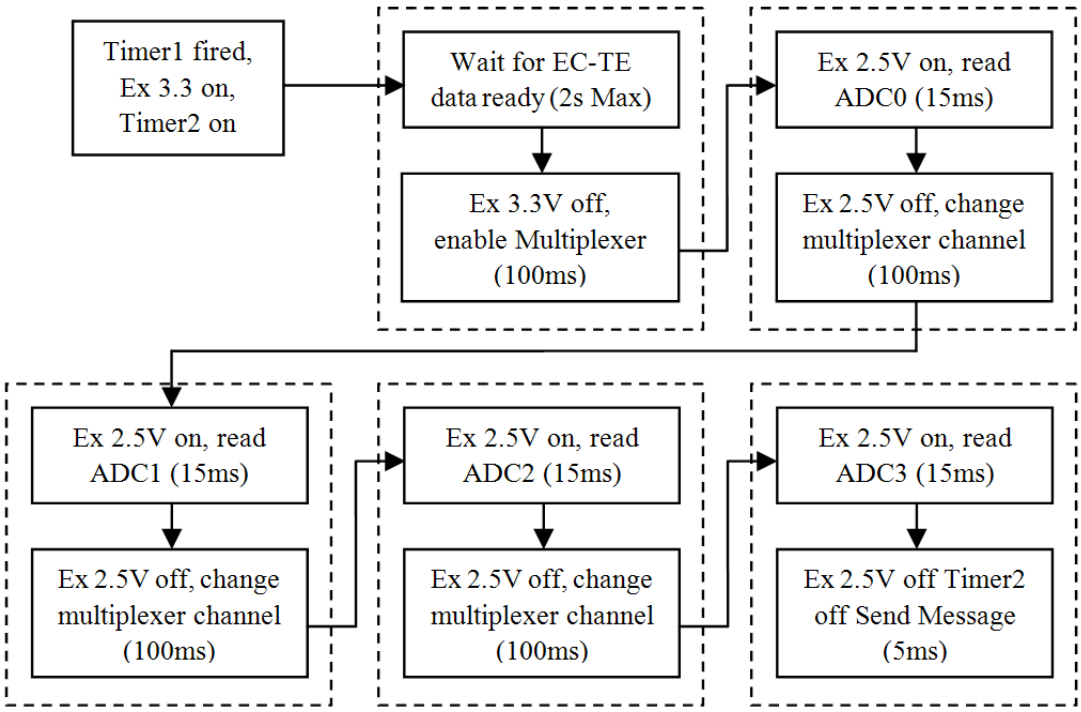

Figure 3-9 Steps and timing within a regular measurement procedure nested in Timer2

2) In-field wireless communication protocol. The in-field star-topology wireless communications included: sensor nodes to the central node, a sensor or the central node to the base node, and the base node to a sensor or the central node. The base node could be either a stable base node connected to the gateway or a mobile base node for on-the-go data acquisition connected to a laptop PC. Messages for in-field wireless communication between different nodes were constructed based on the TinyOS standardized protocol data unit (PDU, Figure 3-10). User data structures were designed to be uniform for different types of communication.

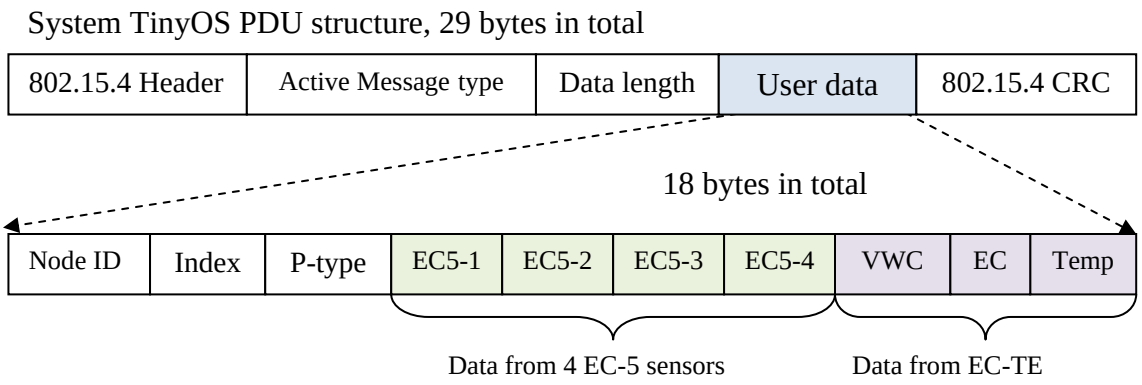

Figure 3-10 The format of the TinyOS protocol data unit (PDU)

The total length of the user data segment was 18 bytes. Names, size, and descriptions of each field within the user data segment of a PDU are explained in Table 3-2.

Table 3-2 Explanation of the data fields within a protocol data unit (PDU) for a soil property measurement

Names	Size	Descriptions
Node ID	1 byte	Indicating packet origination or packet destination depends on "P-type"
Index	2 bytes	Sequential packet identifier
P-type	1 byte	Packet type, current values include: 0x00: central or sensor node to base data upload, Node ID indicates origination; 0x01: sensor node to central node data upload, Node ID indicates origination; 0x02: base to central or sensor node command, Node ID indicates destination.
EC5-1	2 bytes	Soil moisture reading of EC-5 from 60.96cm underground
EC5-2	2 bytes	Soil moisture reading of EC-5 from 30.48cm underground
EC5-3	2 bytes	Soil moisture reading of EC-5 from 15.24cm underground
EC5-4	2 bytes	Soil moisture reading of EC-5 from 05.08cm underground
VWC	2 bytes	Dielectric content reading of EC-TE*
EC	2 bytes	Electrical conductivity reading of EC-TE*
Temp	2 bytes	Temperature reading of EC-TE*

*Readings from EC-TE were reformatted from ASCII to regular hex values before data upload

Long range communication network

1) States of Central Node. A central node worked at three states named: Normal, Uploading, and Renewing. In "Normal" state, the central node stored measurement data from sensor nodes to its on-board flash and waited for a data uploading request from the

gateway. “Uploading” was the state in which data-upload was executed. “Renewing” was the state in which data packets were transferred from temporary buffer to the regular storage. The maximum time for a central node to remain in Renewing state was about 110ms. An assumption was made that there was no incoming communication during that period of time within a measurement interval of one hour. Relationships between different states and situations for transportation are depicted in Figure 3-11a.

2) Data Upload Protocol between the Central Node and the Gateway. As shown in Figure 3-11b, after the gateway waked up from a power loop, it sent data-upload requests wirelessly to the central node. If there were measurement data stored within its flash, the central node would enter Uploading mode and start uploading data. To guarantee no packet loss during data upload, an acknowledgement (ACK) packet would be replied from the gateway after receiving each packet. Once the central node finished sending a packet, a 10-second time-out routine was activated. If an ACK could not be received before the time-out, the central node would exit the Uploading mode and maintain the last uploaded packet. Otherwise, the central node cleared the last packet and started uploading a new one.

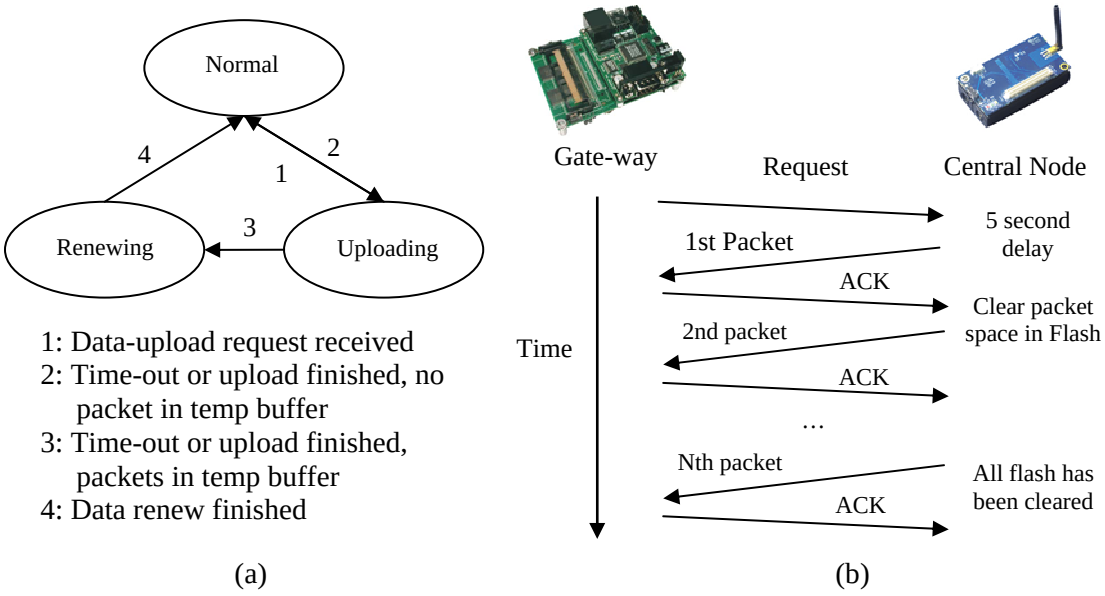

Figure 3-11 The communication protocol between the gateway and the central node: (a) the three states of the central node, and (b) the communication protocol

3) Software Design for the Gateway. A gateway software named Mote-Gate program was developed to forward field data to the remote server machine. The Mote-Gate program consisted of three modules (Figure 3-12):

1) Communication Handler module
2) Receiver module
3) Reporter module

The *Communication Handler* module was a collection of functions to implement socket level communication between the Mote-Gate program and the central node, and also between the Mote-Gate program and the *Mote-Server* program. In other words, it was an abstraction layer between the Mote-Gate program and the outside world.

The *Receiver* module was in charge of communicating with the central node. At the startup time of the Mote-Gate program, this module sent a data-upload request to the

central node, and once a packet is received it would reply with an ACK to the central node to confirm successful arrival of the packet.

The *Reporter* module on the other hand was in charge of communicating with the Mote-Server program. Every time that a packet was successfully received by the Receiver module, it would be reported to the Mote-Server program through this module.

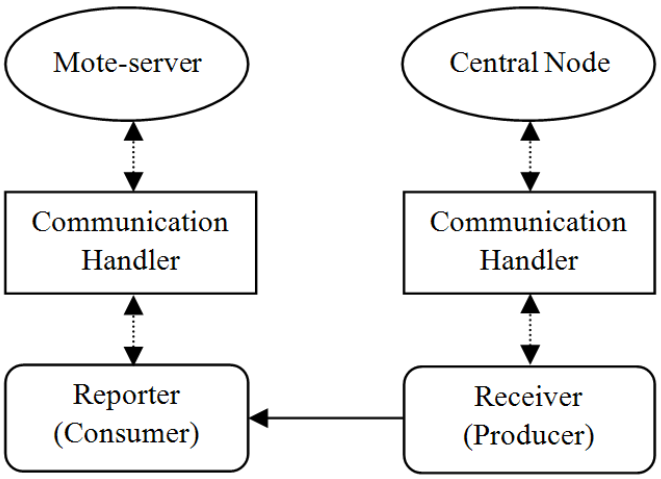

Figure 3-12 The modules within mote-gate program

4) GPRS Service (completed by Aaron Franzen). A GPRS of 5MB per month was purchased for data transmission. The current regular monitoring needed only 220kB monthly. The service had great extension capability for handling more monitoring locations with higher sampling frequencies.

5) Mote-server Program Design (completed by Peyman Taher). The *Mote-Server* program was installed on the server machine and was mainly used to store the data received from Mote-Gate program into a *MySQL* database. Program structure is displayed in Figure 3-13. Basically it is a daemon which listened on a specific port for incoming connections from the Mote-Gate program. Once a connection was established, after a successful handshake between the two ends, the Mote-Server program started receiving

packets. Each successfully received packet went through a validation phase so that faulty packets were properly logged and then all packets were stored in the database. Besides, an *alarm* mechanism was implemented in the Mote-Server program which was responsible for sending a digest email to the system administrator every night at exactly 12:00am to report the number of received packets from each sensor. The Mote-Server program consisted of the following modules:

The *Communication Handling module* was very similar to the communication handler module in the Mote-Gate program. The only difference was that the Mote-Gate program was actually implemented in the C programming language, while the Mote-Server program was implemented in the Java programming language. So generally, this module was responsible for handling the communication between the Mote-Server program and the Mote-Gate program using TCP Sockets.

The *Persistence Layer* was a layer between the Mote-Server program and the MySQL database. It was an Object-Relational Mapping (ORM) implementation which provided a mapping between Plain Old Java Objects (POJO) and records in a relational database system. Hibernate 3 was used which was an open-source ORM library for Java.

The *Data Access Object (DAO) Layer* was the actual mapping between the Java Beans used in the Mote-Server program and their respective tables in the database. The DAO layer also implemented the generic methods used for Create, Read, Update and Delete (CRUD) functions in the database, as well as methods that were internal to individual classes.

The *Alarming module* was a stand-alone thread by itself that sleeps for 24 hours and then wakes up at exactly 12:00am. Once it was running, first it collected certain statistics

from the database and then generated a digest of the packets received during the past 24 hours and finally sent this digest message to the system administrator and went to sleep until the next midnight.

The *Packet Validating module* was used to validate packets that were received from the gateway program based on certain criteria such as the packet delimiters and number of bytes in each packet. Once a packet was found faulty, it would be logged into the database for further analysis.

The *Raw Data Interpreting module* was used to parse the raw data load in each packet and generated human readable values which would be stored in the database.

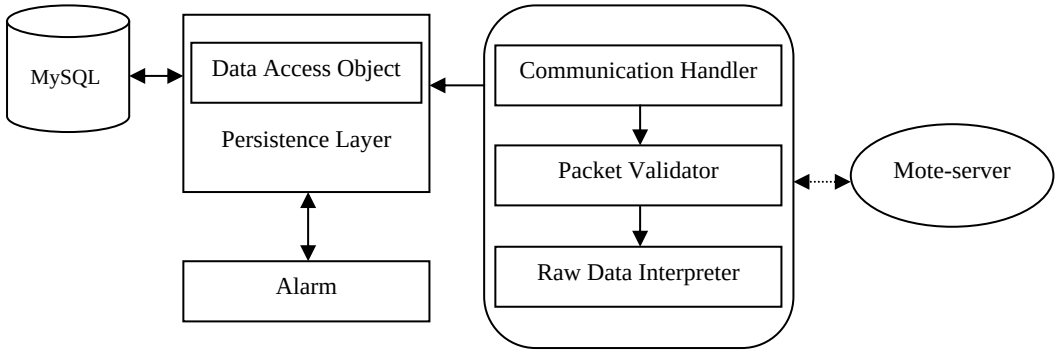

Figure 3-13 The modules within the mote-server program

3.2.3 System Performance Tests

Soil property monitoring

The soil property data was obtained from all the sensor nodes after system deployment in May 4th, 2009. Concurrently, rain fall and air temperature data were accessed from the Oklahoma MESONET's Lake Carl Blackwell station which was 262*m* away from the test field to verify the correctness of the data received from the HWSSN.

Volumetric water content (VWC) of EC-5 was calculated based the calibration equation from previous study (Li, et al., 2008) as Equation 3.3:

$$\theta = 125 \times V_{out} - 33.70 \qquad (3.3)$$

Where θ was the volumetric water content in % and V_{out} was the received EC-5 sensor reading after A/D conversion in volt.

VWC of the EC-TE was calculated as using the equation provided by the manufacturer (Decagon Device, 2006) as Equation 3.4:

$$\theta = 0.1087 \times Raw - 62.9 \quad (3.4)$$

Where θ was the volumetric water content in % and *Raw* was the received sensor reading from the EC-TE.

Electrical conductivity readings from the EC-TE sensor were used directly and near surface temperature was retrieved using Equation 3.5:

$$T = \frac{T_1 - 400}{10} \qquad (3.5)$$

Where T was the real temperature in $°C$ with one decimal space and T_1 is the reading from EC-TE.

Data transmission performance tests

Two wireless communications were included during data transmission in current system including those among local wireless sensors and the long range cellular communication. In-field vegetation led to physical signal attenuation while packet competition introduced logical failures. System stability depended greatly upon successful data transmission. The indexed packets from each sensor node arrived at the web-server, their final destination, during a certain period (between May 4th and May 14th, 2009) was counted. Total packets sent from each node during that period were obtained from the subtraction of the last and first received packet index inside database. A packet delivery rate ($N_{R,pdr}$) was defined as Equation 3.6:

$$N_{R,pdr} = \frac{Nr}{Nt} \times 100\% \qquad (3.6)$$

Where *Nt* was the packet transmitted in a certain period of time by one sensor node and *Nr* was the packet arrived at data base during the same period from the same node.

System reliability

Even though a packet could propagate through different network layers and arrive at the database, it was detected that fields of the PDU might contain invalid values due to protocol failure of TinyOS 1.1 in serial communication. Each invalid data were marked "NULL" within the database and excluded from graphical monitoring result generating. A valid data rate ($N_{R,val}$) was defined as Equation 3.7:

$$N_{R,val} = \frac{Nv}{Nr} \times 100\% \qquad (3.7)$$

Where *Nr* was the number of packets arrived during a certain period of time (between May 4th and May 14th, 2009) of one sensor station and *Nv* was the number of valid data of each sensor within one sensor node during the same time. The same sample space for the transmission performance verification was utilized.

In-field data error rate

The in-field data error rate was defined to determine whether or not and how much if any differences between data coming in and out of the central node. An extra pseudo sensor station (Node 21) with only an IRIS and a MDA320 was programmed to send PDUs in a shortened time interval as 10 seconds. A mobile base node connected to a laptop was applied to supervise communication in and out of the central node. Test duration was limited in between two central node data uploads since the extra buffer for

central node to use in Uploading mode was only 10 packets. Data error rate ($N_{R,err}$) was calculated using Equation 3.8:

$$N_{R,err} = \frac{Ne}{Nt} \times 100\% \qquad (3.8)$$

Where *Nt* was the total number of PDU transmitted by the pseudo station and *Ne* was the number of PDUs which had field difference.

3.3 Results and Discussion

3.3.1 Soil Property Monitoring Results

Examples of monitored data from Node 9 from May 4th, 2009 to June 10th, 2009 are as displayed in Figure 3-14 and Figure 3-15. Figure 3-14 reflected the soil moisture changes and Figure 3-15 reflected the soil electrical conductivity and near-surface temperature changes. Two types of sensor were connected to sensor node 9 including three EC-5 sensors buried at the depths of 609.6, 304.8, and 152.4mm underground and one EC-TE sensor at 50.8mm underground.

There was continuous rain fall from April 26, 2009 to the day of system deployment on May 4, 2009. Maximum recorded rain fall were on April 26 and April 29, both of the readings were over 25mm, resulting the soil moisture in different depths received high readings, especially for the one located closest to the surface.

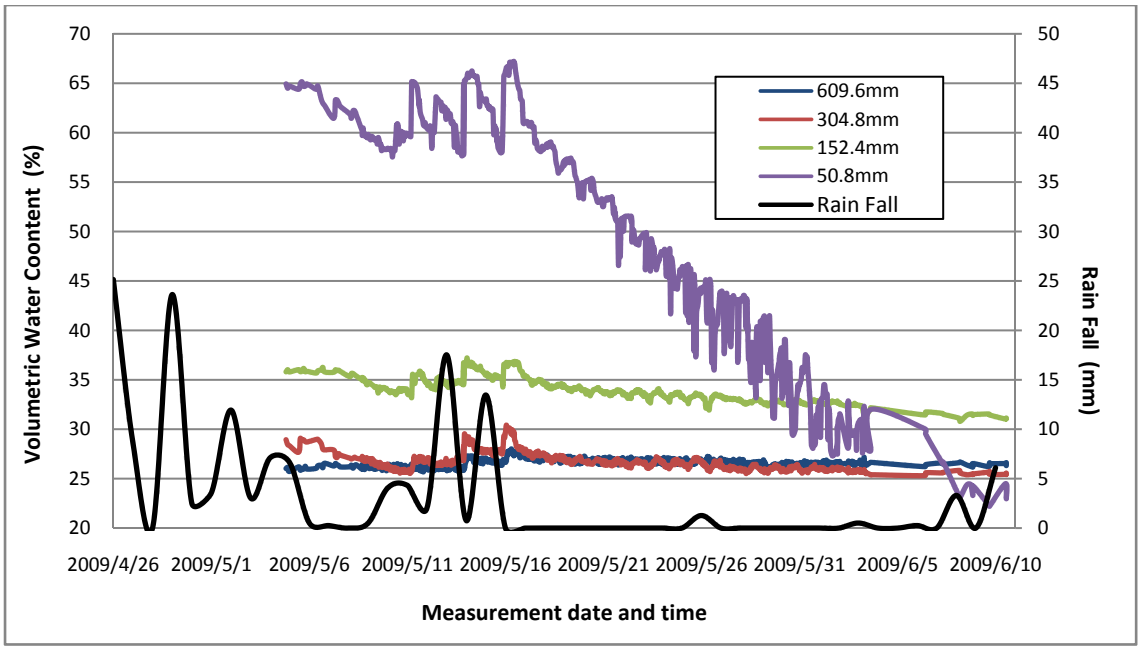

Figure 3-14 System soil moisture monitoring results from sensor node 9

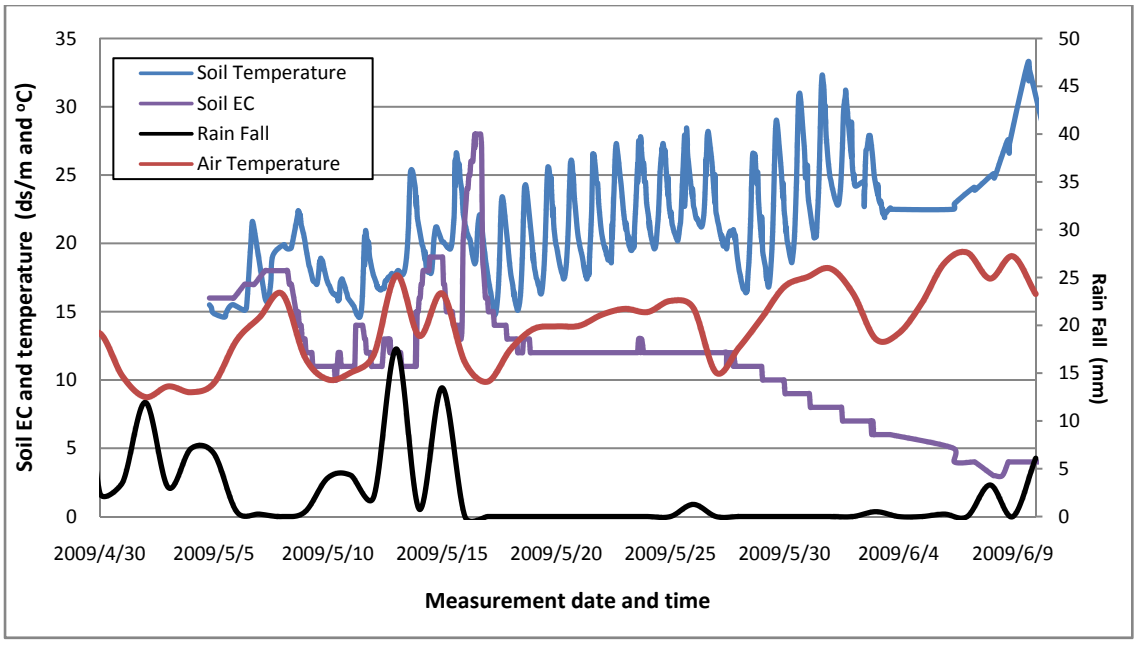

Figure 3-15 System soil electrical conductivity and temperature monitoring results from sensor node 9

In Figure 3-15, rain fall and air temperature were obtained from MESONET. It indicated that monitored soil electrical conductivity changed also along with the rain and there was a lag between changes of the electrical conductivity to the rain. The air temperature was the averaged daily temperature. The trend of the measured near-surface temperature changed accordingly to the air temperature. It was clear that peaks and valleys appeared in near surface temperature readings, which meant that the soil temperature at 50.8mm underground could still be influenced by the air temperature.

3.3.2 Data Transmission Performance

Data transmission performance evaluation results are displayed in Figure 3-16. The averaging system $N_{R,pdr}$ is 95.05% while the $N_{R,pdr}$ of sensor node 2 was excluded for its extra low reading since sensor node 2 located at the furthest distance from the central node and was most influenced by the plant canopy attenuation.

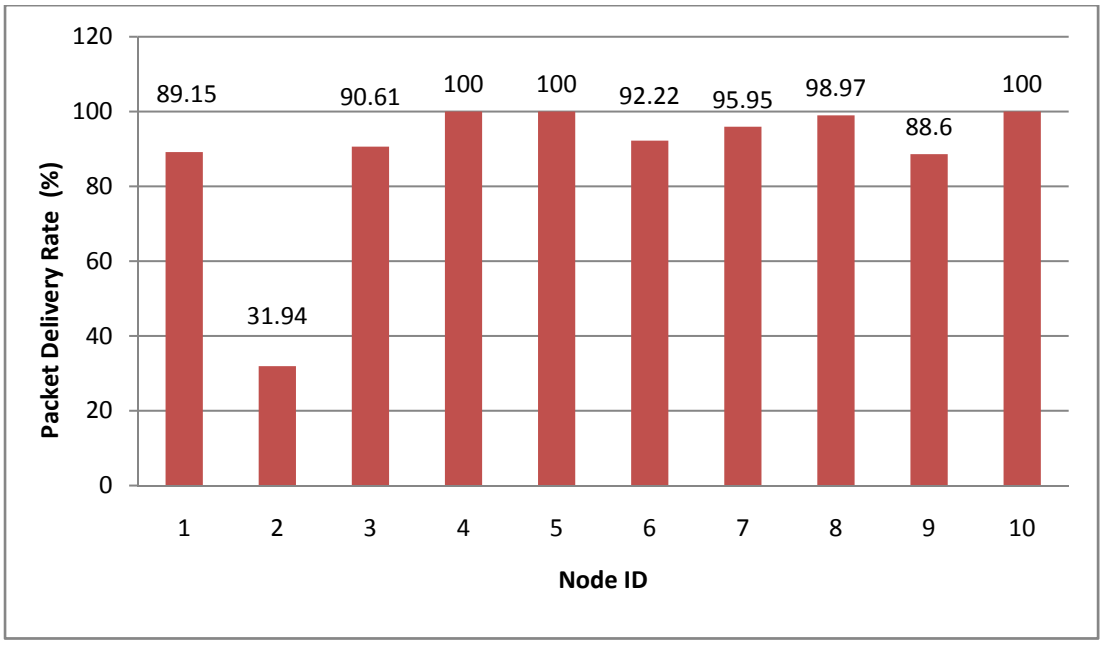

Figure 3-16 Packet delivery rate results

3.3.3 System Reliability

System reliability results are shown in Table 3-3. The minimum valid data rate was 91.9% obtained in Node 10's VWC reading while the majority valid data rates of sensors in each sensor node were above 97%.

Table 3-3 Valid data rate for each sensor node's sensors

Node ID	$N_{R,val}$ (%)						
	EC5-1	EC5-2	EC5-3	EC5-4*	VWC*	EC*	Temp*
1	98.5	98.5	100	100	N/A	N/A	N/A
2	100	98.2	100	100	N/A	N/A	N/A
3	99.0	99.5	98.0	98.5	N/A	N/A	N/A
4	98.9	98.9	100	98.9	N/A	N/A	N/A
5	99.5	99	99.5	99.0	N/A	N/A	N/A
6	100	99.4	100	N/A	100	100	99.4
7	99.5	99.5	100	N/A	99.5	100	98.9
8	100	95.7	99.0	N/A	100	100	100
9	100	98.9	99.5	N/A	97.8	100	100
10	99.0	100	99	N/A	91.9	100	100
Average	**99.4**	**98.8**	**99.5**	**99.3**	**97.8**	**100**	**99.7**

*Sensor Nodes 1 to 5 did not have EC-TE thus the $N_{R,val}$ for EC-TE are N/A; sensor nodes 6 to 10 did not have EC5-4, thus the readings were N/A.

3.3.4 In-filed Data Error Rate

During the tests, 246 pseudo PDUs were transmitted in about 45 minutes and the $N_{R,err}$ was 0%.

3.4 Conclusions and Future Work

This paper described the development of a two tier hybrid sensor network system for un-supervised, real-time, in-field soil property monitoring. Within the system, a local wireless sensor network was developed to acquire soil properties include water content, electrical conductivity and temperature at different underground depth. A combination of cellular network and a webserver worked for data storage and querying to provide easy data access to final users everywhere through Internet. The system was deployed and

tested since May 4th, 2009. The quality of service of the system was calculated based on the average packet delivery rate and in-field data error rate, which were 95.05% and 0% respectively until day of test. The averaged valid data rate was above 97% in general for each sensor node.

The system has high flexibility and robustness in the data acquisition layer that (1) new sensor nodes could added or removed without special re-configurations, (2) data were backed up in every single node as well as in the gateway and (3) monitoring results could be uploaded manually in the field without cellular connections.

Future works may take the following issues into concern as: (1) Currently, base node, central node, and sensor nodes are sharing one Node ID field within the PDU. Network expansion will be constrained since the Node ID space is limited. Extra PDU fields may be added; (2) There is no acknowledgement packet from the central node to sensor nodes which may lead to data loss.

Acknowledgements

The authors would like to acknowledge the support from the National Science Foundation CNS-0709329.

References

Beckwith, R., C. Teibel, P. Bowen. 2004. Report from the field: results from an agricultural wireless sensor network. Local Computer Networks. In *Proc.* 29th Annual IEEE International Conference, 471-478.

Bellis, S.J., K. Delaney, B. O'Flynn, J.Barton, K.M. Razeeb, C.O'Mathuna. 2005. Development of field programmable modular wireless sensor network nodes for ambient systems. *Computer Communications.*28 (13): 1531-1544.

Campbell, C. S. 2002. Response of the ECH2O soil moisture probe to variation in water content, soil type, and solution electrical conductivity. Available at: http://www.madgetech.com/pdf_files/app_notes/ec-probe-analysis.pdf. Accessed 2009.07.05.

Cassman, K.G., D.N. Munns. 1980. Nitrogen mineralization as affected by soil moisture, temperature, and depth. *Soil Sci Soc Am J.* 44: 1233-1237.

Corwin, D.L., S.M. Lesch. 2005. Apparent soil electrical conductivity measurements in agriculture. *Computers and Electronics in Agriculture.* 46(2005):11-43.

Cortez, M., J. Sanchez. 2007. Wireless communication system for a wide area sensor network. *Wireless Sensor and Actor Networks.* 248: 59-69.

Dalton, F.N., W.N. Herkelrath, D.S. Rawlins, J.D. Rhoades.1984. Time-domain reflectometry: simultaneous measurement of soil water content and electrical conductivity with a single probe. *Science.* 224: 989–990.

Davidson, E.A., F. Belk, R.d. Boone. 1998. Soil water content and temperature as independent or confounded factors controlling soil respiration in a temperate mixed hardwood forest. *Global Change Biology.* 4:217-227.

Decagon Device. 2006. EC-TE/TM Operator's Manual. Available at: http://www.decagon.com/support/literature/index.php?pg=ectm. Accessed 2009.06.10

Decagon Device. 2008. 5TE Operator's Manual. Available at: http://www.decagon.com/pdfs/manuals/5TE_v3.pdf. Accessed 2009.07.17

Demirbas, M., K. Y.Chow, C. S. Wan. 2006. INSIGHT: Internet-Sensor Integration for Habitat Monitoring, In *Proc.* of the 2006 International Symposium on World of Wireless, Mobile and Multimedia Networks: 553-558.

Dinh, T. L., W. Hu, P. Sikka, P. Corke, L. Overs, S. Brosnan. 2007. Design and Deployment of a Remote Robust Sensor Network: Experiences from an Outdoor Water Quality Monitoring Network. *Local Computer Networks*. 2007: 799-806.

Fukatsu, T., M. Hirafuji, T. Kiura. 2006. An agent system for operating Web-based sensor nodes via the Internet. *Journal of Robotics and Mechatronics*. 18(2): 186-194.

Han, W., N. Q. Zhang, Y. L. Zhang. 2008. A two-layer wireless sensor network for remote sediment monitoring. ASABE Paper No. 084548. Providence, Rhode Island, USA.

Hefeeda, M. and M. Bagheri. 2007. Wireless Sensor Networks for Early Detection of Forest Fires. In MASS.

Huisman, J.A., C. Sperl, W. Bouten J.M. Verstraten. 2001. Soil water content measurements at different scales: accuracy of time domain reflectometry and ground-penetrating radar. *Journal of Hydrology*. 245(1), 48-58.

Huisman, J.A., J.J.J.C. Snepvangers, W. Bouten, G.B.M. Heuvelink. 2002. Mapping spatial variation in surface soil water content: comparison of ground-penetrating radar and time domain reflectometry. *Journal of Hydrology*. 269(3), 194-207.

Kelleners, T.J., R.W.O. Soppe, J.E. Ayars, T.H. Skaggs. 2004. Calibration of Capacitance Probe Sensors in a Saline Silty Clay Soil. *Soil Science Society of America Journal*. 68: 770-778.

Kitchen, N.R., S.T. Drummond, E.D.lund, K.A. Sudduth, G.W. Bucheiter. 2003. Soil electrical conductivity and topography related to yield for three constrasting soil – crop systems. *Agronomy Journal*. 95: 483-495.

Li, Z., N. Wang, A. Franzen, X. Li. 2008. Development of a Wireless Sensor Network for Field Soil Moisture Monitoring. ASABE Paper No.083835. Providence, Rhode Island, USA.

Liu, H., Z.J. Meng, S.H. Cui. 2007. A Wireless Sensor Network Prototype for Environmental Monitoring in Greenhouses. Wireless Communications, Networking and Mobile Computing. In *Proc.* WiCom 2007 International Conference: 2344-2347.

Lund, E.D., P.E. Colin, D. Christy, P.E. Drummond. 1999. Applying soil electrical conductivity to precision agriculture. In *Proc.* of the Fourth International Conference on Precision Agriculture, 1089-1100. St. Paul, MN, USA.

Panchard, J., S. Rao, T. V. Prabhakar, H. S. Jamadagni, J. P. Hubaux. 2006. COMMON-Sense Net: Improved Water Management for Resource-Poor Farmers via Sensor Networks, In *Proc.* Intern. Conference on Communication and Information Technologies and Development ICTD.

Pierce, F. J., T. V. Elliott. 2008. Regional and on-farm wireless sensor networks for agricultural systems in Eastern Washington. *Computers and Electronics in Agriculture*. 61(1): 32-43.

Sakaki, T., A. Limsuwat, K.M. Smits, T.H. Illangasekare. 2008. Empirical two-point α-mixing model for calibrating ECH2O EC-5 soil moisture sensor, Water Resour. Res., Speciall Issue on Measurement Methods. In revision.

Reed, D., Stewart, J. B. Solie. 2007. Foraging Detection of Free-grazing Cattle using a Wireless Motion Sensing Device and Micro-GPS. ASABE Paper No.071133. Minneapolis, Minnesota, USA.

Tolle,G., J. Polastre, R. Szewczyk, D. Culler, N. Tuner, K. Tu, S. Burgess. 2005. A Macroscope in the Redwoods. Sensys '05, 51-63. San Diego, Califonia, USA.

Valente, A., R. Morais, A. Tuli, J.W. Hopmans, G.J. Kluitenberg. 2006. Multi-functional probe for small-scale simultaneous measurements of soil thermal properties, water content, and electrical conductivity. *Sensors and Actuators A.* 132: 70-77.

Wan, Z., and Z. Li. 1997. A physics-based algorithm for retrieving land-surface emissivities and temperature from EOS/MODIS data. *IEEE Transactions on Geoscience and Remote Sensing*. 35: 980-996.

Werner-Allen, G., J. Johnson; M. Ruiz, J. Lees, M. Welsh. 2005. Monitoring volcanic eruptions with a wireless sensor network, Wireless Sensor Networks. In *Proc*. of the Second European Workshop: 108-120.

CHAPTER IV

ESTABLISHMENT OF A RADIO-WAVE PATH-LOSS MODEL TO PREDICT RECEIVED SIGNAL STRENGTH FOR WIRELESS SENSOR NETWORK USED IN WHEAT FIELDS

Zhen Li[1,2], Ning Wang[1], Haixia Li[1], Aaron Franzen[1], Kevin Stunkel[1]

1. Biosystems and Agricultural Engineering, Oklahoma State University, USA;

2. College of Engineering, South China Agricultural University, China.

Abstract

The promising wireless sensor network (WSN) technology provides great potential for in-situ soil property monitoring. Quality of service (QoS) is crucial for successful development and deployment of wireless sensor networks and is highly dependable on reliable communications. Therefore, it is important to understand system configuration and vegetation impacts on radio wave propagation at typical WSN carrier frequencies. Radio propagation at two carrier frequencies of 915MHz and 2470MHz was evaluated in a test wheat field. An experimental platform was established which consisted of commercial wireless sensor nodes as transmitters and a spectrum analyzer as a receiver. Packet reception rate was obtained concurrently with the path loss measurements. The experiment was divided into three blocks by two plant heights as 0.05m and 0.4m. The

factors affecting radio transmissions were considered including logarithmic transmission distance, transmitter height, receiver height, carrier frequency, and antenna gain. Three widely used models as COST-Hata model, free space model and plane earth model were included for verifying their feasibility in field path loss prediction. Four multivariate linear regression models were developed validated using field experimental data. Paired sample t-tests were conducted to compare the predicted path loss from the developed models, the Free Space models, the Plane Earth models, and the COST-Hata model to the measured path loss. Results indicated that the COST-Hata model yielded the highest difference while free space model came at the second place. The R^2 for the four regressed models were 0.822, 0.810, 0.843 and 0.899, respectively. The special regressed models were superior in path loss prediction to the general models. A threshold of 70m was obtained for reliable communication in the experimental scenarios of this research.

Keywords: path loss; wireless sensor network; wireless communication; packet reception rate, radio propagation

4.1 Introduction

Detailed soil physical property information as soil moisture, temperature and electrical conductivity (EC) are useful for agricultural activities such as precision irrigation, nitrogen application, plant growth, and yield prediction (Sadler et al, 2005; Jackson et al., 2007). Commonly, the commercially available sensors are used to measure soil physical properties at a single location inside a field and the data has to be collected by technicians or machines using portable data acquisition devices or stationary data-loggers with a preset sampling frequency. As a result, the temporal and special density of sampling points is limited.

Wireless sensor network (WSN*)* is one of the most promising technologies with nearly unlimited installation flexibility, outstanding mobility and reduced maintenance complexity. This has particular benefits for field physical property monitoring since a WSN can transfer data without a cable and be merged into other networks like cellular or Internet. The sensor nodes could be left in the field for un-supervised intensive monitoring. Successful agricultural WSN implementations have demonstrated improved understandings of field status as well as aerial macro- or microclimates (Beckwith et al, 2004; Tolle et al, 2005; Liu et al, 2007).

An on-going WSN research project by Oklahoma State University had wireless sensor nodes deployed in an experimental wheat field to measure soil moisture, temperature and EC (Li et al. 2008, 2009). A big challenge of the current in-field WSN applications is that the wireless communication is strongly affected by various factors including system configuration, vegetation, and environment. The theoretical radio propagation models such as the free space model (FRIIS, 1946) and plane earth model (Wait, 1974) are not effective to describe the radio propagation under crop field conditions.

Packet reception rate (PRR) is a major measure to the quality of services (QoS) in a WSN design. It is highly related to the received signal strength which is dependable on the path loss in condition of known transmission power. As a result, propagation algorithms that determine path loss and broadcast signal coverage will be essential to design a reliable, high-performance WSN. It will be convenient to apply sufficient in-site radio wave path loss models during node deployment instead of conducting propagation measurements every time to predict received signal strength and have an image of communication performance.

Each individual telecommunication link is influenced by different terrain, transmission distance, obstructions, environmental conditions, vegetation and other phenomena. It is impractical to formulate an exact path loss model for all types of communication in a single mathematical expression. As a result, different types of radio links should have their unique models. As categorized, there are three major types of near-earth propagation models as Foliage, Terrain and City models. Vegetation influence were not taken into consideration in most of terrain and city models while the existing foliage signal attenuation models mainly focused on forests (Li et al, 1998; Dapper et al, 2003; Richter et al, 2005). Some other field specific models described radio propagation and signal attenuation around plants like maize and soybean (Vine et al, 1996) or potato (Thelen et al, 2005). The reviewed signal attenuation models were determined by impact factors like plant canopy height and moisture content on it, communication distance, antenna height and gain, surface roughness as well as the carrier frequency. Although there's little concrete information about radio wave propagation pattern in wheat field for low-power short-distance wireless sensor network applications, the carrier frequency, communication distance, station height as well as antenna gain are considered to be the most regular impact factors in wave propagation models besides plant canopy height and shape.

The objective of this research was to quantify the system configuration, vegetation and environmental influences on WSN communications within a wheat field and to develop predictive models for robust WSN deployment. The specific objectives include:

1) To find and analyze the major factors which affect in-field wireless path loss during wheat growing stages;

2) To evaluate applicability of existing, widely used path loss models for WSNs under wheat field conditions;
3) To develop and evaluate multivariable radio path loss models for predicting in-field signal path loss during transmission under wheat field conditions; and
4) To determine the maximum separation distance for reliable communication.

4.2 Methods and Materials

4.2.1 Impact Factor Selection

Path loss (*PL*) measures the average RF attenuation along the path of radio propagation imposed on the transmitted signal when it arrives at the receiver. Generally, a path loss within a distance *d* could be expressed as Equation 4.1(Sarkar, et al., 2003):

$$PL(d) = 10\log\frac{P_t}{P_r} \qquad (4.1)$$

Where *PL(d)* is the path loss in *dB*, P_t and P_r are the transmitted and received power in *mW*, respectively. In our experiments, the measured transmitted power (P_{tm}) and received power (P_{rm}) were in the unit of *dBm* where: $P_{tm}(dBm) = 10\log P_t$ and $P_{rm}(dBm) = 10\log P_r$. The path loss calculation can be reformulated as Equation 4.2:

$$PL(d) = P_{tm} - P_{rm} \qquad (4.2)$$

However, Equation 4.2 won't hold in situations in which the distance of d=0 where the measured received power equals to the measured transmitted power (Sarkar, et al., 2003) resulting that the actual power coming out of the antenna is inaccessible. Therefore, a different representation for a close-in distance, d_0, is usually applied in path loss calculations as the received-power reference point (Sarkar, et al., 2003). In our experiments, d_0 was 1*m* and the path loss within a distance of *d* was calculated using Equation 4.3:

$$PL(d) = PL(d_0) + P_{rmd_0} - P_{rmd} \qquad (4.3)$$

Where P_{rmd0} is the measured signal strength at d_0=1m in *dBm*, P_{rmd} is the measured signal strength at d in *dBm*, $PL(d)$ is the path loss within d in *dB* and $PL(d_0)$ is the path loss within d_0 calculated using the free space mode. It was assumed that there was no significant difference between signal attenuation at the distance of 1m in free space and in field applications.

Potential impact factors in a crop field were considered which included: distance between base and sensor nodes (d), transmitter height (h_t), receiver height (h_r), carrier frequency (f), antenna gain of both transmitter and receiver (G_t and G_r), wheat height (h_p), field temperature (T) and relative humidity (RH). Wheat height served as a blocking factor while temperature and relative humidity acted as referencing factors during the process since it's difficult to control their readings. Impacts from the rest of the factors would be tested and empirical models would be constructed by relating measured *PL* to these factors. Experimental values of the impact factors are shown in Table 4-1:

Table 4-1 The impact factors considered

Factors	Communication Distance (m)	Transmitter Height (m)	Receiver Height (m)	Carrier frequency (MHz)	Antenna Gain (*dBi*)
Values	20~130 with 10 interval	1 2 3	1 2 3	915 2470	0 (node) 2.15 (base)

*Values of plant height intervals will be calculated and explained in the later session

The maximum separation distance was determined based on our preliminary tests to maintain communication without extra signal amplification or directional antenna.

4.2.2Criterion of Using Plant Canopy Height as Blocks

In the field, wheat canopy is the major reflection surface and obstacle along the transmission path. The attenuation introduces by plant height is as depicted in Figure 4-1.

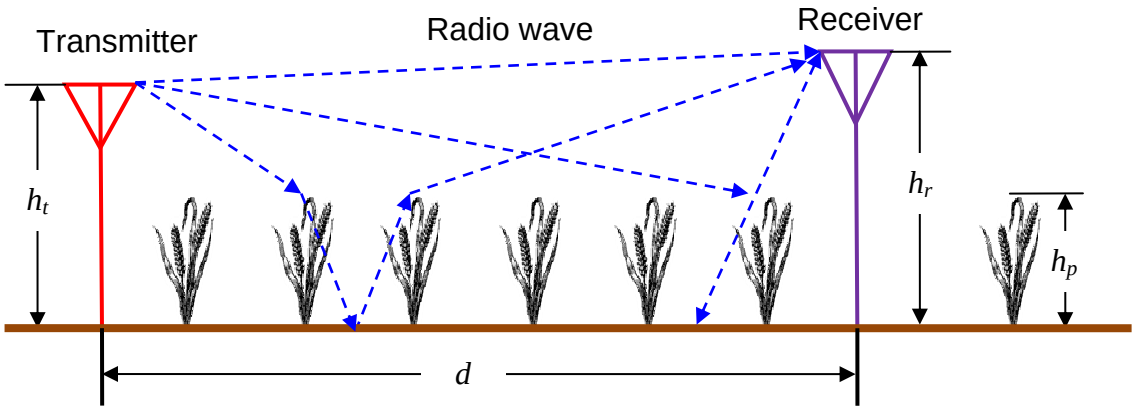

Figure 4-1 Sketch map of plant influences on radio wave propagation inside wheat field. h_t and h_r are transmitter and receiver height, h_p is plant height and d is the separation distance between a transmitter and a receiver

The canopy height changes during wheat growth and makes the attenuation sources contribute differently. To reduce experimental error from the wheat, canopy height was applied as a blocking criterion to make signal attenuation pattern similar within each block. Typical plant heights as thresholds were calculated using concepts as the Rayleigh roughness (Sizum, 2005) and the Fresnel zone clearance (Sheriff, 1996) to divide the wheat growth into certain stages (blocks).

Equation 4.4 is derived from the Rayleigh roughness criterion but takes the transmitter/receiver height into consideration as:

$$H_1 = \frac{\lambda\sqrt{d^2 + (h_t^2 + h_r^2)}}{8(h_t + h_r)} \qquad (4.4)$$

Where H_1 is the threshold of crop height in m, h_t and h_r is the heights of a transmitter and a receiver in m, respectively, d is the separation distance in m and λ is the wavelength in m. If the wheat height is lower than H_1, then the reflected waves from both the ground and plant are in phase and it leads to the case of specular reflection. If the wheat height is higher than H_1, then the reflection becomes diffusion reflection which means waves are not in phase. By putting the values from Table 1 into Equation 4.8, the minimum H_1 for 915MHz carrier frequency is 0.14m and that for 2470MHz is 0.05m. As a result, H_1=0.05m is determined as the first plant height threshold.

The second concept applied for plant height threshold determination is the Fresnel zone clearance for analyzing interference introduced by obstacles near the path of a radio beam for line-of-sight communications (Figure 4-2).

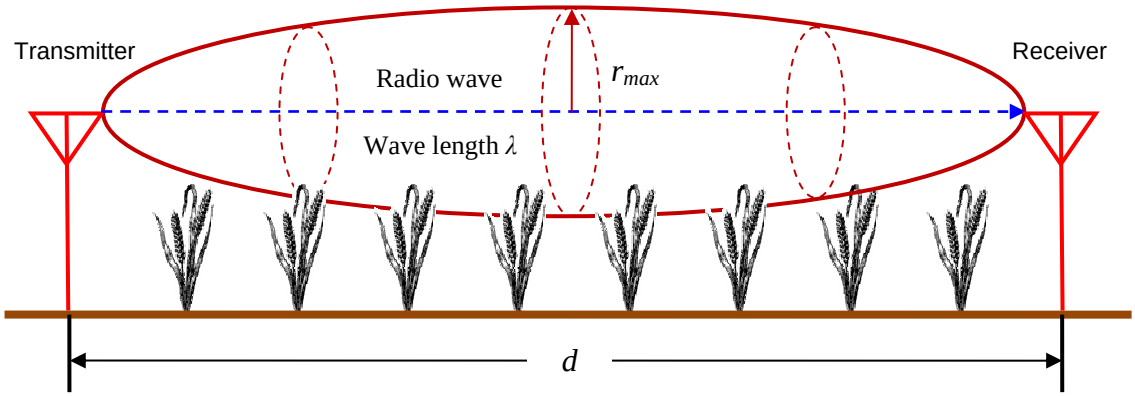

Figure 4-2 Sketch map of Fresnel zone clearance. r_{max} is the maximum radius of the first ellipsoid, d is the separation distance

Maximum radius of the first ellipsoid within each communication distance at both 915MHz and 2470MHz carrier frequency were calculated using Equation 4.5 as:

$$r_{max} = \frac{1}{2}\sqrt{\lambda d} \qquad (4.5)$$

Where r_{max} is the maximum radius in m, λ is the wavelength in m and d is the communication distance in m. r_{max} ranges from 1.28m to 3.26m for 915MHz at different distances and from 0.78m to 1.99m for 2470MHz. Here we considered the situation in which both sensor and base station are at a 3m height. For 2470MHz, the Fresnel zone is clear for all separation distances, but for 915MHz there's some obstruction when the distance is 130m. A 20% clearance tolerance was introduced and the allowed plant height at the largest r_{max} was re-calculated as Equation 4.6:

$$H_2 = 3 - (3.26 - 3.26 \times 20\%) \qquad (4.6)$$

H_2 equals to 0.4m and serves as the second threshold for the plant height. As shown in Figure 4-3(a), the growth of wheat was divided into three stages (blocks) based on plant canopy height (h_p) using the two calculated thresholds as:

Stage 1: 0m $\leq h_p < H_1$, specular reflection, Fresnel zone clear;

Stage 2: $H_1 \leq h_p < H_2$, diffusion reflection, Fresnel zone clear;

Stage 3: $H_2 \leq h_p <$ 1m, diffusion reflection, obstacles within Fresnel zone.

Where H_1=0.15m as the threshold for dividing specular and diffusion reflection and H_2=0.4m for Fresnel zone clearance when transmitter and receiver were at the height of 3m.

Figure 4-3 (b), (c) and (d) show the wheat plants at different growth stages. The actual height for the third stage was around 0.8m. The three stages of wheat growth were referred to as plant height 1, 2, and 3, respectively.

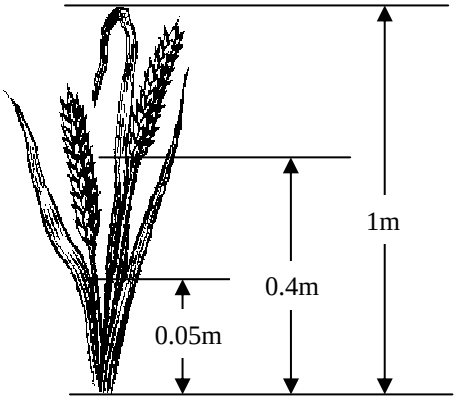

(a) Different thresholds of wheat growth

(b) Stage 1, wheat height lower than 0.05m

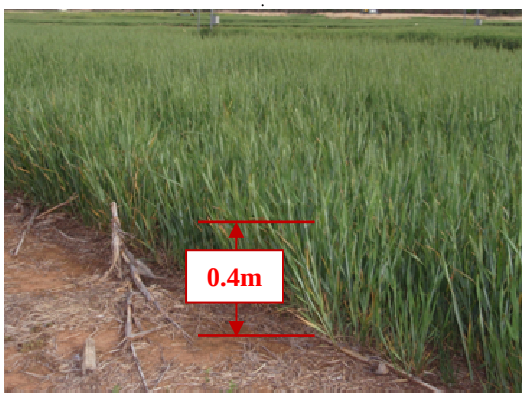

(c) Stage 2, wheat height between 0.05m and 0.4m

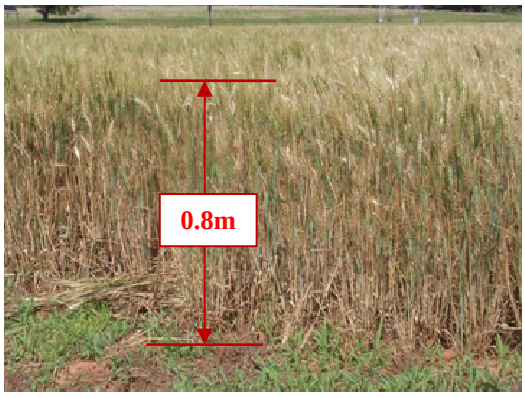

(d) Stage 3, actual wheat height 0.8m

Figure 4-3 Different Stages of wheat growth (canopy height)

4.2.3 Experimental Setup

The experiments were conducted with both commercial off-shelf and self-designed wireless sensor nodes to measure the impacts of each impact factor on wireless communications and to determine the key factors to develop an in-site path loss model.

Hardware

1) Transmitters: Two types of wireless sensor nodes, the IRIS mote from Crossbow Technology (Crossbow, 2004) and the one developed by the Department of Biological and Agricultural Engineering at Oklahoma State University (Steward, et al., 2007) referred as "*cattle node*" were applied in the field tests as transmitters. Once the nodes

received a predefined request from a separate controller, they transmitted indexed packets to a receiver for measuring both received signal strength and packet delivery rate (*PDR*).

The IRIS mote uses Atmel's AT86RF230 (Atmel Crop., San Jose, CA, USA) as the IEEE 802.15.4 compliant RF transceiver and the data transmission rate could be as high as 250kbps (Atmel, 2009). The RF frequency band ranges from 2405MHz to 2480MHz within the ISM band. 16 channels are programmable in 5MHz steps with 34dB or 36dB adjacent channel rejection. The highest transmit power is +3.2*dBm*, and the receiver sensitivity is -101*dBm*. The modulation technique is the *DSSS*/*QPSK* (direct-sequence spread-spectrum and quadratic phase shift keying). The antenna applied is ¼ wave dipole antenna with 0*dBi* gain. For our experiments, the transmission power was +3.2*dBm* and the selected carrier frequency was 2470MHz (Channel 24) for not disturbing the working nodes in the same field using Channel 11 as 2405MHz.

The cattle node is based on the CC1010 low power UHF wireless data transceiver. It is programmable from 300MHz to 1000MHz with 4 typical carrier frequencies as 315/433/868and 915MHz. Data transmit rate could be up to 76.8kbps. The maximum output power is 10*dBm* at 315/433MHz and 4*dBm* at 868/915MHz, the receiving sensitivity is -107*dBm*. In our experiments, the CC1010 (Texas Instruments, TX, USA) configuration is as: 915MHz carrier frequency, Manchester Encoding, 19.2kbps data transmit rate, 4*dBm* transmission power, *FSK* modulation, and connected to a 0*dBi* omni-directional compact antenna.

A tri-pole was built to fix the transmitters at different heights of 1, 2 and 3 meters, respectively, as shown in Figure 4-4. A piece of plastic pad was fixed at each height. The nodes were attached to the pads using valcro as shown in Figure 4-4 b and c. The tri-pole

could be carried to any spot inside the field and introduces minimum interference to the antenna polarization pattern.

(a) Tri-pole overview (b) Cattle node fixture (c) IRIS mote fixture

Figure 4-4 Sensor nodes fixture

2) Base station: The base station contained receivers for different measurements. It was composed of four major components as: a handheld RF spectrum analyzer (N9340B, Agilent Technology, USA), a IRIS mote with MIB510 programming board, a cattle node with CC1010 development kit board, and a Laptop computer (Toughbook, Dell, USA) for displaying and restoring experimental results including spectrum and packets in real-time. Key specifications of the spectrum analyzer are: 100kHz to 3GHz frequency range, 30Hz to 1MHz RBW in 1-3-10 sequence, -144*dBm* displayed average noise level (*DANL*) with pre-amplifier etc. Received signal strength was measured using the spectrum analyzer rather than directly reading *RSSI* values from both types of the nodes. Key configurations of the analyzer are: pre-amplifier on, carrier frequency: 2470MHz and 915MHz, frequency span: 15MHz, resolution bandwidth (RBW): 100kHz, video bandwidth: 30kHz, attenuation: -10*dB*, reference level: -30*dBm*. By using the configurations above, the *DANL* is -100*dBm* in the experiments. The other two boards

with nodes attached were used to receive the indexed packets for packet delivery rate calculation.

A frame was built to contain the analyzer while the other two boards were mounted on the side for retrieving similar heights (Figure 4-5). A flag-pole was placed on the edge of the field with the frame mounted to it so that the height of the base station (Laptop not included) was adjustable.

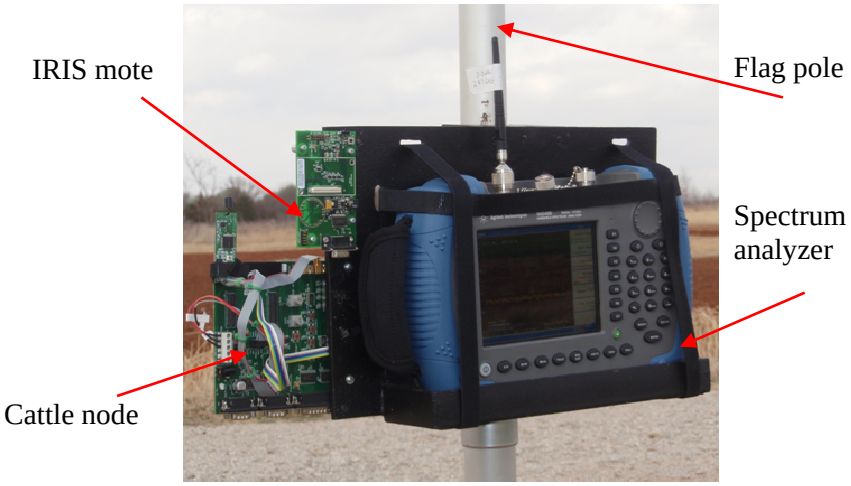

Figure 4-5 Base station mounted to a flagpole

Field layout

The field experiments started at January 6th, 2009 and ended at May 22nd, 2009 which covered a complete wheat growing season. The testing spots were located in the experimental field where a WSN for soil property monitoring was deployed (Li et al., 2008). As shown in Figure 4-6, the base station was located on one edge of the field. Twelve spots, namely "*source spots*", were marked in a lane inside the field. Separation distance between the first source spot and base is 20m±0.5m. Each of the following spots heading another field edge has a 10m±0.5m increase in distance away from the previous spot. The tri-pole with the transmitting nodes was placed at each source spot. Received

signal strengths at the base were recorded for path loss calculation. Seven other spots, namely the "*verification spots*", were selected at each mid-point between two source spots with distances to base ranging from 25m to 85m. The tri-pole with motes transmitting signal was also placed at each verification spot and received signal strengths at base were recorded. However, path loss calculated at verification spots were not included in model development but applied for model verification.

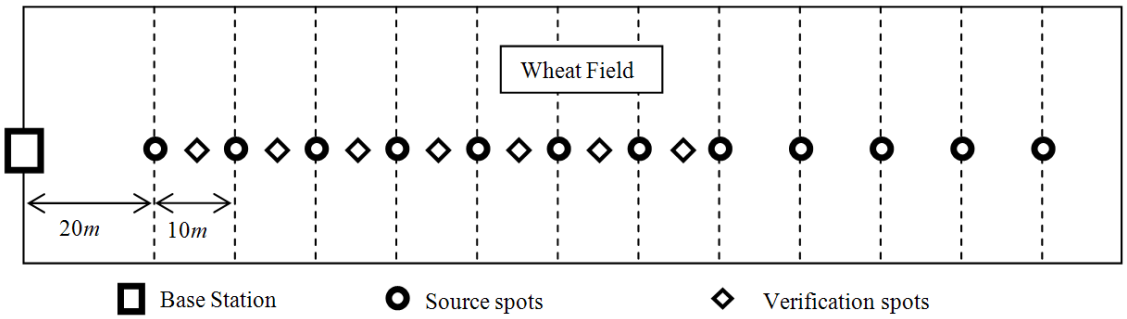

Figure 4-6 Experimental field layout

Software

Three different software were used in field experiments as *Agilent N9340 PC Software* (Version A.01.04, Agilent Technologies, USA), *XSniffer* (Version 1.0.3, Crossbow Technology, USA) and *Realterm* (Version 2.0.0.43, open source) The *N9340* could (1) display real-time graphical *RF* power spectrum in span of certain carrier frequency, (2) export power spectrum to spread sheets, and (3) make some basic configurations of the analyzer. The *XSniffer* and *Realterm* were used to display and restore the received indexed data for packet transmission rate calculations.

4.2.4 Data Processing and Analysis

Received signal strength (*RSS*) was measured at each distinct distance as well as at the received-power reference point. Values of the path loss under certain impact factor combinations were calculated by insert the *RSS* values measured at a certain distance and

at the received-power reference point into Equation 4.3. Statistical analysis was carried out off-line in SPSS (Version 14.0, USA). Measured as well as predicted path loss using *FS*, *PE*, COST-Hata models and the constructed models based on data obtained from field experiments of this research were employed for analysis on each impacting factor.

Regression analysis was conducted to relate the path loss to multiple impact factors of separation distance, transmitter and receiver height, base antenna gain and carrier frequency. Stepwise method was applied for impact factors' entry or removal. Experimental data from each influencing factor combinations were included with outlier exclusion using the Box plots. Four regressed models would be obtained with one without plant height blocking and the other three were blocked into different plant heights under which the signal strength was measured and path loss was calculated.

4.2.5 Feasibility Verification of Three Widely Used Path Loss Prediction Models

Three widely used path loss models were used to compare their performance and verify their applicability for wheat field applications as: Free Space (FS) model (Sarkar, et al., 2003), Plane Earth (PE) (Bianchi and Sivaprasad, 1998) model, and COST-Hata model (suburban area, Okamura, et al., 1968). Predicted path losses from these three models were compared with the measured path loss under each influencing factor combinations using the paired samples t-test to determine whether or not and to what extent these general models could be applied to the WSN application in wheat field.

Free space model

This model is used to calculate the loss in signal strength of an electromagnetic wave from a line-of-sight communication without obstacles nearby to cause reflection or diffraction. Path loss from this model could be calculated using Equation 4.7 as:

$$PL_{fs} = 32.45 + 20\log(f) + 20\log(d) - Gt - Gr \quad (4.7)$$

Where PL_{fs} is the free space path loss in dB, f is the carrier frequency in MHz, d is the separation distance in km, Gt and Gr is the transmitter and receiver antenna gain in *dBi*, respectively.

Plane earth model

This model takes the effect of the earth surface into consideration during free space propagation. When reflected off the earth surface, they may partially cancel the line-of-sight wave. Path loss from this model could be calculated using Equation 4.8 as:

$$PL_{pe} = 40\log(d) - 20\log(ht) - 20\log(hr) - Gt - Gr \quad (4.8)$$

Where PL_{pe} is the plane earth path loss in dB, d is the separation distance in m, ht and hr is the transmitter height and receiver height in m, respectively. Gt and Gr is the transmitter and receiver antenna gain in *dBi*, respectively.

COST-Hata model for suburban areas

This model predicts the total path loss along a link of microwave transmission just outside cities with less dense man-made structures, which fits the scenario of most agricultural wireless sensor network applications. Path loss from this model is calculated using Equation 4.9 as:

$$PL_{ch} = 46.3 + 33.9\log(f) - 13.82\log(h_B) - a(h_T) + [44.9 - 6.55\log(h_B)]\log(d) + C \quad (4.9)$$

Where PL_{ch} is the COST-Hata path loss in dB, f is the carrier frequency in MHz, d is the separation distance in km, h_T and h_B is the transmitter height and receiver height in m, respectively. a(h_T) is calculated using Equation 4.10, C is a constant and its value is 0*dB* for medium cities and sub-urban areas.

$$a(h_T) = 0.8 + [1.1 log(f) - 0.7] h_M - 1.56 log(f) \quad (4.10)$$

Where $a(h_T)$ is the mobile station antenna height correction factor, f is the carrier frequency in MHz, d is the separation distance in km and h_M is the height of mobile station antenna in m.

4.2.6 Packet Reception Rate Analysis

The packet reception rates (PRR, $N_{R.packet}$) under all scenarios were achieved using indexed packets received concurrently with signal strength measurements using Equation 4.11:

$$N_{R,packet} = \frac{N_{received}}{N_{transmitted}} \times 100\% \quad (4.11)$$

Where $N_{R.packet}$ is the packet reception rate, $N_{transmitted}$ is the total number of packets transmitted by the transmitter and $N_{received}$ is the number of packets received by the receiver.

4.3 Results and Discussion

4.3.1 Signal Strength at the Received-power Reference Point

To determine the signal strength at the received-power reference point, both base station and motes were kept at 1 meter in height and 1 meter away from each other. Labeled transmission power was 4.0*dBm* for the cattle node and 3.2*dBm* for IRIS node. The calculated free space path loss at this point was 31.67*dB* and 40.29*dB* for 915MHz and 2470MHz carrier frequency, respectively. The measured signal strength at the received-power reference point was -55.17*dBm* and -59.03*dBm* for the two kinds of nodes, respectively. The sum of $PL(d_0)$ and P_{rmd0} applied for further distance path loss calculations was -23.50*dBm* and -18.76*dBm* respectively for the two carrier frequencies.

4.3.2 Feasibility Verification of the Three Widely Used Models

The minimum difference between measured path loss and predicted ones from COST-Hata model (suburban area) was 24.14*dBm* and the maximum one was 90.56*dBm*. The maximum difference from comparing measured loss to predicted ones using FS and PE models were 14.42*dBm* and 28.74*dBm*, respectively. Also, standard deviation from comparing to COST-Hata model was no less than to FS or PE models. As a result, COST-Hata model had the least feasibility in predicting in-field path loss for our applications. Thus, no further comparisons would be made for analyzing factor impacts concerning this model. On the other hand, the free space and plane earth models showed potential feasibility. Their predicted path loss would be compared to the measured loss for applicability verification.

4.3.3 Impact of Linear Distance on Path Loss

Impact of separation distance on path loss for 915MHz carrier frequency

There were totally 27 path loss readings forming a data group at each distance. The factor combinations included 1 carrier frequency (915MHz), 3 plant heights, 3 heights of the base station, and 3 heights of the transmission node. Box plots (Figure 4-7) were applied to detect and exclude group outliers. Statistical results including number of remained readings (*N*), group mean, and 95% confidence interval inside each group is shown in Table 4-2. Standard deviation within each group increased after 90m, which means when the separation distance increased, impact factors had more complicated impacts on path loss.

Figure 4-8 shows how path loss changed along with the distance changes between transmission nodes and base station. The dashed line was obtained from using the Free

Space model with separation distances ranging from 20~130m with a 10m interval. Group means after outlier exclusion were plotted as the solid line for each 10m sampling interval. As shown in Figure 4-8, the averaged path loss at each distance was less than the theoretical one calculated from *FS* model.

Table 4-2 Path loss statistical results after outlier exclusion for radio wave with 915MHz carrier frequency

Distance (*m*)	*N*	Mean (*dB*)	Std. Deviation	95% Confidence Interval	
				Lower (*dB*)	Upper (*dB*)
20	24	42.7368	2.3929	41.7263	43.7473
30	27	48.6170	3.1222	47.3818	49.8521
40	26	49.9783	3.1088	48.7226	51.2341
50	26	54.0995	3.2014	52.8064	55.3926
60	27	55.4579	3.4837	54.0798	56.8360
70	26	57.9002	2.6571	56.8270	58.9735
80	26	58.9432	2.7933	57.8149	60.0714
90	27	62.1295	4.4724	60.3603	63.8988
100	27	63.8468	5.3320	61.7375	65.9561
110	27	65.8047	5.1655	63.7613	67.8482
120	26	66.6175	3.9991	65.0022	68.2328
130	27	68.1237	4.2512	66.4420	69.8055

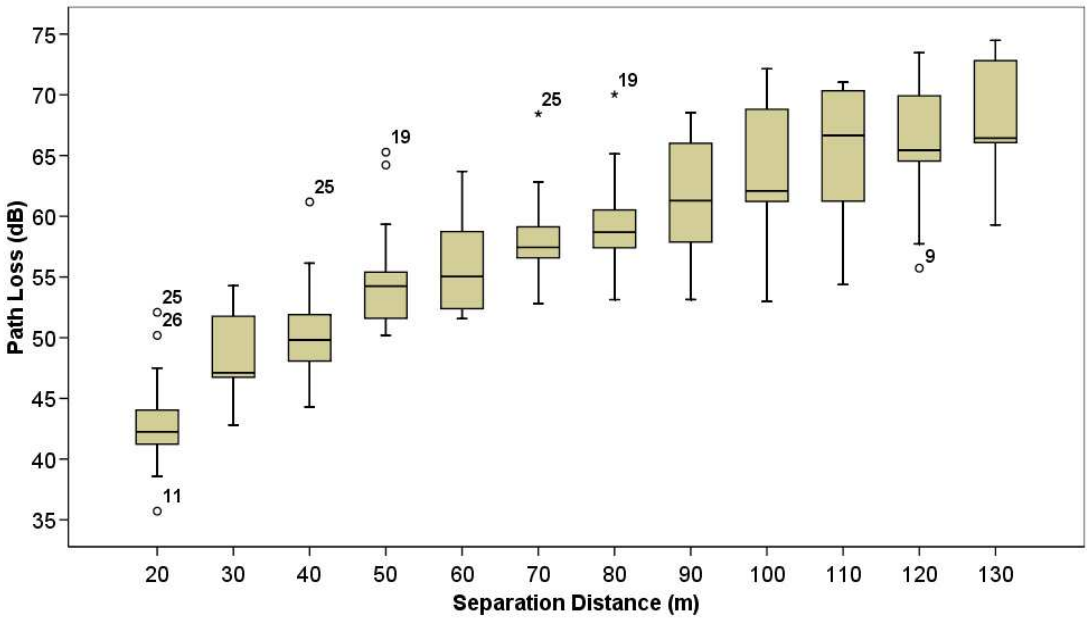

Figure 4-7 Box plots for path loss data groups at each separation distance, the carrier frequency is 915MHz, 27 readings included for each distances, single dots outside boxes are considered outliers.

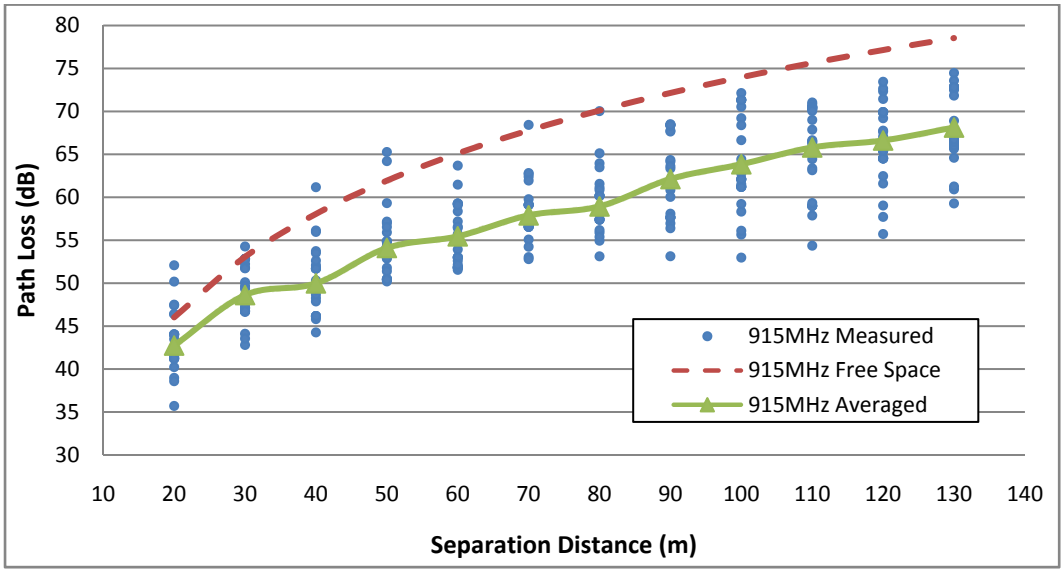

Figure 4-8 Path loss vs. distance for radio wave with 915MHz carrier frequency from using both averaged results after outliers exclusion and the Free Space model.

A single variable linear regression function for the 915MHz carrier frequency was obtained as Equation 4.12 by calculating the logarithmic transmission distance and the path loss at each distinct distance after outlier exclusion, influences of other factors were ignored:

$$PL(d) = 3.110 \times 10 log_{10}(d) + 1.365 \qquad (4.12)$$

Where *PL(d)* was the path loss in *dB* and *d* is the separation distance in *m*. The R^2 for Equation 4.12 was 0.790.

Impact of separation distance on path loss for 2470MHz carrier frequency

Similar analysis was applied for radio wave with a carrier frequency of 2470MHz, box plots and statistical results after outlier exclusion are shown in Figure 4-9 and Table 4-3. For 2470MHz carrier frequency, the standard deviation changed less thus was more stable within the whole range than 915MHz carrier frequency.

Figure 4-10 displays how path loss increased along with the separation between nodes and base station. The solid line was plotted using group means from Table 4-3. A single slope linear regression function for the 2470MHz carrier frequency was obtained similar to the one for 915MHz as Equation 4.13:

$$PL(d) = 1.916 \times 10 log_{10}(d) + 34.693 \qquad (4.13)$$

Where *PL(d)* was the path loss in *dB* and *d* is the separation distance in m. The R^2 for Equation 4.13 was 0.601.

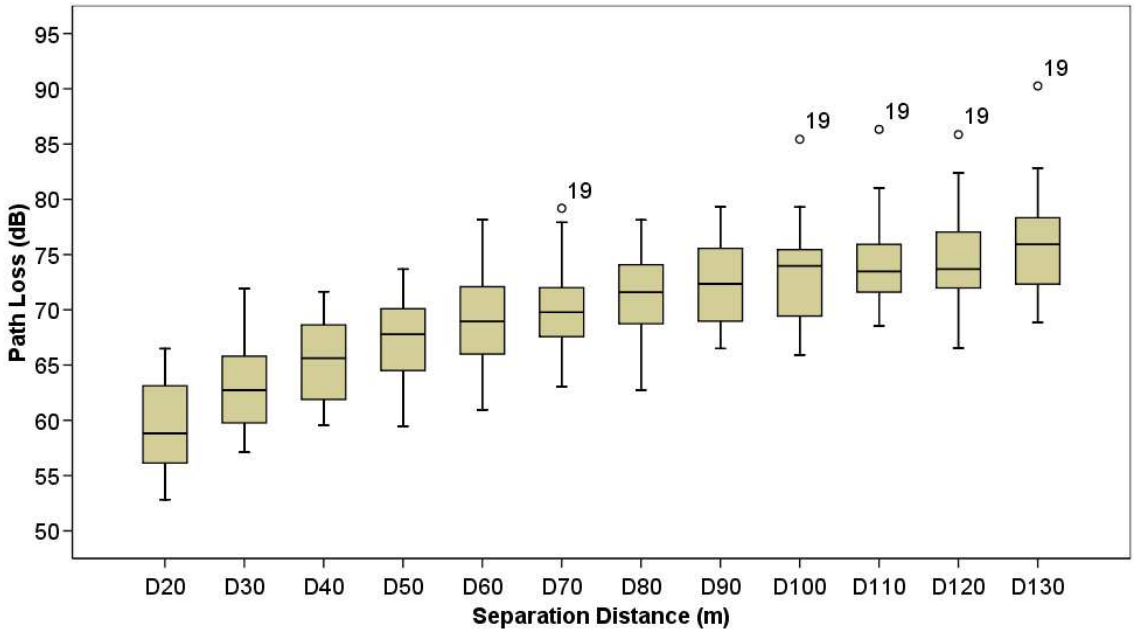

Figure 4-9 Box plots for path loss data groups at each separation distance, the carrier frequency is 2470MHz, 27 readings included for each distances, single dots outside boxes are considered outliers.

Table 4-3 Path loss statistical results after outlier exclusion for 2470MHz carrier frequency

Distance (*m*)	*N*	Mean (*dB*)	Std. Deviation	95% Confidence Interval	
				Lower (*dB*)	Upper (*dB*)
20	27	59.4393	4.2069	57.7751	61.1035
30	27	63.0560	3.8965	61.5146	64.5974
40	27	65.4483	3.6845	63.9907	66.9058
50	27	66.8787	4.0116	65.2918	68.4657
60	27	69.6033	4.5983	67.7843	71.4224
70	26	69.9632	3.5749	68.5192	71.4071
80	27	71.1674	3.8195	69.6564	72.6783
90	27	72.3704	4.0321	70.7753	73.9655
100	26	72.7376	3.6927	71.2461	74.2291
110	26	73.8233	3.3125	72.4854	75.1613
120	26	74.0599	3.4754	72.6562	75.4637
130	26	75.4239	3.8327	73.8758	76.9720

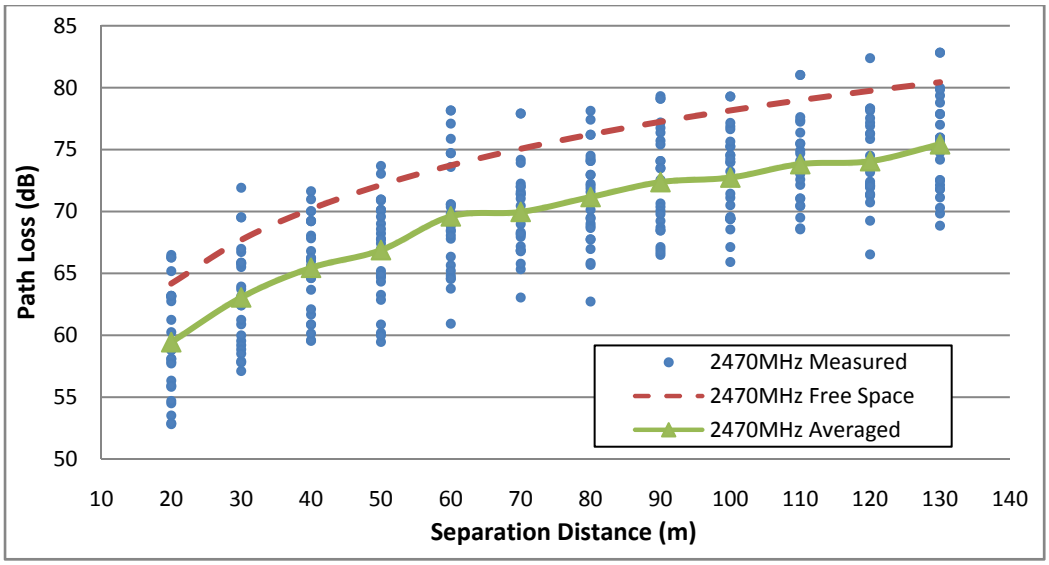

Figure 4-10 Path loss vs. distance for radio waves with a carrier frequency of 2470MHz from using both averaged results after outliers exclusion and the Free Space model.

4.3.4 Impact of Transmitter/receiver Height on Path Loss

To study the effects from transmitter/receiver height on wireless signal path loss, readings from setting both transmitter and receiver at the same height as 1m-1m, 2m-2m and 3m-3m under each carrier frequency and plant height were employed and grouped using plant height.

Impact of transmitter/receiver height on path loss for 915MHz carrier frequency

Figure 4-11 depicts how path loss increased along with separation distance changes when transmitter and receiver were at the same height under different plant canopy height (block) situations. The dashed line within each graph is free space loss. As shown in Figure 4-11, all path loss, except for the one measured from transmitter/receiver height 1(T1R1) in plant height 3, were lower than free space model. Paired samples t-tests were applied for comparing measured path loss to predicted path loss using free space model and plane earth model. Compared means and p-values are shown in Table 4-4.

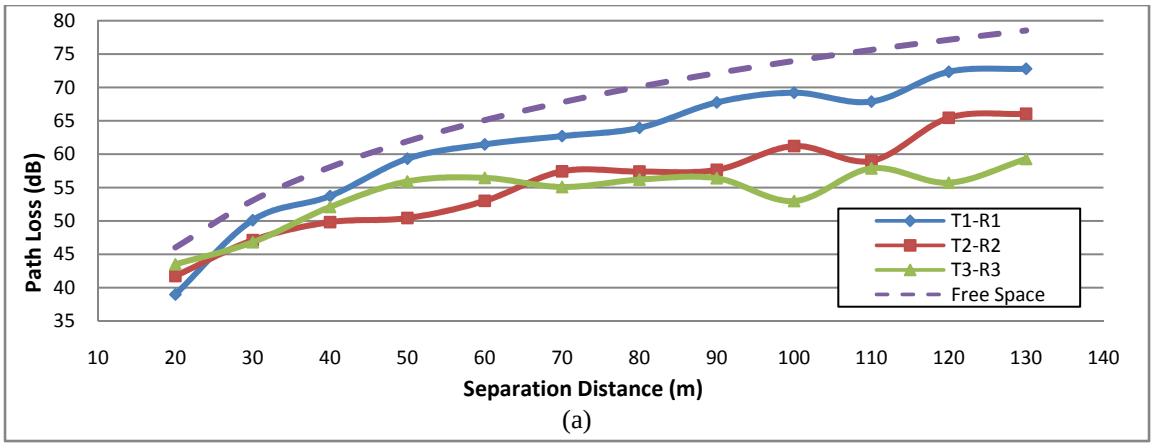

(a)

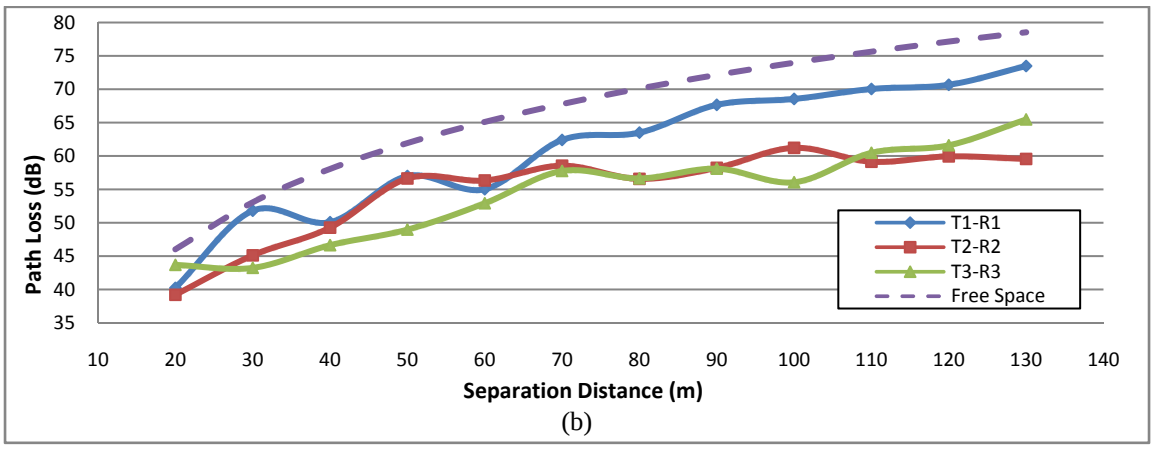

(b)

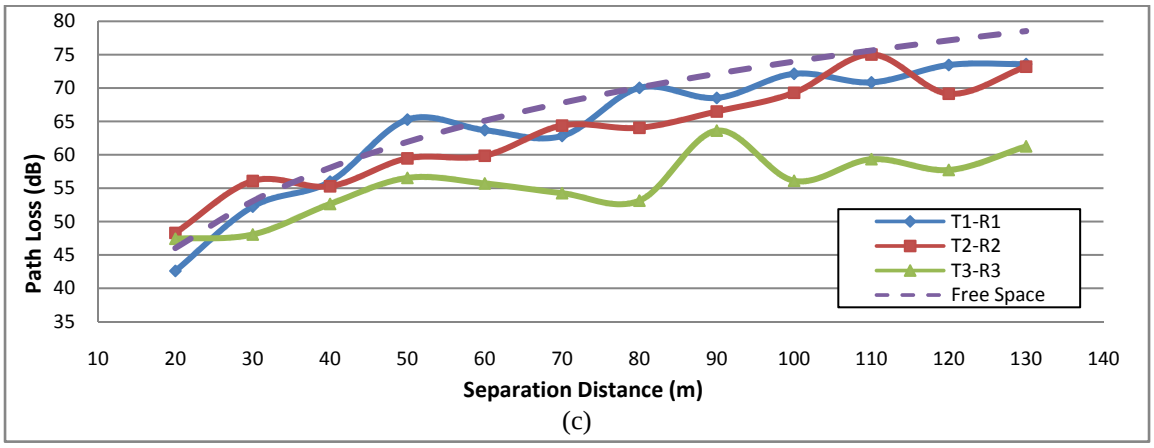

(c)

Figure 4-11 Path loss *vs*. separation distance for 915MHz carrier frequency under different plant and node heights. Tx-Rx stands for transmitter and receiver heights at xm. (a) plant height 1; (b) plant height 2; (c) plant height 3.

Table 4-4 Compared samples t-test result for analyzing impact on transmitter/receiver height under each plant height for 915MHz

Compared Pairs*	Plant Height 1		Plant Height 2		Plant Height 3	
	Mean (*dB*)	P-Value	Mean (*dB*)	P-Value	Mean (*dB*)	P-Value
T1R1-T2R2	6.1602	0.000	5.8897	0.002	0.8817	0.458
T1R1-T3R3	7.6666	0.001	6.5697	0.000	8.7850	0.001
T2R2-T3R3	1.5063	0.289	0.6799	0.552	7.9032	0.000
T1R1-FS	-4.9356	0.000	-5.7565	0.000	-2.3595	0.006
T2R2-FS	-11.0958	0.000	-11.6463	0.000	-3.2413	0.007
T3R3-FS	-12.6022	0.000	-12.3263	0.000	-11.144	0.000
T1R1-PE11	-10.9562	0.000	-11.7771	0.000	-8.3801	0.000
T2R2-PE22	-5.0752	0.000	-5.6257	0.001	2.7792	0.015
T3R3-PE33	0.4620	0.812	0.7379	0.525	1.9196	0.340

*TxRx stands for transmitter/receiver height at xm; PExx stands for plane earth loss from transmitter/receiver height xm/xm

From Table 4-4, the results indicated that: (1) All the mean differences were positive for compared pairs of path loss from lower node heights to higher heights, revealing that path loss changed inversely with the transmitter/receiver height. (2) All measured path loss were less than free space loss; (3) Measured path loss was less than the corresponding predicted plane earth loss under T1R1 in all plant heights and T2R2 in plant heights 1 and 2 but greater under T2R2 in plant height 3 and T3R3 in all plant heights.

Based on the p-values, results indicated that: (1) For plant heights 1 and 2, p-values from comparing path loss from T1R1 to other two transmitter/receiver heights were less than 0.005, reveling significant difference of path loss between T1R1 and T2R2 or T3R3. There is no significant difference between T2R2 and T3R3 in plant heights 1 and 2 since the p-values were 0.289 and 0.552. (2) For plant height 3, there is no significant difference between T1R1 and T2R2 but there is significant difference between T3R3 and the other two transmitter/receiver heights; (3) There is significant difference between

measured and *FS* loss. (4) There is significant difference between measured path loss and plane earth loss for T1R1 and T2R2 in all plant heights but no sig difference for T3R3 in all plant heights.

For 915MHz carrier frequency, path loss decreased when transmitter/receiver increased due to less attenuation introduced by both earth terrain and vegetation. Impacts from node height were similar in plant heights 1 and 2 when the Fresnel zone was blocked for T1R1but still clear for T2R2 and T3R3. This led to difference between T1R1 and the higher two node heights but similarity within the two higher node heights. In plant height 3, both T1R1 and T2R2 had obstacles inside their Fresnel zones but the zone for T3R3 was still clear. As a result, path loss patterns were similar for the lower two but different from the top one. It could be concluded that obstruction had more influence than reflection to path loss for 915MHz in-field communication. However, the effect of reflection could not be ignored since though the Fresnel zone is clear for T3R3 under all plant heights, measured path loss increased along with the plant growth, resulting in mean values from compared to *PE* loss increased from 0.462 to 1.919 while p-value decreased from 0.812 to 0.340 due to attenuation introduced by plant canopy reflection.

Impact of transmitter/receiver height on path loss for 2470MHz carrier frequency

Similar analysis was applied to path loss from using 2470MHz carrier frequency. Results are as shown in Figure 4-12 and Table 4-5. As shown in Figure 4-12, it is similar to results from using 915MHz carrier frequency that all path losses, except for the one measured under T3R3 in plant height 3, were lower than free space loss. The higher was the plant canopy, the closer that measured loss was to the predicted free space loss.

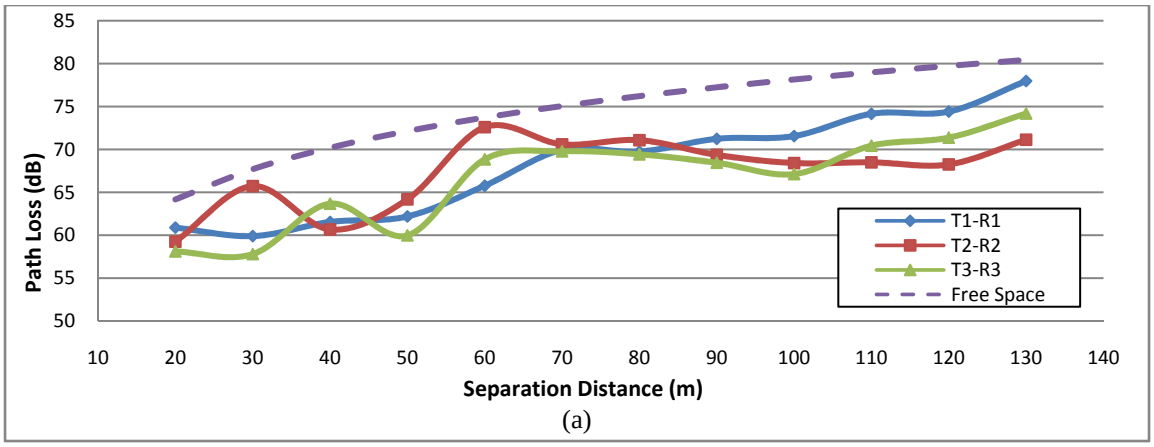

(a)

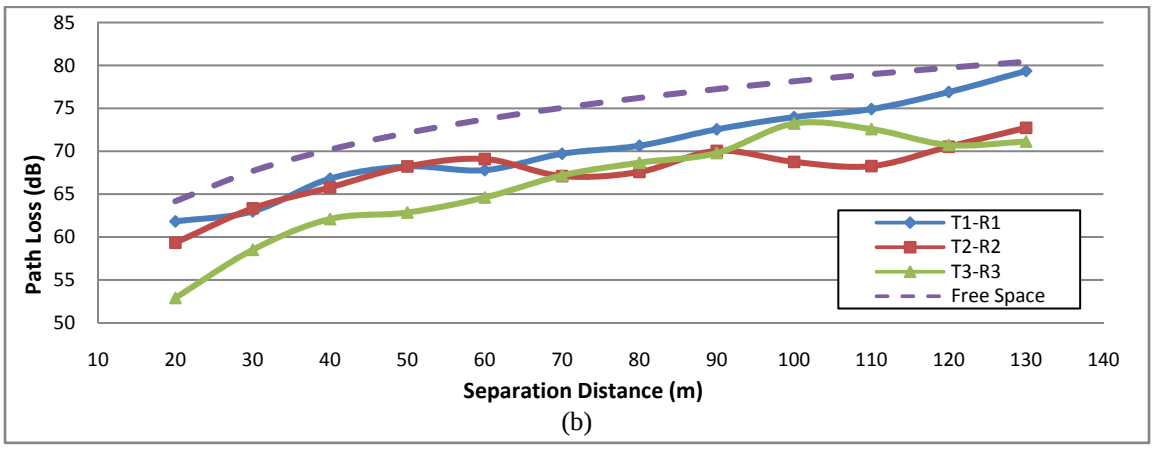

(b)

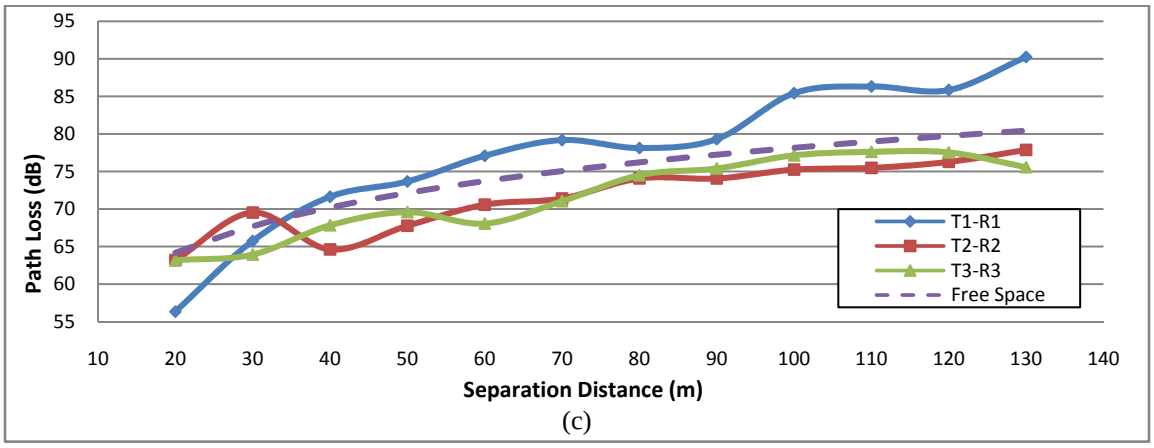

(c)

Figure 4-12 Path loss *vs*. separation distance for 2470MHz carrier frequency under different plant and node heights. Tx-Rx stands for transmitter and receiver heights at xm. (a) plant height 1; (b) plant height 2; (c) plant height 3.

Table 4-5 Compared samples t-test result for analyzing impact on transmitter/receiver height under each plant heights for 2470MHz

Compared Pairs	Plant Height 1		Plant Height 2		Plant Height 3	
	Mean	P-Value	Mean	P-Value	Mean	P-Value
T1R1-T2R2	0.7947	0.544	2.9079	0.004	5.7385	0.005
T1R1-T3R3	1.6761	0.033	4.2822	0.000	5.6302	0.004
T2R2-T3R3	0.8813	0.383	1.2891	0.322	-0.1083	0.883
T1R1-FS	-6.2003	0.000	-4.0020	0.000	2.9391	0.053
T2R2-FS	-6.9951	0.000	-6.9100	0.000	-2.7994	0.000
T3R3-FS	-7.8765	0.000	-8.2843	0.000	-2.6910	0.000
T1R1-PE11	-2.2202	0.148	-0.0219	0.989	6.9193	0.000
T2R2-PE22	9.0261	0.002	9.1113	0.000	13.2219	0.000
T3R3-PE33	15.1884	0.000	14.7806	0.001	20.3739	0.000

Analyzed using the means in Table 4-5, results from using 2470MHz carrier frequency were similar as those from using 915MHz as: (1) path loss changed inversely with transmitter/receiver heights except for rising from T2R2 to T3R3 in plant height 3; (2) All except for one measured path loss were less than the free space loss; (3) under each plant height, differences between measured and theoretical plane earth path loss inclined to increase along with the node height ascended.

Analyzed from the p-values, it could be seen that: (1) In plant height 1, there was no significant difference between adjacent node heights. In the other two plant heights, path loss from T2R2 was similar to that from T3R3 but the loss from T1R1 was different to the other two heights; (2) All measured loss, except for the one from T3R3 under plant height 3, were significantly different from free space loss; (3) Path loss from T1R1 in plant height 1 and 2 were similar to the plane earth loss while the rest of the measured loss were significantly different from the plane earth loss.

4.3.5 Impact of Plant Height on Path Loss

To study the effect of plant height on wireless signal path loss, results from the same data set for analyzing impacts of transmitter/receiver height were used. The experimental records were grouped by transmitter/receiver height.

Impact of plant height on path loss for 915MHz carrier frequency

Experimental results for 915MHz carrier frequency in Figure 4-13 and Table 4-6 indicated that:

(1) As from Table 4-6, all except two of the means from paired comparisons between measured path loss were negative, indicating that in general the higher the plant height, the more signal strength loss in accordance to the wheat growth. Plant height affected more obviously on T2R2 since there is a larger variation of the means from 0.5504 to -8.4049 than others'.

(2) All the paired means between measured path loss and FS loss were negative, indicating that the theoretical FS loss was higher than measured ones in all conditions within this scenario.

(3) For T1R1, all the paired means with PE yielded negative results, indicating all measured loss were lower than corresponding PE theoretical values; for T2R2, measured loss were still lower than PE values under plant height 1 and 2 but in plant 3 the measured loss became greater; for T3R3, all the measured loss were greater than the PE values.

(4) The p-values were greater than 0.05 for compared pairs of PH1-PH2 under each transmitter/receiver height, indicating little impact on path loss from plant height before PH2; p-values were less than 0.005 when path loss from PH3 were compared for both

B1H1 and B2H2 but B3H3, indicating plant height yielded more impact on path loss after PH2 for both T1R1 and T2R2; p-value decreased, though still greater than 0.05, for PH1-PH2 and PH2-PH3 under T3R3, indicating plant height has impacts, though not so obvious on path loss under T3R3.

(5) The p-values were less than 0.05 when comparing measured loss to PE loss for both T1R1 and T2R2 but greater for T3R3. The results were in consistency with the ones obtained from analyzing impacts of transmitter/receiver height that Fresnel zone dominates signal attenuation but effects from reflection pattern could not be ignored.

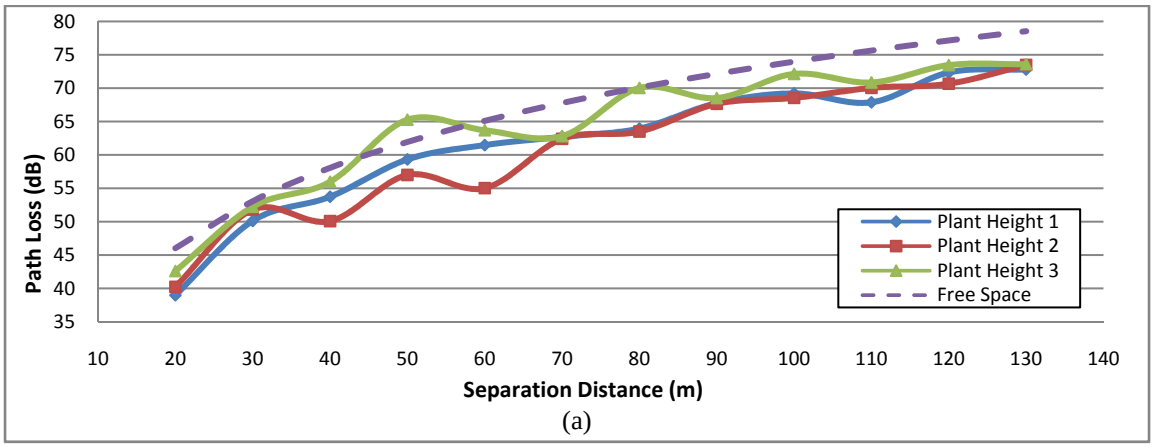

(a)

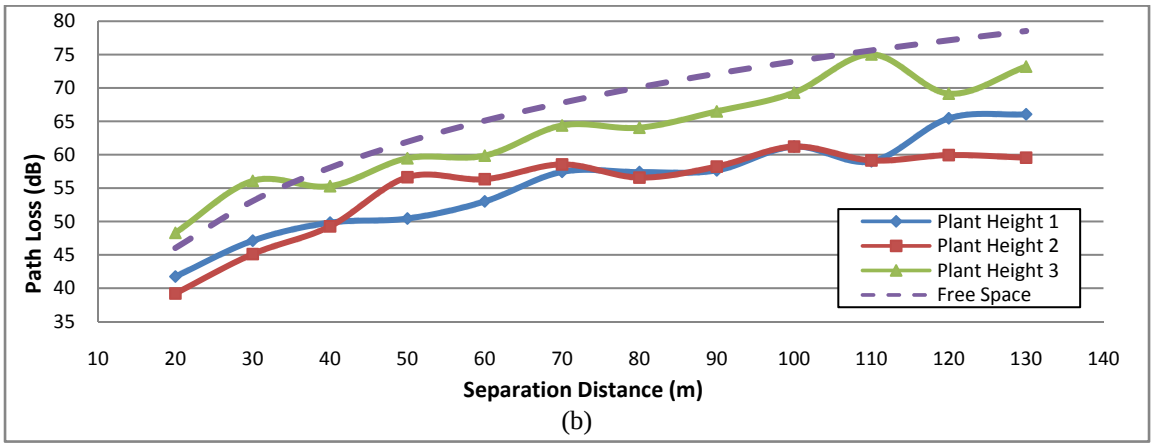

(b)

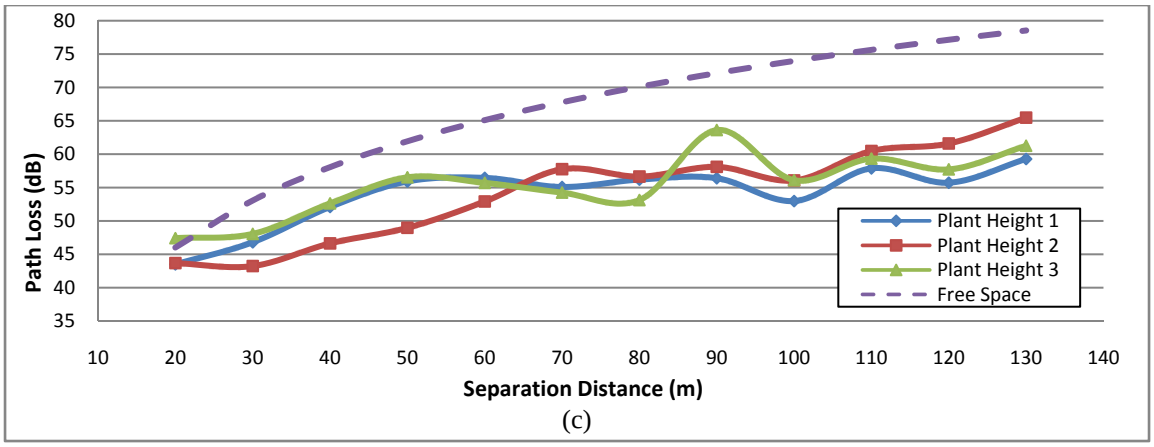

(c)

Figure 4-13 Path loss *vs*. separation distance for 915MHz carrier frequency under different plant and node heights. Plant Height x stands for plant height at the *x*th stage. Chart (a), (b) and (c) were obtained when transmitter/receiver heights were 1m, 2m and 3m, respectively.

Table 4-6 Compared samples t-test results for analyzing impact on plant height under each node height for 915MHz

Compared Pairs*	T1R1		T2R2		T3R3	
	Mean	P-Value	Mean	P-Value	Mean	P-Value
PH1-PH2	0.8209	0.268	0.5504	0.592	-0.2759	0.828
PH1-PH3	-2.5760	0.001	-7.8545	0.000	-1.4576	0.079
PH2-PH3	-3.3969	0.003	-8.4049	0.000	-1.1817	0.370
PH1-FS	-4.9356	0.000	-11.0958	0.000	-12.6022	0.000
PH2-FS	-5.7565	0.000	-11.6463	0.000	-12.3263	0.000
PH3-FS	-2.3595	0.006	-3.2413	0.007	-11.1445	0.000
PH1-PE	-10.9562	0.000	-5.0752	0.000	0.4620	0.812
PH2-PE	-11.7771	0.000	-5.6257	0.001	0.7379	0.525
PH3-PE	-8.3801	0.000	2.7792	0.015	1.9196	0.340

*PHx stands for plant height at xm; for T1R1, PE11 was used, for T2R2 it was PE22, for T3R3 it was PE33

Impact of plant height on path loss for 2470MHz carrier frequency

Experimental results for 2470MHz carrier frequency in Figure 4-14 and Table 4-7 indicated that:

(1) Eight out of nine paired means were negative which reflected that in general the path loss along with the wheat growth. Plant height affected no specialty on each group.

(2) All the paired means between measured path loss and FS loss were negative, indicating that the theoretical FS loss was higher than measured ones in all conditions within this scenario.

(3) In T1R1, measured loss were less than PE loss in plant height 1 and 2 but higher in plant height 3; in the other two groups, all measured loss were higher than corresponding PE loss.

(4) The p-values were greater than 0.05 for compared pairs of PH1-PH2 under T2R2 and T3R3 but less under T1R1, indicating little impact on path loss from plant height before PH2 for higher transmitter/receiver heights; p-values were less than 0.005 when path loss from PH3 were compared for all transmitter/receiver heights, indicating plant height yielded more impact on path loss after PH2; p-value was greater than 0.05 for PH1-PH2 and less than 0.05 for PH2-PH3 under T3R3, indicating PH2 was a threshold for plant height impacts in B3H3.

(5) The p-values were greater than 0.05 for comparing measured loss from PH1 and PH2 under T1R1 to PE loss, indicating no significant difference for these two pairs. It could be concluded from previous results that both reflection pattern and Fresnel zone clearance related to plant height had significant impacts on signal attenuation for lower transmitter/receiver height. When transmitter/receiver went higher, Fresnel zone clearance dominates the attenuation, which is in consistency with the results from using 915MHz carrier frequency.

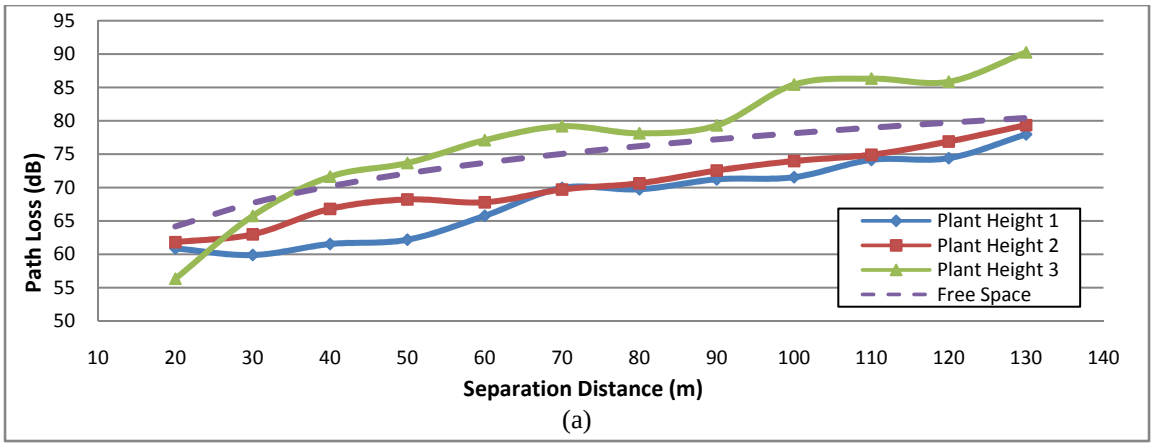

(a)

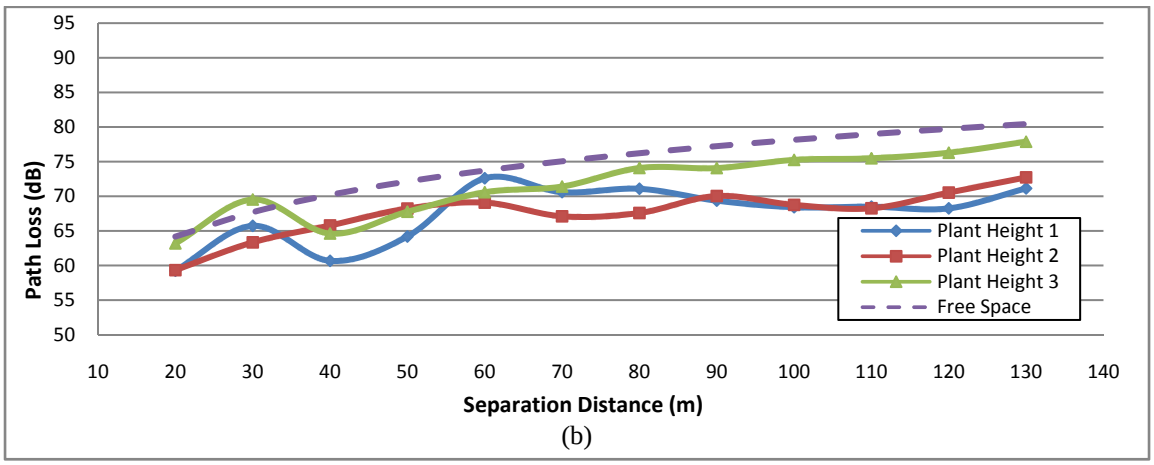

(b)

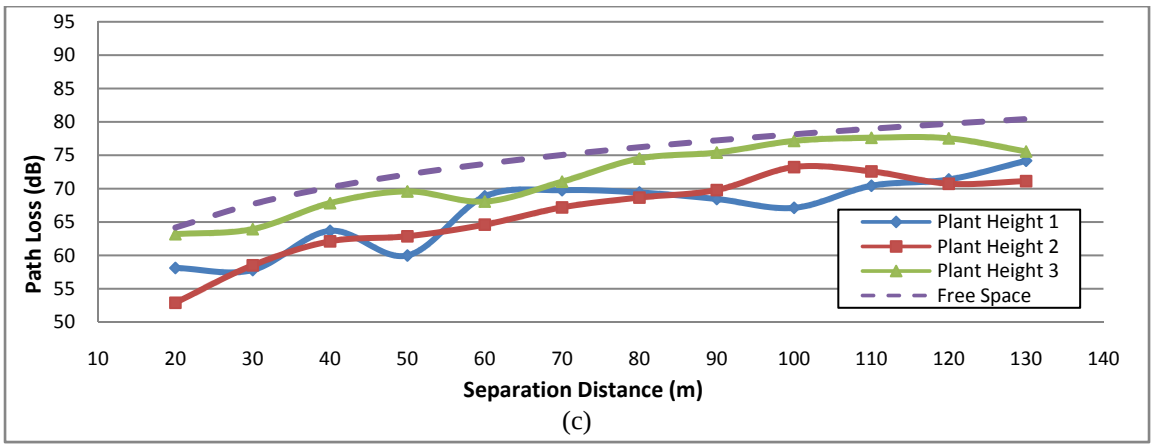

(c)

Figure 4-14 Path loss *vs*. separation distance for 2470MHz carrier frequency under different plant and node heights. Plant Height x stands for plant height at the *x*th stage. Chart (a), (b) and (c) were obtained when transmitter/receiver heights were 1m, 2m and 3m, respectively.

Table 4-7 Compared samples t-test result for analyzing impact on plant height under each node height for 2470MHz

Compared Pairs	T1R1		T2R2		T3R3	
	Mean	P-Value	Mean	P-Value	Mean	P-Value
PH1-PH2	-2.1982	0.002	-0.0851	0.921	0.4077	0.671
PH1-PH3	-9.1395	0.000	-4.1957	0.000	-5.1855	0.000
PH2-PH3	-6.9412	0.000	-4.1106	0.000	-5.5932	0.000
PH1-FS	-6.2003	0.000	-6.9951	0.000	-7.8765	0.000
PH2-FS	-4.0020	0.000	-6.9100	0.000	-8.2843	0.000
PH3-FS	2.9391	0.053	-2.7994	0.000	-2.6910	0.000
PH1-PE	-2.2202	0.148	9.0261	0.002	15.1884	0.000
PH2-PE	-0.0219	0.989	9.1113	0.001	14.7806	0.000
PH3-PE	6.9193	0.000	13.2219	0.000	20.3739	0.000

4.3.6 Multi-variable Path Loss Model Regression and Verification

Regressed model without plant height blocking

A regressed equation was obtained from combining the measured path loss at each plant height as:

$$PL(d) = 15.092 + 24.863\log_{10}(d) - 5.631\log_{10}(h_t) - 3.449\log_{10}(h_b) + 5.397G_b \quad (4.14)$$

Where *PL(d)* is the path loss in *dB*, *d* is the separation distance in m, h_b is the base height in m, h_t is the node height in m and G_b is base antenna gain in *dBi*. The R^2 for Equation 4.14 is 0.822. The influence of carrier frequency was excluded. The p-values were less than 0.000 for the rest factors as independents, indicating a high level of significance in the factors for offset, separation distance, base height, node height and base antenna gain.

Regressed model with plant height blocking

In this analysis, path loss from each plant height was applied separately and three equations each for one plant height were generated as:

(1) Regression model blocked inside plant height 1(Equation 4.15):

$$PL(d) = 18.897 + 22.216\log_{10}(d) - 7.171\log_{10}(h_b) + 5.071G_b \quad (4.15)$$

Where *PL(d)* is the path loss in *dB*, *d* is the separation distance in m, h_b is the node height in m and G_b is base antenna gain in *dBi*. The R^2 for Equation 4.15 is 0.810. The influence of node height and carrier frequency were excluded. The p-values were less than 0.000 for all the rest regression factors, indicating a high level of significance in the factors for offset, separation distance, base height and base antenna gain.

(2) Regression model blocked inside plant height 2 (Equation 4.16):

$$PL(d) = 12.147 + 26.239\log_{10}(d) - 7.529\log_{10}(h_t) + 4.808G_b \quad (4.16)$$

Where *PL(d)* is the path loss in *dB*, *f* is the carrier frequency in MHz, *d* is the separation distance in m, h_t is the base height in m and G_b is base antenna gain in *dBi*. The R^2 for Equation 4.16 is 0.843. The influence of carrier frequency and antenna gain were excluded. The p-values were less than 0.000 for all the rest regression factors, indicating a high level of significance in the factors for offset, separation distance, node height and antenna gain.

(3) Regression model blocked inside plant height 3 (Equation 4.17):

$$PL(d) = -80.369 + 31.674\log_{10}(f) + 26.363\log_{10}(d) - 2.484\log_{10}(h_b) - 8.438\log_{10}(h_t) \quad (4.17)$$

Where *PL(d)* is the path loss in *dB*, *d* is the separation distance in m, *f* is the carrier frequency in MHz, h_b is the base height in m, h_t is the node height in m, and G_b is base antenna gain in *dBi*. The R^2 for Equation 4.17 is 0.889. The influence of base antenna gain was excluded. The p-values were less than 0.000 for all the rest regression factors, indicating a high level of significance in the factors for offset, separation distance, base height, node height, and carrier frequency.

The R^2 for each individual blocked regression was 0.810, 0.843 and 0.889, respectively while the R^2 from regression of combining path loss under each plant height was 0.822. This indicated that there is less variation for individual equations inside each block within plant height 2 and 3 and it would be more precise to use the blocked regressions rather than the combined one for path loss prediction. The R^2 from models of taking multiple factors into consideration were higher than the ones from which only relating path loss to separation distance (0.790 and 0.601). This confirmed that distance alone was inadequate for predicting in-field path loss.

It could be seen from the three individual regressions that the first two for lower plant heights are more similar to plane earth model which ignores the influence of carrier frequency but takes node height into consideration. The one for plant height 3 is more likely as a combination of both free space and plane earth models since it takes both carrier frequency and node heights into consideration.

Model verification

Three sets of data taken at the "*verification spots*" under different plant height were used to verify the regressed model. Paired sample t-test was applied for comparing measured path loss to predicted loss from FS model, PE model, combined (COM) and individual regressed model (IND). Means and p-values for each comparison are shown in Table 4-8. In plant height 1, though all the predicted losses were statistically different from the measured loss (p-values<0.005), the mean difference between the measured loss and predicted loss from FS, PE, COM and IND were -6.3741, 4.9662, -1.7590, -1.8038 *dBm*, respectively, indicating that both types of the regressed models had less differences for path loss prediction than FS or PE models. In plant height 2 and 3, predicted loss from

regressed models yielded no significant difference from the measured ones (p-values>0.05). However, the least variation in plant height 3 came from comparing measured loss and predicted PE path loss, which is also in consistency with former conclusions that in plant height 3, PE model is suitable for path loss prediction.

Table 4-8 Results from paired sample t-tests for model verification

Compared Pairs*	Plant Height 1		Plant Height 2		Plant Height 3	
	Mean	P-Value	Mean	P-Value	Mean	P-Value
MS-FS	-6.3741	0.000	-9.6011	0.000	-9.8891	0.000
MS-PE	4.9662	0.000	7.8017	0.004	-0.3208	0.580
MS-COM	-1.7590	0.002	-0.1577	0.750	1.1268	0.169
MS-IND	-1.8038	0.001	-0.3876	0.512	0.7809	0.260

*MS: measured, FS: free space, PE: plane earth, COM: combined regression, IND: individual regression

4.3.7 Packet Reception Rate Analysis

Previous results indicated that signal attenuation alters in proportion to the separation distance and plant height but inversely with transmitter/receiver height. Consequently in the field experiments of this research, the scenario when both transmitter and receiver heights are 1m under plant height 3 should be the worst case and generates the highest signal attenuation along with the test path though using the maximum transmission power. Another extreme case is that both transmitter and receiver heights were 3m under plant height 1. This should be the best case and generates the least signal attenuation.

$N_{R.packet}$ for the best and worst cases was plotted in Figure 4-15. A threshold $T_{R.packet}$ was defined at the distance after which $\Delta N_{R.packet} > 50\%$.

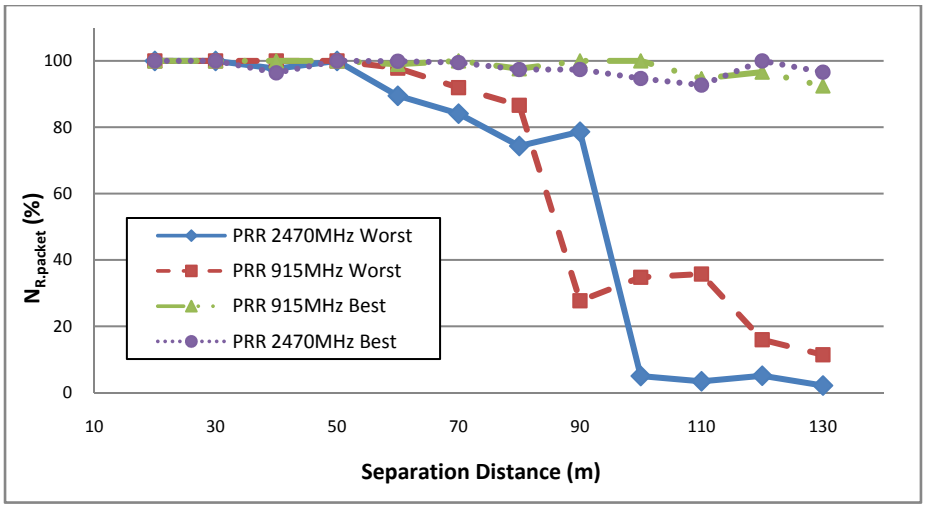

Figure 4-15 PDR vs. separation distance for both best and worst cases

As in Figure 4-15, $N_{R.packet}$ stayed stable above 95% for all cases until the separation distance arrived 50m. After that, curves from the worst case start to drop. $N_{R.packet}$ was above 80% within 70m in all scenarios including the plotted best and worst situations. In the best case, minimum *RSSs* were obtained at 130m as -92.9*dBm* for IRIS and -82.78*dBm* for cattle node using CC1010 radio. These *RSSs* were still higher than their receiving sensitivity as -101*dBm* and -107*dBm*. $N_{R.packet}$ in the best case stayed above 95% and $T_{R.packet}$ was larger than 130m for both kinds of nodes. In the worst case for IRIS, $N_{R.packet}$ dropped more than 50% along with separation distance increased from 90m to 100m where the *RSS* was -98.06*dBm* and -104.18*dBm*. As a result, $T_{R.packet}$ for IRIS in the worst case was 90m. For CC1010, $N_{R.packet}$ dropped more than 50% between 80m and 90m where the *RSS* was -92.02*dBm* and -93.53*dBm*. As a result, $T_{R.packet}$ for CC1010 in the worst case was 80m. Although $T_{R.packet}$ for IRIS was further than CC1010, $N_{R.packet}$ for CC1010 stayed higher before and after the drop. The minimum $N_{R.packet}$ achieved was 2.12% for IRIS and 11.4% for CC1010 at 130m.

We observed that $N_{R.packet}$ dropped to an un-acceptable level even the *RSS* was still above labeled receiving sensitivity. Since all *RSS* was obtained from the spectrum analyzer, it is quite possible that the node's radio design is worse than the analyzer's thus introduces more attenuation resulting lower actual received signal strength at the node than that displayed in the analyzer.

4.3.8 Limitations of the Current Path Loss Model

Radio propagation models are empirical in nature, which means, large groups of data has to be collected for developing. Due to time and research facility constraints, the collection of experimental data was not yet sufficiently large to provide enough probabilities (or enough scope) to all kind of environmental situations which can happen during wheat growth.

Similar to other empirical models, the developed regressed path loss models did not provide exact behavior of radio wave propagations in wheat field, rather, they only predict the most likely behavior the radio might exhibit under the specified conditions inside the wheat field where the experiments were carried out. To improve the robustness of the models, systematic field experiments are needed.

4.4 Conclusions

This research provides a systematic analysis of in-field wireless signal attenuation and path loss within a wheat growth season. The results have significance to provide a reference to the development and deployment of wireless sensor networks with optimized node density, distribution, flexibility and service quality.

From the field experiments, COST-Hata model yielded large differences and standard deviation between predicted and measured path loss. It is not suitable to analyze radio

wave propagation for a WSN used in wheat fields. The configuration and vegetation related parameters, including transmission distance, transmitter height, receiver height, carrier frequency, antenna gain and plant height, had significant impacts on signal attenuation during transmission. There was no significant difference between path loss under each transmitter/receiver height in stages of plant height 1 and 2 while there was significant difference between path loss in stages of plant height 2 and 3, indicated that the Fresnel zone clearance dominated signal attenuation concerning plant height. For in-field applications, a special regressed multi-variable model could be applied to predict path loss within different stages of wheat growth. Model improvements were achieved using plant heights as blocks to obtain separate models with R^2 as 0.810, 0.843, and 0.899, respectively. Comparisons of the predicted path loss from both widely accepted and specially regressed models to the measured path loss at both tested and verification spots showed that, in general, *FS* model generated the highest difference than the rests while *PE* model generated more difference than special regressed models. A separation distance of 70m could be considered the threshold for a reliable communication in the tested field layout. More repetitions will be in need for improving model accuracy.

References

Atmel, 2009. AVR Z-Link for IEEE 802.15.4 and ZigBee Applications. Available at: http://www.atmel.com/dyn/resources/prod_documents/doc7911.pdf. Accessed 2009.07.16

Beckwith, R., C. Teibel, P. Bowen. 2004. Report from the field: results from an agricultural wireless sensor network, Local Computer Networks. In *Proc.* 29th Annual IEEE International Conference, 471-478.

Bianchi, C.H. and K. Sivaprasad. 1998. A Channel Model for Multipath Interference on Terrestrial Line-of-sight Digital Radio. IEEE Transactions on Antennas and Propagation, 46(6): 891-901.

Crossbow Technology. 2004. IRIS Datasheet. Available at: http://www.xbow.com/Products/Product_pdf_files/Wireless_pdf/IRIS_Datasheet.pdf. Accessed 9 June 2009.

Dapper, M., J. Wells, T. Schwallie, L. Huon. 2003. RF propagation in short-range sensor communications. In *Proc.* of the SPIE Conference on Unattended Ground Sensor Technologies and Applications V, 5090:330-340. Orlando, FL, USA.

Friis, H.T.. 1946. A node on a simple transmission formula. *PROC. IRE,* 34.

Jackson ,T., K. Mansfield, M. Saafi, T. Colman, P. Romine. 2007. Measuring soil temperature and moisture using wireless MEMS sensors. *Journal of Measurement.* 41(4):381-390.

Li, L., P.Lk.T. Yeo, M. Leong.1998. Radio wave propagation along mixed paths through a four-layered model of rain forest: An analytic approach. *IEEE Transactions on Antennas and Propagation*. 46(7): 1098-1111.

Li, Z., N. Wang, A. Franzen, C. Godsey. 2008. Development of a Wireless Sensor Network for Field Soil Moisture Monitoring. ASABE Paper No. 083835. Rhode Island, Providence, USA.

Liu, H., Z.J. Meng, S.H. Cui. 2007. A Wireless Sensor Network Prototype for Environmental Monitoring in Greenhouses. Wireless Communications, Networking and Mobile Computing. In *Proc.* WiCom 2007 International Conference: 2344-2347.

Okamura, Y. 1968. Field strength and its variability in VHF and UHF land-mobile radio service. *Rev. Elec. Coom. Lab.* 9-10: 825-873.

Richter, J., R.F.S. Caldeirinha, M.O. Al-Nuaimi, A. Seville, N.C. Roggers, N. Savage. 2005. A generic narrowband model for radio wave propagation through vegetation. Vehicular Technology Conference, 1: 39-43.

Sadler, E.J., R.G. Evans, K.C. Stone, C.R. Camp. 2005. Opportunities for conservation with precision irrigation. *Journal of soil and water conservation*. 60(6): 371-379.

Sarkar, T. K., Z. Ji, K. Kim, A. Medouri, M. Salazar-Palma,. 2003. A Survey of Various Propagation Models for Mobile Communication. *IEEE Antennas and Propagation Magazine.* 45(3): 51-83.

Sizun, H.. 2005. Radio Wave Propagation for Telecommunication Applications. Springer-Verlag Berlin Heidelberg, Germany. Page 45-46.

Sheriff, R.E. 1996. Understanding the Fresnel Zone. Geophysical Corner. Available at: http://www.searchanddiscovery.net/documents/geophysical/sheriff/images/sheriff.pdf. Accessed 2009.07.09.

Thelen, J., D. Goense, K. Langendoen.2005. Radio wave propagation in potato fields. In First workshop on Wireless Network Measurements (co-located with WiOpt 2005). Rivadel Garda, Italy.

Tolle, G., J. Polastre, R. Szewczyk, D. Culler, N. Tuner, K. Tu, S. Burgess. 2005. A Macroscope in the Redwoods. Sensys ’05, 51-63. San Diego, Califonia, USA.

Vine, D.L., M. Karam. 1996. Dependence of attenuation in a vegetation canopy on frequency and plant water content. *IEEE Transactions on Geoscience and Remote Sensing.* 34(5): 1090-1096.

Wait, J.R.. 1974. Recent analytical investigations of electromagnetic ground wave propagation over inhomogeneous earth models. *Proceedings of the IEEE.* 62(8): 1061-1072.

CHAPTER V

CONCLUSIONS AND FUTURE WORK

The purpose of the author throughout the composition of this thesis was that, the design, development, deployment, and tests of applying WSN technology for in-situ, real-time soil property monitoring to be sufficiently explained to readers. Also, it is expected that the developed wheat field specific radio wave path-loss prediction models to be applicable for other in-field agricultural WSN communications with similar system configuration and environmental conditions. Though this thesis considered only a particular implementation of the in-field communication, it is hoped that the analytical process of impact factors' impacts on signal attenuation pattern can act as a guide for analyzing system communication performance in other agricultural and environmental WSN applications.

5.1 Conclusions

5.1.1 Soil Property Monitoring Systems

The problems of using wireless sensor network technology for unsupervised, in-field, and real-time soil property monitoring in terms of soil moisture content, soil electrical conductivity and near surface soil temperature have been successfully addressed in this thesis.

In order to measure, aggregate and transmit the monitored soil property parameters including soil moisture, soil electrical conductivity and near surface soil temperature through different tiers of networks and ultimately arrived the infrastructure facilities, wireless sensor networks demonstrated considerable advantages over other traditional supervised or invasive data collection methods. A Zigbee based wireless sensor network was selected for message communication for its capabilities as: a maximum communication distance of 300m under line-of-sight configuration, low-power consumption rate of 8mA per hour under 3.3V power supply for each node, enough bandwidth to support 16 channels in 5MHz frequency steps with 34dB or 36dB adjacent channel rejection, 250kbps high data transmission rate and the cost of each sensor node was around 1000 dollars, including sensors, data acquisition boards, WSN mote, and other accessories.

System QoS tests for the second generation WSN soil property monitoring system resulted: (1) the average packet delivery rate was 95%; (2) valid data rate ranged from 91% to 100% for different sensors on different sensor nodes and the majority of the valid data rates (48 out of 50) was higher than 97%; (3) the in-field data error rate was 0% during the field test in which 246 test packets was received and uploaded by the central node. The system's monitored soil property data reflected a trend in accordance with corresponding rain fall and average air temperature changes observed from MESONET

Soil moisture sensor (EC-5) calibration using soil samples taken from the WSN deployment field resulted that, though soil samples from different strips close to each other in physical locations yielded similar relationships between soil moisture content and sensor output, the saturation levels for different soil samples were different. R^2 of the

equations relating soil moisture content to sensor output though calibration were 0.958, 0.967, 0.962 and 0.977 for using soil obtained at three different in-field locations and using the averaged data, respectively.

5.1.2 In-field Radio Signal Path-loss Modeling

By statistically analyzing the experimental in-field radio path loss obtained in different stages of plant growth and comparing the measured readings to the corresponding theoretical values from using COST-Hata model, free space model and plane earth model, results indicated that: (1) the COST-Hata model yielded the highest difference between theoretical values and experimental readings, values from using the free space model came at the second place in difference while the values from using the plane earth model was similar to the measured readings in some situations; (2) plant canopy height had impacts on the signal propagation and attenuation patterns, during our experiments, plant height influenced more when the nodes were in lower vertical locations; (3) in general, Fresnel zone clearance acted as the major cause to signal attenuation but the influences of reflection patterns to signal attenuation could not be ignored.

One combined and three separate high performance multi-variable signal path-loss prediction models relating signal path loss to impact factors based on different stages of plant canopy height which in return reflecting different signal attenuation patterns were regressed and verified using the experimental readings. R^2 for the four models are: 0.822, 0.810, 0.843, and 0.899, respectively. Statistical analysis results indicated that the predicted path loss from using these multi-variable models yielded no significant difference to the measured path loss under wheat growing stages 2 and 3 while under stage 1 the difference between predicted path loss from our own models and the

measured path loss was much lower than the difference between predicted path loss from using free space or plane model and the measured loss.

Finally, by analyzing the packet delivery rate changing patterns, it was found that when both of the transmitter and receiver were kept at 3m above ground and the plant height was lower than 0.05m, the packet delivery rate for both kinds of the nodes were still above 95% at the maximum tested separation distance of 130m. However, when both of the transmitter and receiver were kept at 1m above ground and the plant height was higher than 0.4m, a 50% drop of the packet reception rate happened at 90m for cattle node using 915MHz carrier frequency and 80m for IRIS mote using 2470MHz carrier frequency. As a result, a separation distance of 70m was put forward as the threshold for reliable wireless communication in our soil property monitoring WSN field layout.

5.2 Future Work

5.2.1 Soil Property Monitoring System

Improvements could be made to the current configuration of the soil property monitoring system in relation to the following points:

(1) To enable the in-field WSN with multi-hop abilities between nodes upgrade the current system topology from “star” to “mesh” for longer message transmission range thus larger monitored areas;

(2) To make more reliable and intelligent communication protocols so that sensor nodes inside the field could maintain good communication with each other while fall asleep most of the time for energy conservation;

(3) To add handshaking and acknowledgement protocols for the on-going communication between sensor node and both central node or base station to handle the potential packet loss problem;

(4) To add more data fields to the TinyOS PDU for enabling the in-field WSN system with extension abilities to enlarge the monitoring areas with more nodes forming clusters and meshes based on physical in-field locations; and

(5) To improve web-based data accessing interfaces for researchers to utilize the monitored soil property data.

5.2.2 Radio Path Loss Predicting Model

The current regressed path loss predicting models have proved to be sufficient for the purpose of in-field signal strength predicting. However, additional improvements could be considered as follows:

(1) To measure path loss in more repetitions under impacts from equal impact factors as the previous experiments to increase predicting accuracy;

(2) To include more influencing factors such as plant biomass, relative humidity to the in-field radio signal attenuation; and

(3) To include more values for each impact factors and measure the corresponding introduced path loss to recognize more detailed in-field signal propagation patterns.

5.2.3 Other Related Research

Other future work related to the studies within this thesis may as follows:

(1) To carry out soil specific electrical conductivity and volume metric water content calibration for the EC-TE soil property sensor; and

(2) To relate the soil property sensors' monitoring results to the plant growth performance.

VITA

Zhen LI

Candidate for the Degree of

Master of Science

Thesis: DEVELOPMENT OF WIRELESS SENSOR NETWORK TECHNOLOGY FOR SOIL PROPERTY MONITORING

Major Field: Biosystems Engineering

Biographical:

Personal Data: Born in Guangzhou, Guangdong, China on August 16, 1981

Education:
Completed the requirements for the Master of Science in Biosystems Engineering at Oklahoma State University, Stillwater, Oklahoma in July, 2009.

Completed the requirements for the Bachelor of Engineering in Telecommunication at South China Agricultural University, Guangzhou, Guangdong, China in July, 2004.

Studying for Master of Engineering and Ph.D of Engineering degree in Agricultural Electrification and Automation at South China Agricultural University, Guangzhou, Guangdong, China from September, 2004 to June, 2007.

Experience:

Professional Memberships:

ASABE Student Member

Name: Zhen Li Date of Degree: July 24, 2009

Institution: Oklahoma State University Location: Stillwater, Oklahoma

Title of Study: DEVELOPMENT OF WIRELESS SENSOR NETWORK TECHNOLOGY FOR SOIL PROPERTY MONITORING

Pages in Study: 140 Candidate for the Degree of Master of Science

Major Field: Biosystems Engineering

Scope and Method of Study:
In the first part of this thesis, we designed and developed a soil property monitoring system with two generation evolutions. Soil property parameter data including soil moisture, soil electrical conductivity and near-surface soil temperature were collected from using two kinds of sensors embedded in four different depths as 50.8, 152.4, 304.8 and 609.6mm underground. A hybrid sensor network (HSN) conceptual system module including in-field wireless sensor network, cellular network and the Internet was put forward and realized for transmitting in-field data to the lab infrastructure. In the second part of this thesis, outdoor as well as off-line laboratory statistical experiments were carried out for analyzing impacts of impact factors as plant height, antenna gain, transmitter & receiver height, and separation distance to in-field radio propagation and modeling radio wave path loss to make the communication performance predictable. The experiments were divided into three blocks by two plant heights as 0.05m and 0.4m. Three widely used path loss models as COST-Hata, free space and plane earth models were included for verifying their applicability for in-field scenarios. Multi-variable linear regression was applied for relating the path loss to the impact factors.

Findings and Conclusions:
Results from the first part of the thesis indicated that wireless sensor network technologies had considerable advantages in field data collection and transmission over the traditional invasive methods. System quality of service testing results as: the average packet delivery rate and in-field data error rate were 95.05% and 0% until day of test while the averaged valid data rate was above 97% in general for each node. Results from the second part of the thesis indicated that the blocking criteria selection was proper and the Fresnel clearance dominated the in-field radio wave attenuation while the influence of reflection patterns was non-ignorable. R^2 for the four regressed path loss prediction model was 0.822, 0.810, 0.843, and 0.899, respectively. By comparing measured path loss to predicted ones using general and regressed models, COST-Hata model yielded the highest difference, free space model yielded the second highest difference, and specific regressed models generated the least difference in most cases. A threshold of 70m was obtained for reliable communication in the worst cases of our experimental scenarios.

ADVISER'S APPROVAL: Ning Wang

0.5 Ω CMOS 1.65 V TO 3.6 V 4-Channel Multiplexer

ADG804

FEATURES

0.5 Ω typical on resistance
0.8 Ω maximum on resistance at 125°C
1.65 V to 3.6 V operation
Automotive temperature range: –40°C to +125°C
High current carrying capability: 300 mA continuous
Rail-to-rail switching operation
Fast switching times <25 ns
Typical power consumption (<0.1 µW)

APPLICATIONS

MP3 players
Power routing
Battery-powered systems
PCMCIA cards
Cellular phones
Modems
Audio and video signal routing
Communication systems

GENERAL DESCRIPTION

The ADG804 is a low voltage 4-channel CMOS multiplexer comprising four single channels. This device offers ultralow on resistance of less than 0.8 Ω over the full temperature range. The digital inputs can handle 1.8 V logic with a 2.7 V to 3.6 V supply.

The ADG804 switches one of four inputs to a common output, D, as determined by the 3-bit binary address lines, A0, A1, and EN. A Logic 0 on the EN pin disables the device. The ADG804 has break-before-make switching.

The ADG804 is fully specified for 3.3 V, 2.5 V, and 1.8 V supply operation. It is available in a 10-lead MSOP package.

FUNCTIONAL BLOCK DIAGRAM

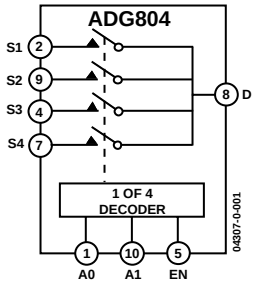

Figure 1.

PRODUCT HIGHLIGHTS

1. <0.8 Ω over full temperature range of –40°C to +125°C.
2. Single 1.65 V to 3.6 V operation.
3. Operational with 1.8 V CMOS logic.
4. High current handling capability (300 mA continuous current at 3.3 V).
5. Low THD + N (0.02% typ).
6. Small 10-lead MSOP package.

Rev. 0

One Technology Way, P.O. Box 9106, Norwood, MA 02062-9106, U.S.A.
Tel: 781.329.4700 **www.analog.com**
Fax: 781.326.8703

TABLE OF CONTENTS

REVISION HISTORY

Revision 0: Initial Version

SPECIFICATIONS

V_{DD} = 2.7 V to 3.6 V, GND = 0 V, unless otherwise noted.[1]

Table 1.

Parameter	+25°C	−40°C to +85°C	−40°C to +125°C	Unit	Test Conditions/Comments
ANALOG SWITCH					
Analog Signal Range			0 V to V_{DD}	V	
On Resistance (R_{ON})	0.5			Ω typ	V_{DD} = 2.7 V; V_S = 0 V to V_{DD}, I_S = 10 mA; Figure 18
	0.65	0.75	0.8	Ω max	
On Resistance Match between	0.04			Ω typ	V_{DD} = 2.7 V; V_S = 0.65 V, I_S = 10 mA
Channels (ΔR_{ON})		0.075	0.08	Ω max	
On Resistance Flatness ($R_{FLAT(ON)}$)	0.1			Ω typ	V_{DD} = 2.7 V; V_S = 0 V to V_{DD},
		0.15	0.16	Ω max	I_S = 10 mA
LEAKAGE CURRENTS					V_{DD} = 3.6 V
Source Off Leakage I_S (OFF)	±0.1			nA typ	V_S = 0.6 V/3.3 V; V_D = 3.3 V/0.6 V; Figure 19
	±1			nA max	
Drain Off Leakage I_D (OFF)	±0.1			nA typ	V_S = 0.6 V/3.3 V; V_D = 3.3 V/0.6 V; Figure 19
	±1			nA max	
Channel On Leakage I_D, I_S (ON)	±0.1			nA typ	V_S = V_D = 0.6 V or 3.3 V; Figure 20
	±1			nA max	
DIGITAL INPUTS					
Input High Voltage, V_{INH}			2	V min	
Input Low Voltage, V_{INL}			0.8	V max	
Input Current I_{INL} or I_{INH}	0.005			μA typ	V_{IN} = V_{INL} or V_{INH}
			±0.1	μA max	
C_{IN}, Digital Input Capacitance	4			pF typ	
DYNAMIC CHARACTERISTICS[2]					
$t_{TRANSISTION}$	24			ns typ	R_L = 50 Ω, C_L = 35 pF
	30	32	35	ns max	V_S = 1.5 V/0 V; Figure 21
t_{ON} ENABLE	23			ns typ	R_L = 50 Ω, C_L = 35 pF
	29	30	31	ns max	V_S = 1.5 V/0 V; Figure 23
t_{OFF} ENABLE	5			ns typ	R_L = 50 Ω, C_L = 35 pF
	6	7	8	ns max	V_S = 1.5 V; Figure 23
Break-Before-Make Time Delay (t_{BBM})	20			ns typ	R_L = 50 Ω, C_L = 35 pF
			5	ns min	V_{S1} = V_{S2} = 1.5 V; Figure 22
Charge Injection	28			pC typ	V_S = 1.5 V, R_S = 0 Ω, C_L = 1 nF; Figure 24
Off Isolation	−67			dB typ	R_L = 50 Ω, C_L = 5 pF,f = 100 kHz; Figure 25
Channel-to-Channel Crosstalk	−75			dB typ	R_L = 50 Ω, C_L = 5 pF, f = 100 kHz; Figure 27
Total Harmonic Distortion (THD+N)	0.02			%	R_L = 32 Ω, f = 20 Hz to 20 kHz, V_S = 2 V p-p
Insertion Loss	0.06			dB typ	R_L = 50 Ω, C_L = 5 pF, f = 100 kHz
−3 dB Bandwidth	33			MHz typ	R_L = 50 Ω, C_L = 5 pF; Figure 26
C_S (OFF)	24			pF typ	
C_D (OFF)	105			pF typ	
C_D, C_S (ON)	125			pF typ	
POWER REQUIREMENTS					V_{DD} = 3.6 V
I_{DD}	0.003			μA typ	Digital inputs = 0 V or 3.6 V
		1.0	4	μA max	

[1] Temperature range, Y version: −40°C to +125°C.
[2] Guaranteed by design, not subject to production test.

V_{DD} = 2.5 V ± 0.2 V, GND = 0 V, unless otherwise noted.[1]

Table 2.

Parameter	+25°C	−40°C to +85°C	−40°C to +125°C	Unit	Test Conditions/Comments
ANALOG SWITCH					
Analog Signal Range			0 V to V_{DD}	V	
On Resistance (R_{ON})	0.65			Ω typ	V_{DD} = 2.3 V; V_S = 0 V to V_{DD}, I_S = 10 mA; Figure 18
	0.77	0.8	0.88	Ω max	
On Resistance Match between	0.4			Ω typ	V_{DD} = 2.3 V; V_S = 0.7 V; I_S = 10 mA
Channels (ΔR_{ON})		0.08	0.085	Ω max	
On Resistance Flatness ($R_{FLAT(ON)}$)	0.16			Ω typ	V_{DD} = 2.3 V; V_S = 0 V to V_{DD}; I_S = 10 mA
		0.23	0.24	Ω max	
LEAKAGE CURRENTS					V_{DD} = 2.7 V
Source Off Leakage I_S (OFF)	±0.1			nA typ	V_S = 0.6 V/2.4 V, V_D = 2.4 V/0.6 V; Figure 19
	±1			nA max	
Drain Off Leakage I_D (OFF)	±0.1			nA typ	V_S = 0.6/2.4 V, V_D = 2.4/0.6 V; Figure 19
	±1			nA max	
Channel On Leakage I_D, I_S (ON)	±0.1			nA typ	V_S = V_D = 0.6 V or 2.4 V; Figure 20
	±1			nA max	
DIGITAL INPUTS					
Input High Voltage, V_{INH}			1.7	V min	
Input Low Voltage, V_{INL}			0.7	V max	
Input Current I_{INL} or I_{INH}	0.005			μA typ	V_{IN} = V_{INL} or V_{INH}
			±0.1	μA max	
C_{IN}, Digital Input Capacitance	4			pF typ	
DYNAMIC CHARACTERISTICS[2]					
$T_{TRANSISTION}$	25			ns typ	R_L = 50 Ω, C_L = 35 pF
	31	33	35	ns max	V_S = 1.5 V/0 V; Figure 21
t_{ON} ENABLE	25			ns typ	R_L = 50 Ω, C_L = 35 pF
	30	32	34	ns max	V_S = 1.5 V/0 V; Figure 22
t_{OFF} ENABLE	5			ns typ	R_L = 50 Ω, C_L = 35 pF
	7	8	9	ns max	V_S = 1.5 V; Figure 22
Break-Before-Make Time Delay (t_{BBM})	20			ns typ	R_L = 50 Ω, C_L = 35 pF
			5	ns min	V_{S1} = V_{S2} = 1.5 V; Figure 22
Charge Injection	20			pC typ	V_S = 1.25 V, R_S = 0 Ω, C_L = 1 nF; Figure 24
Off Isolation	−67			dB typ	R_L = 50 Ω, C_L = 5 pF, f = 100 kHz; Figure 25
Channel-to-Channel Crosstalk	−75			dB typ	R_L = 50 Ω, C_L = 5 pF, f = 100 kHz; Figure 27
Total Harmonic Distortion (THD + N)	0.022			%	R_L = 32 Ω, f = 20 Hz to 20 kHz, V_S = 1.5 V p-p
Insertion Loss	−0.06			dB typ	R_L = 50 Ω, C_L = 5 pF, f = 100 kHz
−3 dB Bandwidth	33			MHz typ	R_L = 50 Ω, C_L = 5 pF; Figure 26
C_S (OFF)	25			pF typ	
C_D (OFF)	110			pF typ	
C_D, C_S (ON)	128			pF typ	
POWER REQUIREMENTS					V_{DD} = 2.7 V
I_{DD}	0.003			μA typ	Digital inputs = 0 V or 2.7 V
		1	4	μA max	

[1] Temperature range, Y version: −40°C to +125°C.
[2] Guaranteed by design, not subject to production test.

V_{DD} = 1.65 V ± 1.95 V, GND = 0 V, unless otherwise noted.[1]

Table 3.

Parameter	+25°C	−40°C to +85°C	−40°C to +125°C	Unit	Test Conditions/Comments
ANALOG SWITCH					
Analog Signal Range			0 V to V_{DD}	V	
On Resistance (R_{ON})	1			Ω typ	V_{DD} = 1.8 V; V_S = 0 V to V_{DD}, I_S = 10 mA
	1.4	2.2	2.2	Ω max	
	2.2	4	4	Ω max	V_{DD} = 1.65 V, V_S = 0 V to V_{DD}, I_S = 10 mA; Figure 18
On Resistance Match between Channels (ΔR_{ON})	0.1			Ω typ	V_{DD} = 1.65 V, V_S = 0.7 V, I_S = 10 mA
LEAKAGE CURRENTS					V_{DD} = 1.95 V
Source Off Leakage I_S (OFF)	±0.1			nA typ	V_S = 0.6 V/1.65 V, V_D = 1.65 V/0.6 V;
	±1			nA max	Figure 19
Drain Off Leakage I_D (OFF)	±0.1			nA typ	V_S = 0.6/1.65 V, V_D = 1.65/0.6 V;
	±1			nA max	Figure 19
Channel On Leakage I_D, I_S (ON)	±0.1			nA typ	V_S = V_D = 0.6 V or 1.65 V; Figure 20
	±1			nA max	
DIGITAL INPUTS					
Input High Voltage, V_{INH}			0.65 V_{DD}	V min	
Input Low Voltage, V_{INL}			0.35 V_{DD}	V max	
Input Current I_{INL} or I_{INH}	0.005			μA typ	V_{IN} = V_{INL} or V_{INH}
			±0.1	μA max	
C_{IN}, Digital Input Capacitance	4			pF typ	
DYNAMIC CHARACTERISTICS[2]					
$t_{TRANSITION}$	32			ns typ	R_L = 50 Ω, C_L = 35 pF
	40	42	44	ns max	V_S = 1.5 V/0 V; Figure 21
t_{ON} ENABLE	34			ns typ	R_L = 50 Ω, C_L = 35 pF
	39	40	41	ns max	V_S = 1.5 Ω/0 V; Figure 22
t_{OFF} ENABLE	8			ns typ	R_L = 50 Ω, C_L = 35 pF
	10	11	13	ns max	V_S = 1.5 V; Figure 22
Break-Before-Make Time Delay (t_{BBM})	22			ns typ	R_L = 50 Ω, C_L = 35 pF
			5	ns min	V_{S1} = V_{S2} = 1 V; Figure 22
Charge Injection	12			pC typ	V_S = 1 V, R_S = 0 V, C_L = 1 nF; Figure 24
Off Isolation	−67			dB typ	R_L = 50 Ω, C_L = 5 pF, f = 100 kHz; Figure 25
Channel-to-Channel Crosstalk	−75			dB typ	R_L = 50 Ω, C_L = 5 pF, f = 100 kHz, Figure 27
Total Harmonic Distortion (THD + N))	0.14			%	R_L = 32 Ω, f = 20 Hz to 20 kHz, V_S = 1.2 V p-p
Insertion Loss	0.08			dB typ	R_L = 50 Ω, C_L = 5 pF, f = 100 kHz
−3 dB Bandwidth	30			MHz typ	R_L = 50 Ω, C_L = 5 pF; Figure 26
C_S (OFF)	26			pF typ	
C_D (OFF)	115			pF typ	
C_D, C_S (ON)	130			pF typ	
POWER REQUIREMENTS					V_{DD} = 1.95 V
I_{DD}	0.003			μA typ	Digital inputs = 0 V or 1.95 V
		1.0	4	μA max	

[1] Temperature range, Y version: −40°C to +125°C.
[2] Guaranteed by design, not subject to production test.

ABSOLUTE MAXIMUM RATINGS

T_A = 25°C, unless otherwise noted.

Table 4.

Parameter	Rating
V_{DD} to GND	−0.3 V to +4.6 V
Analog Inputs[1]	−0.3 V to V_{DD} + 0.3 V
Digital Inputs[1]	−0.3 V to +4.6 V or 10 mA, whichever occurs first
Peak Current, S or D	(Pulsed at 1 ms, 10% Duty Cycle Max)
3.3 V Operation	500 mA
2.5 V Operation	460 mA
1.8 V Operation	420 mA
Continuous Current, S or D	
3.3 V Operation	300 mA
2.5 V Operation	275 mA
1.8 V Operation	250 mA
Operating Temperature Range	
Automotive (Y Version)	−40°C to +125°C
Storage Temperature Range	−65°C to +150°C
Junction Temperature	150°C
MSOP Package	
θ_{JA} Thermal Impedance	206°C/W
θ_{JC} Thermal Impedance	44°C/W
IR Reflow, Peak Temperature <20 sec	235°C

[1] Overvoltages at IN, S, or D are clamped by internal diodes. Current should be limited to the maximum ratings given.

Stresses above those listed under Absolute Maximum Ratings may cause permanent damage to the device. This is a stress rating only; functional operation of the device at these or any other conditions above those listed in the operational sections of this specification is not implied. Exposure to absolute maximum rating conditions for extended periods may affect device reliability. Only one absolute maximum rating may be applied at any one time.

Table 5. ADG804 Truth Table

A1	A0	EN	ON Switch
x	x	0	None
0	0	1	S1
0	1	1	S2
1	0	1	S3
1	1	1	S4

ESD CAUTION

ESD (electrostatic discharge) sensitive device. Electrostatic charges as high as 4000 V readily accumulate on the human body and test equipment and can discharge without detection. Although this product features proprietary ESD protection circuitry, permanent damage may occur on devices subjected to high energy electrostatic discharges. Therefore, proper ESD precautions are recommended to avoid performance degradation or loss of functionality.

PIN CONFIGURATION

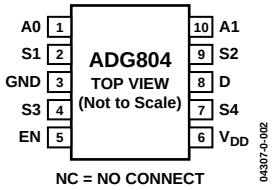

Figure 2. 10-Lead MSOP (RM-10)

Table 6. Terminology

V_{DD}	Most positive power supply potential.
I_{DD}	Positive supply current.
GND	Ground (0 V) reference.
S	Source terminal. May be an input or an output.
D	Drain terminal. May be an input or an output.
EN	Active high logic control input.
A0, A1	Logic control inputs. Used to select which source terminal, S1 to S4, is connected to the drain, D.
V_D, V_S	Analog voltage on terminals D, S.
R_{ON}	Ohmic resistance between D and S.
$R_{FLAT (ON)}$	Flatness is defined as the difference between the maximum and minimum value of on resistance as measured over the specified analog signal range.
ΔR_{ON}	On resistance match between any two channels.
I_S (OFF)	Source leakage current with the switch off.
I_D (OFF)	Drain leakage current with the switch off.
I_D, I_S (ON)	Channel leakage current with the switch on.
V_{INL}	Maximum input voltage for Logic 0.
V_{INH}	Minimum input voltage for Logic 1.
I_{INL} (I_{INH})	Input current of the digital input.
C_S (OFF)	Off switch source capacitance. Measured with reference to ground.
C_D (OFF)	Off switch drain capacitance. Measured with reference to ground.
C_D, C_S (ON)	On switch capacitance. Measured with reference to ground.
C_{IN}	Digital input capacitance.
t_{ON} (EN)	Delay time between the 50% and the 90% points of the digital input and switch on condition.
t_{OFF} (EN)	Delay time between the 50% and the 90% points of the digital input and switch off condition.
$t_{TRANSITION}$	Delay time between the 50% and the 90% points of the digital input and switch on condition when switching from one address state to the other.
t_{BBM}	On or off time measured between the 80% points of both switches when switching from one to another.
Charge Injection	A measure of the glitch impulse transferred from the digital input to the analog output during on-off switching.
Off Isolation	A measure of unwanted signal coupling through an off switch.
Crosstalk	A measure of unwanted signal which is coupled through from one channel to another as a result of parasitic capacitance.
−3 dB Bandwidth	The frequency at which the output is attenuated by 3 dB.
On Response	The frequency response of the on switch.
Insertion Loss	The loss due to the on resistance of the switch.
THD + N	The ratio of the harmonic amplitudes plus noise of a signal to the fundamental.

TYPICAL PERFORMANCE CHARACTERISTICS

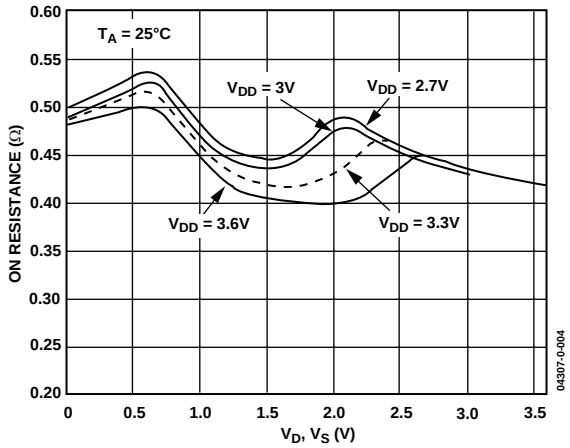

Figure 3. On Resistance vs. V_D (V_S) V_{DD} = 2.7 V to 3.6 V

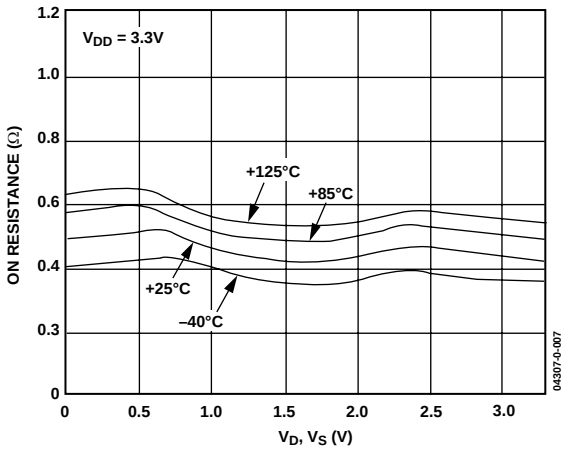

Figure 6. On Resistance vs. V_D (V_S) for Different Temperature, V_{DD} = 3.3 V

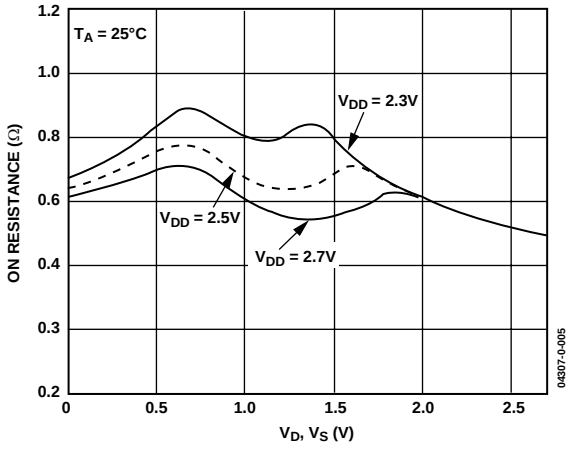

Figure 4. On Resistance vs. V_D (V_S) V_{DD} = 2.5 V ± 0.2 V

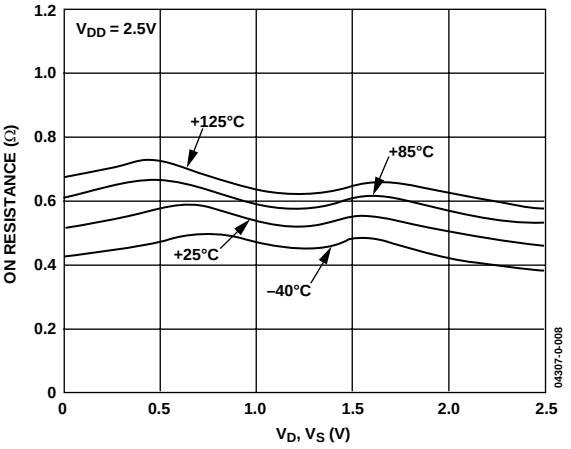

Figure 7. On Resistance vs. V_D (V_S) for Different Temperature, V_{DD} = 2.5 V

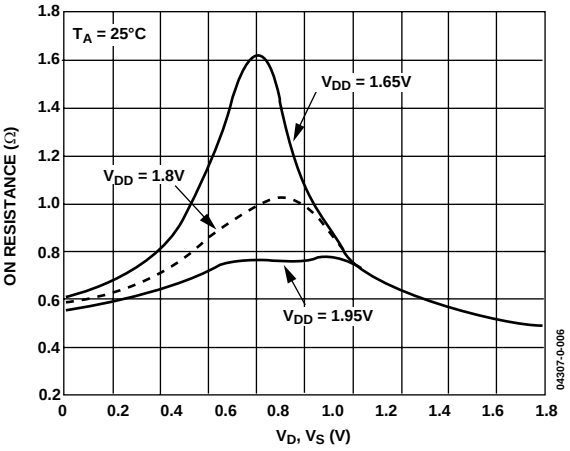

Figure 5. On Resistance vs. V_D (V_S) V_{DD} = 1.8 ± 0.15 V

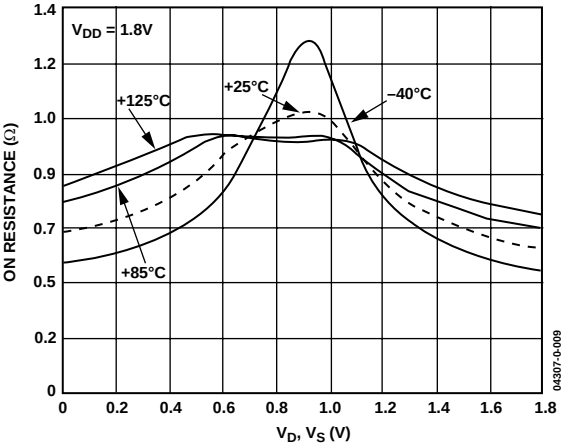

Figure 8. On Resistance vs. V_D (V_S) for Different Temperature, V_{DD} = 1.8 V

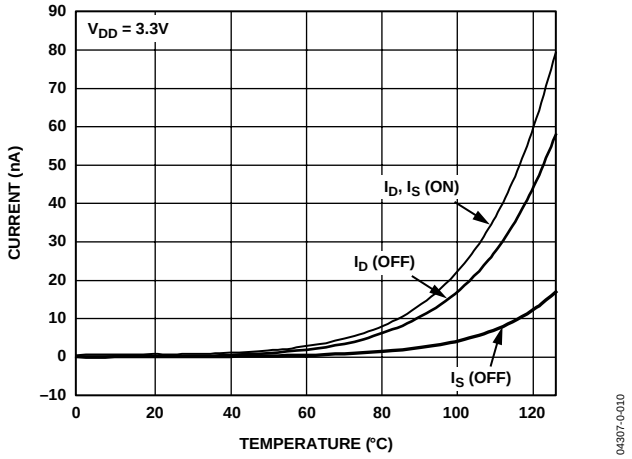

Figure 9. Leakage Current vs. Temperature, V_{DD} = 3.3 V

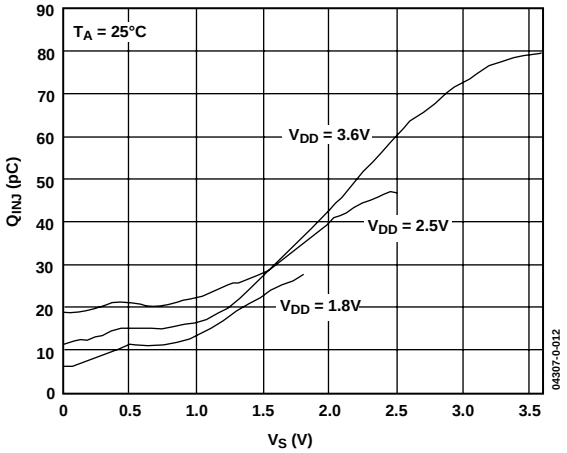

Figure 12. Charge Injection vs. Source Voltage, V_{DD} = 1.8 V

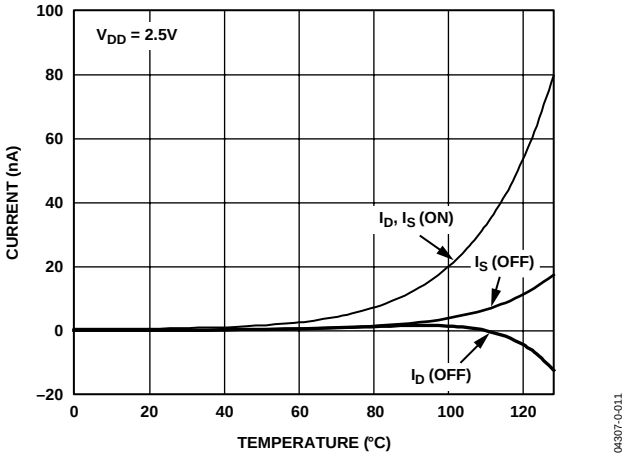

Figure 10. Leakage Current vs. Temperature, V_{DD} = 2.5 V

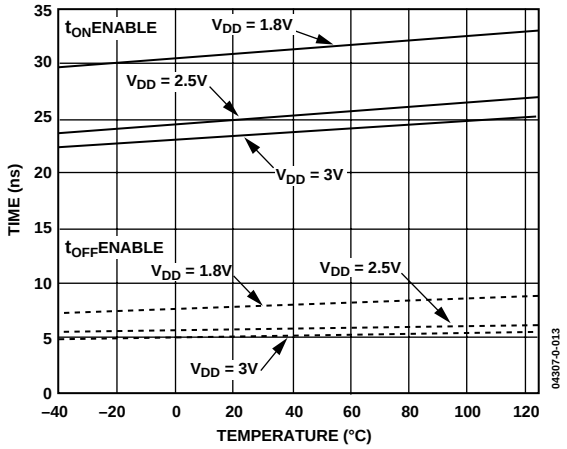

Figure 13. t_{ON}/t_{OFF} Times vs. Temperature

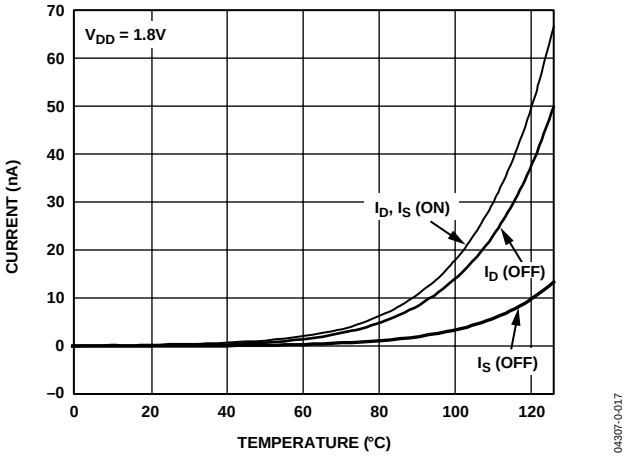

Figure 11. Leakage Current vs. Temperature, V_{DD} = 1.8 V

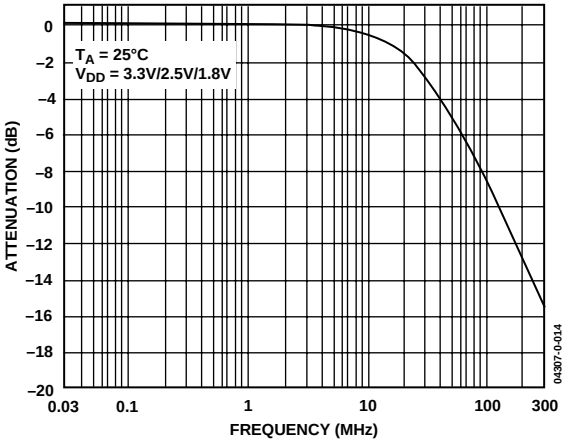

Figure 14. Bandwidth

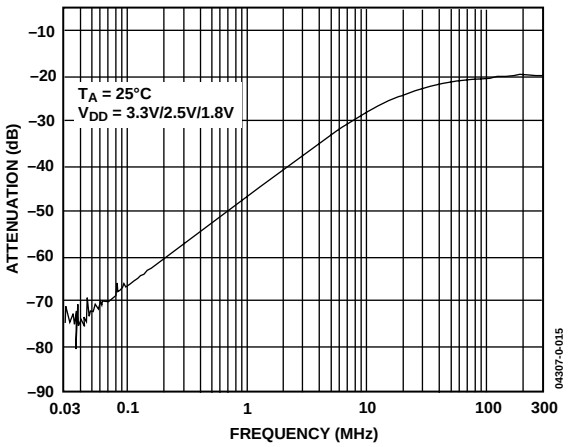

Figure 15. Off Isolation vs. Frequency

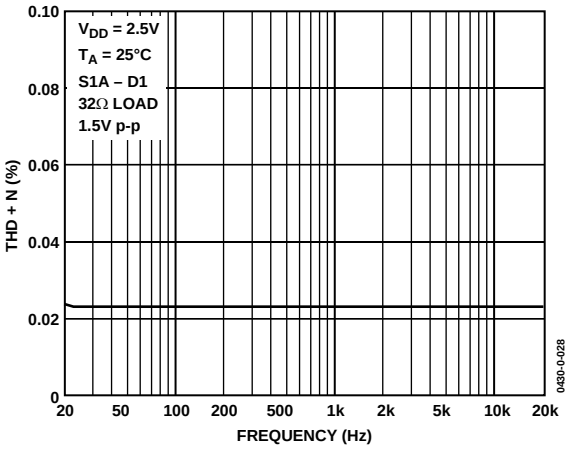

Figure 17. Total Harmonic Distortion + Noise

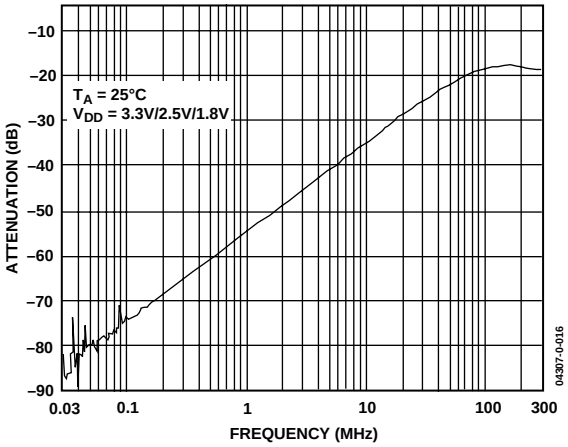

Figure 16. Crosstalk vs. Frequency

TEST CIRCUITS

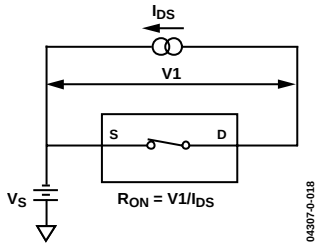

Figure 18. On Resistance

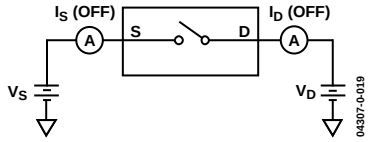

Figure 19. Off Leakage

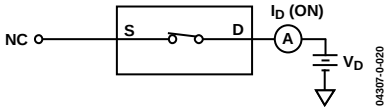

Figure 20. On Leakage

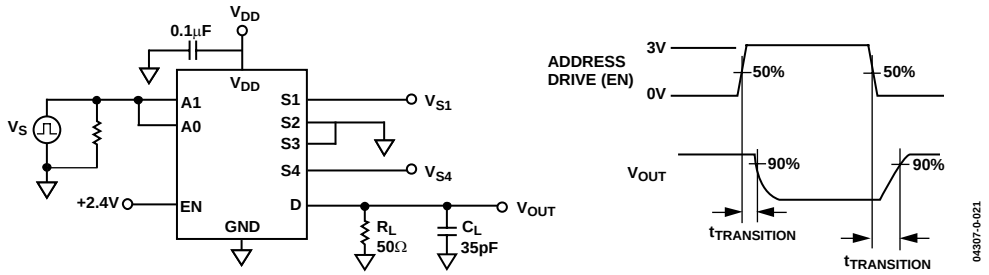

Figure 21. Switching Time of Multiplexer, $t_{TRANSITION}$

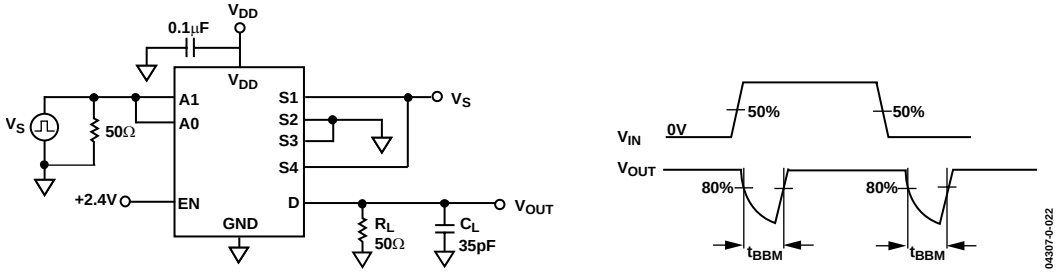

Figure 22. Break-Before-Make Time Delay, t_{BBM}

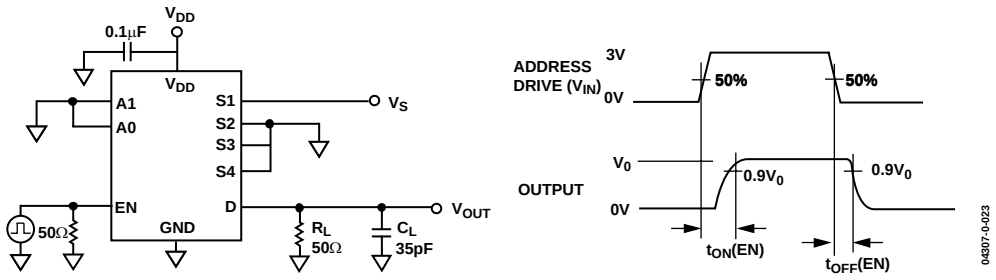

Figure 23. Enable Delay, $t_{ON}(EN)$, $t_{OFF}(EN)$

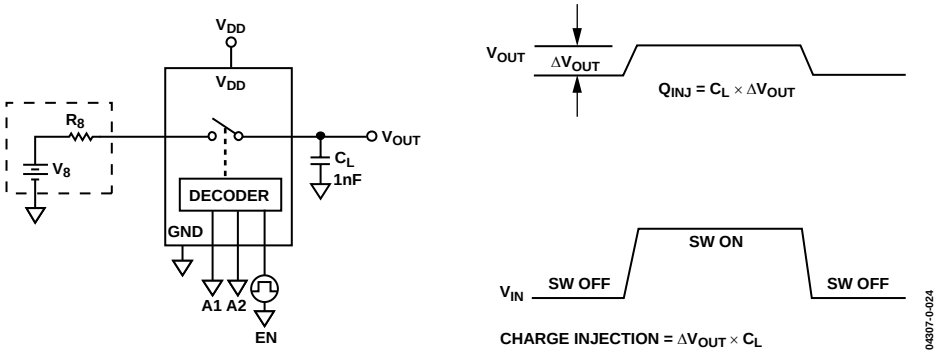

Figure 24. Charge Injection

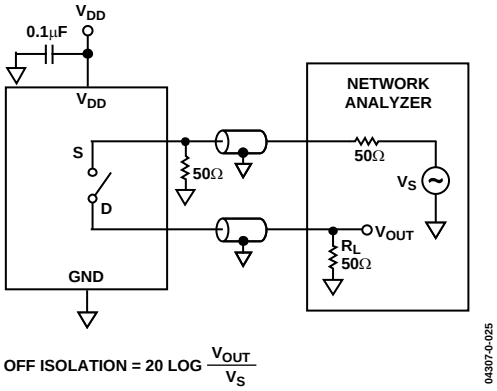

Figure 25. Off Isolation

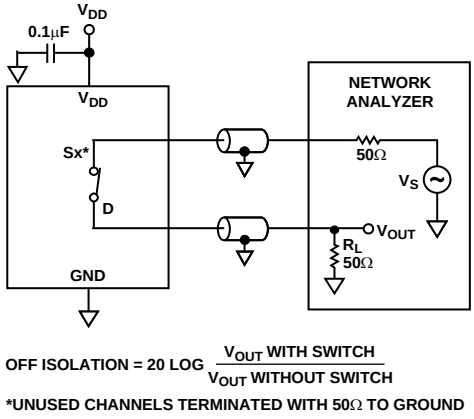

Figure 26. Bandwidth

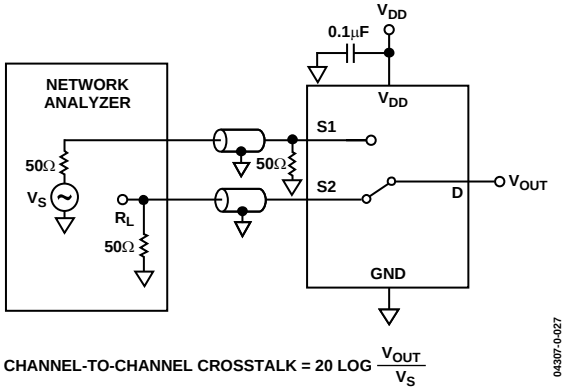

Figure 27. Channel-to-Channel Crosstalk

OUTLINE DIMENSIONS

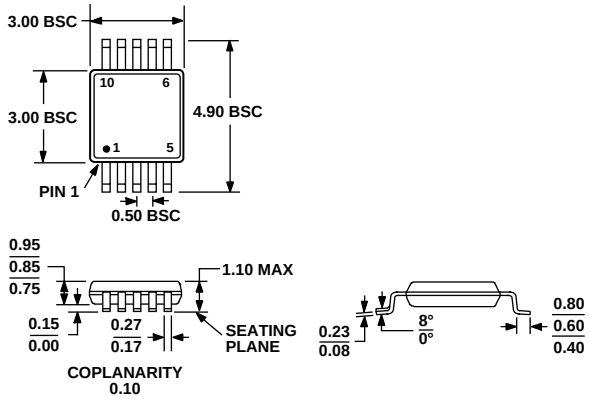

Figure 28. 10-Lead Mini Small Outline Package [MSOP]
(RM-10)
Dimensions shown in millimeters

ORDERING GUIDE

Model	Temperature Range	Package Description	Package Option	Branding[1]
ADG804YRM	–40°C to +125°C	Mini Small Outline Package (MSOP)	RM-10	S1A
ADG804YRM-REEL	–40°C to +125°C	Mini Small Outline Package (MSOP)	RM-10	S1A
ADG804YRM-REEL7	–40°C to +125°C	Mini Small Outline Package (MSOP)	RM-10	S1A

[1] Branding on this package is limited to three characters due to space constraints.

NOTES

NOTES

NOTES

D04307–0–4/04(0)

National Semiconductor

August 2000

LMC6484
CMOS Quad Rail-to-Rail Input and Output Operational Amplifier

General Description

The LMC6484 provides a common-mode range that extends to both supply rails. This rail-to-rail performance combined with excellent accuracy, due to a high CMRR, makes it unique among rail-to-rail input amplifiers.

It is ideal for systems, such as data acquisition, that require a large input signal range. The LMC6484 is also an excellent upgrade for circuits using limited common-mode range amplifiers such as the TLC274 and TLC279.

Maximum dynamic signal range is assured in low voltage and single supply systems by the LMC6484's rail-to-rail output swing. The LMC6484's rail-to-rail output swing is guaranteed for loads down to 600Ω.

Guaranteed low voltage characteristics and low power dissipation make the LMC6484 especially well-suited for battery-operated systems.

See the LMC6482 data sheet for a Dual CMOS operational amplifier with these same features.

Features

(Typical unless otherwise noted)

- Rail-to-Rail Input Common-Mode Voltage Range (Guaranteed Over Temperature)
- Rail-to-Rail Output Swing (within 20 mV of supply rail, 100 kΩ load)
- Guaranteed 3V, 5V and 15V Performance
- Excellent CMRR and PSRR: 82 dB
- Ultra Low Input Current: 20 fA
- High Voltage Gain (R_L = 500 kΩ): 130 dB
- Specified for 2 kΩ and 600Ω loads

Applications

- Data Acquisition Systems
- Transducer Amplifiers
- Hand-held Analytic Instruments
- Medical Instrumentation
- Active Filter, Peak Detector, Sample and Hold, pH Meter, Current Source
- Improved Replacement for TLC274, TLC279

3V Single Supply Buffer Circuit

Rail-to-Rail Input

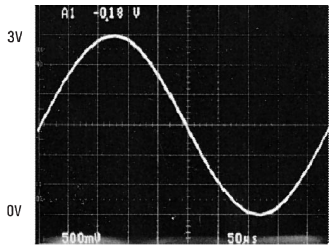

DS011714-1

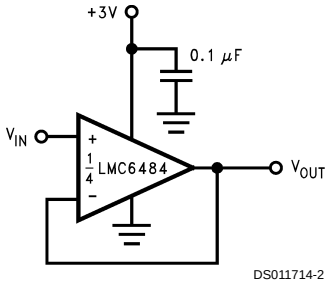

DS011714-2

Rail-to-Rail Output

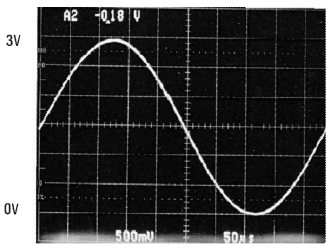

DS011714-3

Absolute Maximum Ratings (Note 1)

If Military/Aerospace specified devices are required, please contact the National Semiconductor Sales Office/ Distributors for availability and specifications.

ESD Tolerance (Note 2)	2.0 kV
Differential Input Voltage	±Supply Voltage
Voltage at Input/Output Pin	(V^+) + 0.3V, (V^-) − 0.3V
Supply Voltage $(V^+ - V^-)$	16V
Current at Input Pin (Note 12)	±5 mA
Current at Output Pin (Notes 3, 8)	±30 mA
Current at Power Supply Pin	40 mA
Lead Temp. (Soldering, 10 sec.)	260˚C
Storage Temperature Range	−65˚C to +150˚C
Junction Temperature (Note 4)	150˚C

Operating Ratings (Note 1)

Supply Voltage	$3.0V \le V^+ \le 15.5V$
Junction Temperature Range	
LMC6484AM	$-55^\circ C \le T_J \le +125^\circ C$
LMC6484AI, LMC6484I	$-40^\circ C \le T_J \le +85^\circ C$
Thermal Resistance (θ_{JA})	
N Package, 14-Pin Molded DIP	70˚C/W
M Package, 14-Pin Surface Mount	110˚C/W

DC Electrical Characteristics

Unless otherwise specified, all limits guaranteed for T_J = 25˚C, V^+ = 5V, V^- = 0V, $V_{CM} = V_O = V^+/2$ and R_L > 1M. **Boldface** limits apply at the temperature extremes.

Symbol	Parameter	Conditions		Typ (Note 5)	LMC6484AI Limit (Note 6)	LMC6484I Limit (Note 6)	LMC6484M Limit (Note 6)	Units
V_{OS}	Input Offset Voltage			0.110	0.750 **1.35**	3.0 **3.7**	3.0 **3.8**	mV max
TCV_{OS}	Input Offset Voltage Average Drift			1.0				µV/˚C
I_B	Input Current	(Note 13)		0.02	**4.0**	**4.0**	**100**	pA max
I_{OS}	Input Offset Current	(Note 13)		0.01	**2.0**	**2.0**	**50**	pA max
C_{IN}	Common-Mode Input Capacitance			3				pF
R_{IN}	Input Resistance			>10				Tera Ω
CMRR	Common Mode Rejection Ratio	$0V \le V_{CM} \le 15.0V$, $V^+ = 15V$		82	70 **67**	65 **62**	65 **60**	dB min
		$0V \le V_{CM} \le 5.0V$ $V^+ = 5V$		82	70 **67**	65 **62**	65 **60**	
+PSRR	Positive Power Supply Rejection Ratio	$5V \le V^+ \le 15V$, $V^- = 0V$, $V_O = 2.5V$		82	70 **67**	65 **62**	65 **60**	dB min
−PSRR	Negative Power Supply Rejection Ratio	$-5V \le V^- \le -15V$, $V^+ = 0V$, $V_O = -2.5V$		82	70 **67**	65 **62**	65 **60**	dB min
V_{CM}	Input Common-Mode Voltage Range	V^+ = 5V and 15V For CMRR ≥ 50 dB		V^- − 0.3	−0.25 **0**	−0.25 **0**	−0.25 **0**	V max
				V^+ + 0.3	V^+ + 0.25 **V^+**	V^+ + 0.25 **V^+**	V^+ + 0.25 **V^+**	V min
A_V	Large Signal Voltage Gain	R_L = 2kΩ (Notes 7, 13)	Sourcing	666	140 **84**	120 **72**	120 **60**	V/mV min
			Sinking	75	35 **20**	35 **20**	35 **18**	V/mV min
		R_L = 600Ω (Notes 7, 13)	Sourcing	300	80 **48**	50 **30**	50 **25**	V/mV min
			Sinking	35	20 **13**	15 **10**	15 **8**	V/mV min

DC Electrical Characteristics (Continued)

Unless otherwise specified, all limits guaranteed for T_J = 25˚C, V^+ = 5V, V^- = 0V, $V_{CM} = V_O = V^+/2$ and R_L > 1M. **Boldface** limits apply at the temperature extremes.

Symbol	Parameter	Conditions	Typ (Note 5)	LMC6484AI Limit (Note 6)	LMC6484I Limit (Note 6)	LMC6484M Limit (Note 6)	Units
V_O	Output Swing	V^+ = 5V	4.9	4.8	4.8	4.8	V
		R_L = 2 kΩ to $V^+/2$		**4.7**	**4.7**	**4.7**	min
			0.1	0.18	0.18	0.18	V
				0.24	**0.24**	**0.24**	max
		V^+ = 5V	4.7	4.5	4.5	4.5	V
		R_L = 600Ω to $V^+/2$		**4.24**	**4.24**	**4.24**	min
			0.3	0.5	0.5	0.5	V
				0.65	**0.65**	**0.65**	max
		V^+ = 15V	14.7	14.4	14.4	14.4	V
		R_L = 2 kΩ to $V^+/2$		**14.2**	**14.2**	**14.2**	min
			0.16	0.32	0.32	0.32	V
				0.45	**0.45**	**0.45**	max
		V^+ = 15V	14.1	13.4	13.4	13.4	V
		R_L = 600Ω to $V^+/2$		**13.0**	**13.0**	**13.0**	min
			0.5	1.0	1.0	1.0	V
				1.3	**1.3**	**1.3**	max
I_{SC}	Output Short Circuit Current	Sourcing, V_O = 0V	20	16	16	16	mA
	V+ = 5V			**12**	**12**	**10**	min
		Sinking, V_O = 5V	15	11	11	11	mA
				9.5	**9.5**	**8.0**	min
I_{SC}	Output Short Circuit Current	Sourcing, V_O = 0V	30	28	28	28	mA
	V^+ = 15V			**22**	**22**	**20**	min
		Sinking, V_O = 12V	30	30	30	30	mA
		(Note 8)		**24**	**24**	**22**	min
I_S	Supply Current	All Four Amplifiers	2.0	2.8	2.8	2.8	mA
		V^+ = +5V, $V_O = V^+/2$		**3.6**	**3.6**	**3.8**	max
		All Four Amplifiers	2.6	3.0	3.0	3.0	mA
		V^+ = +15V, $V_O = V^+/2$		**3.8**	**3.8**	**4.0**	max

AC Electrical Characteristics

Unless otherwise specified, all limits guaranteed for T_J = 25˚C, V^+ = 5V, V^- = 0V, $V_{CM} = V_O = V^+/2$ and R_L > 1M. **Boldface** limits apply at the temperature extremes.

Symbol	Parameter	Conditions	Typ (Note 5)	LMC6484A Limit (Note 6)	LMC6484I Limit (Note 6)	LMC6484M Limit (Note 6)	Units
SR	Slew Rate	(Note 9)	1.3	1.0	0.9	0.9	V/µs
				0.7	**0.63**	**0.54**	min
GBW	Gain-Bandwidth Product	V^+ = 15V	1.5				MHz
ϕ_m	Phase Margin		50				Deg
G_m	Gain Margin		15				dB
	Amp-to-Amp Isolation	(Note 10)	150				dB
e_n	Input-Referred Voltage Noise	f = 1 kHz V_{CM} = 1V	37				$nV/\sqrt{Hz}$
i_n	Input-Referred Current Noise	f = 1 kHz	0.03				$pA/\sqrt{Hz}$

AC Electrical Characteristics (Continued)

Unless otherwise specified, all limits guaranteed for T_J = 25˚C, V^+ = 5V, V^- = 0V, $V_{CM} = V_O = V^+/2$ and $R_L > 1M$. **Boldface** limits apply at the temperature extremes.

Symbol	Parameter	Conditions	Typ (Note 5)	LMC6484A Limit (Note 6)	LMC6484I Limit (Note 6)	LMC6484M Limit (Note 6)	Units
T.H.D.	Total Harmonic Distortion	f = 1 kHz, A_V = −2 R_L = 10 kΩ, V_O = 4.1 V_{PP}	0.01				%
		f = 10 kHz, A_V = −2 R_L = 10 kΩ, V_O = 8.5 V_{PP} V^+ = 10V	0.01				%

DC Electrical Characteristics

Unless otherwise specified, all limits guaranteed for T_J = 25˚C, V^+ = 3V, V^- = 0V, $V_{CM} = V_O = V^+/2$ and $R_L > 1M$

Symbol	Parameter	Conditions	Typ (Note 5)	LMC6484AI Limit (Note 6)	LMC6484I Limit (Note 6)	LMC6484M Limit (Note 6)	Units
V_{OS}	Input Offset Voltage		0.9	2.0 **2.7**	3.0 **3.7**	3.0 **3.8**	mV max
TCV_{OS}	Input Offset Voltage Average Drift		2.0				µV/˚C
I_B	Input Bias Current		0.02				pA
I_{OS}	Input Offset Current		0.01				pA
CMRR	Common Mode Rejection Ratio	0V ≤ V_{CM} ≤ 3V	74	64	60	60	dB min
PSRR	Power Supply Rejection Ratio	3V ≤ V^+ ≤ 15V, V^- = 0V	80	68	60	60	dB min
V_{CM}	Input Common-Mode Voltage Range	For CMRR ≥ 50 dB	V^- − 0.25	0	0	0	V max
			V^+ + 0.25	V^+	V^+	V^+	V min
V_O	Output Swing	R_L = 2 kΩ to $V^+/2$	2.8				V
			0.2				V
		R_L = 600Ω to $V^+/2$	2.7	2.5	2.5	2.5	V min
			0.37	0.6	0.6	0.6	V max
I_S	Supply Current	All Four Amplifiers	1.65	2.5 **3.0**	2.5 **3.0**	2.5 **3.2**	mA max

AC Electrical Characteristics

Unless otherwise specified, V^+ = 3V, V^- = 0V, $V_{CM} = V_O = V^+/2$ and $R_L > 1M$

Symbol	Parameter	Conditions	Typ (Note 5)	LMC6484AI Limit (Note 6)	LMC6484I Limit (Note 6)	LMC6484M Limit (Note 6)	Units
SR	Slew Rate	(Note 11)	0.9				V/µs
GBW	Gain-Bandwidth Product		1.0				MHz
T.H.D.	Total Harmonic Distortion	f = 10 kHz, A_V = −2 R_L = 10 kΩ, V_O = 2 V_{PP}	0.01				%

Note 1: Absolute Maximum Ratings indicate limits beyond which damage to the device may occur. Operating Ratings indicate conditions for which the device is intended to be functional, but specific performance is not guaranteed. For guaranteed specifications and the test conditions, see the Electrical Characteristics.

Note 2: Human body model, 1.5 kΩ in series with 100 pF. All pins rated per method 3015.6 of MIL-STD-883. This is a class 2 device rating.

AC Electrical Characteristics (Continued)

Note 3: Applies to both single supply and split-supply operation. Continuous short circuit operation at elevated ambient temperature can result in exceeding the maximum allowed junction temperature of 150˚C. Output currents in excess of ±30 mA over long term may adversely affect reliability.

Note 4: The maximum power dissipation is a function of $T_{J(max)}$, θ_{JA}, and T_A. The maximum allowable power dissipation at any ambient temperature is $P_D = (T_{J(max)} - T_A)/\theta_{JA}$. All numbers apply for packages soldered directly into a PC board.

Note 5: Typical Values represent the most likely parametric norm.

Note 6: All limits are guaranteed by testing or statistical analysis.

Note 7: V^+ = 15V, V_{CM} = 7.5V and R_L connected to 7.5V. For Sourcing tests, 7.5V ≤ V_O ≤ 11.5V. For Sinking tests, 3.5V ≤ V_O ≤ 7.5V.

Note 8: Do not short circuit output to V^+, when V^+ is greater than 13V or reliability will be adversely affected.

Note 9: V^+ = 15V. Connected as Voltage Follower with 10V step input. Number specified is the slower of either the positive or negative slew rates.

Note 10: Input referred, V^+ = 15V and R_L = 100 kΩ connected to 7.5V. Each amp excited in turn with 1 kHz to produce V_O = 12 V_{PP}.

Note 11: Connected as Voltage Follower with 2V step input. Number specified is the slower of either the positive or negative slew rates.

Note 12: Limiting input pin current is only necessary for input voltages that exceed absolute maximum input voltage ratings.

Note 13: Guaranteed limits are dictated by tester limitations and not device performance. Actual performance is reflected in the typical value.

Note 14: For guaranteed Military Temperature Range parameters see RETSMC6484X.

Typical Performance Characteristics V_S = +15V, Single Supply, T_A = 25˚C unless otherwise specified

Supply Current vs Supply Voltage

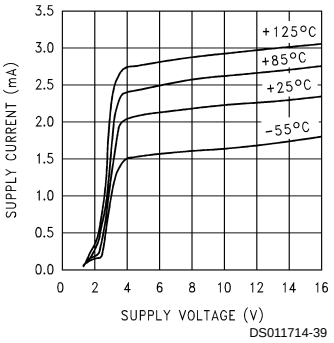

DS011714-39

Input Current vs Temperature

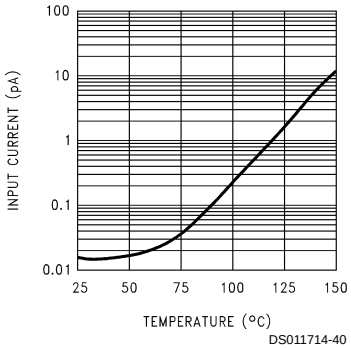

DS011714-40

Sourcing Current vs Output Voltage

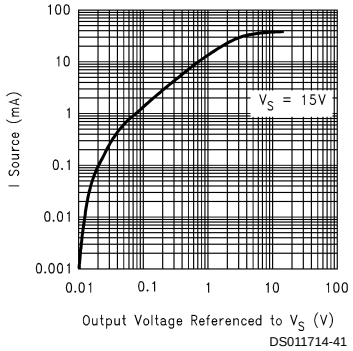

DS011714-41

Sourcing Current vs Output Voltage

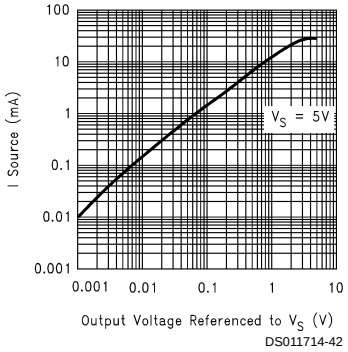

DS011714-42

Sourcing Current vs Output Voltage

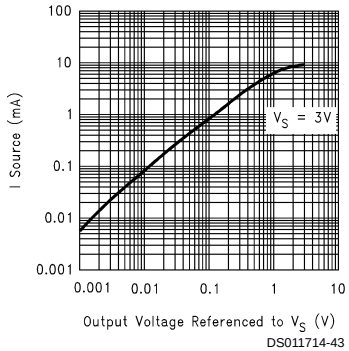

DS011714-43

Sinking Current vs Output Voltage

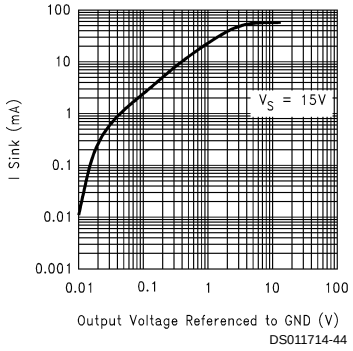

DS011714-44

Typical Performance Characteristics V_S = +15V, Single Supply, T_A = 25˚C unless otherwise specified (Continued)

Sinking Current vs Output Voltage

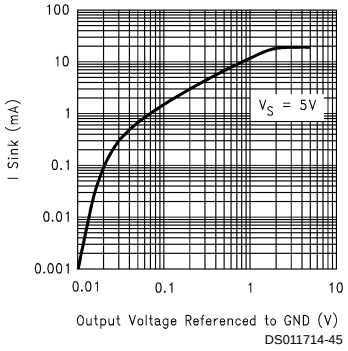

DS011714-45

Sinking Current vs Output Voltage

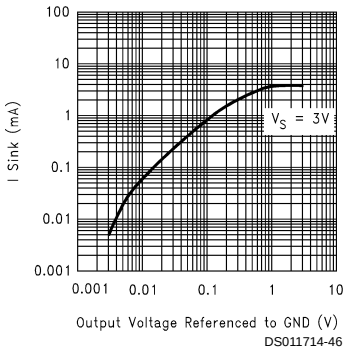

DS011714-46

Output Voltage Swing vs Supply Voltage

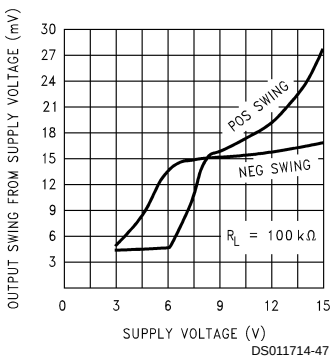

DS011714-47

Input Voltage Noise vs Frequency

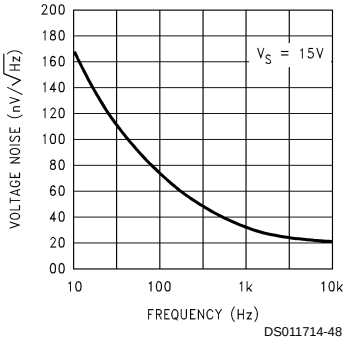

DS011714-48

Input Voltage Noise vs Input Voltage

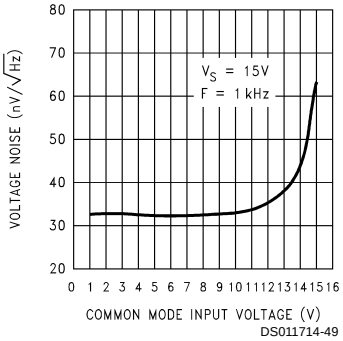

DS011714-49

Input Voltage Noise vs Input Voltage

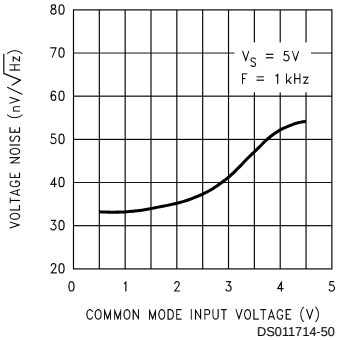

DS011714-50

Input Voltage Noise vs Input Voltage

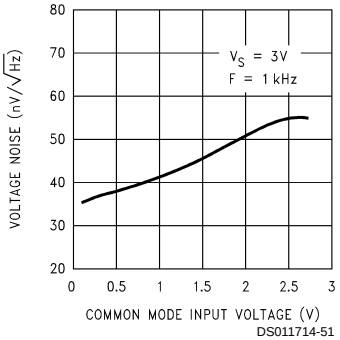

DS011714-51

Crosstalk Rejection vs Frequency

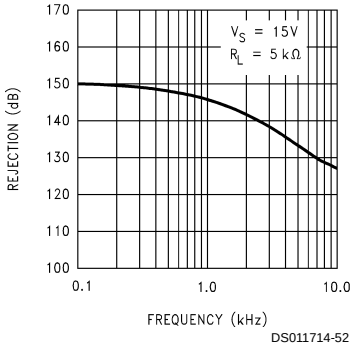

DS011714-52

Typical Performance Characteristics V_S = +15V, Single Supply, T_A = 25˚C unless otherwise specified (Continued)

Crosstalk Rejection vs Frequency

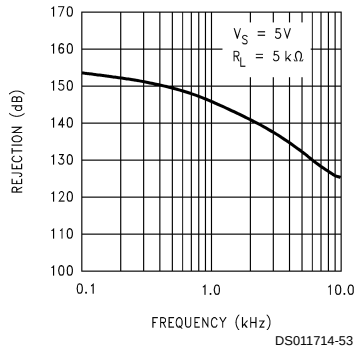

DS011714-53

Positive PSRR vs Frequency

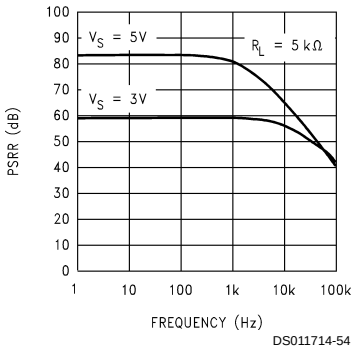

DS011714-54

Negative PSRR vs Frequency

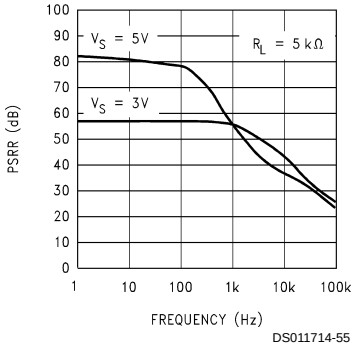

DS011714-55

CMRR vs Frequency

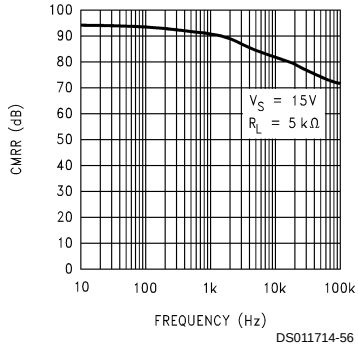

DS011714-56

CMRR vs Input Voltage

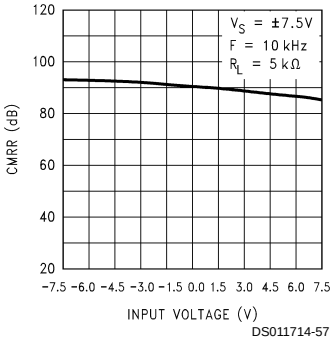

DS011714-57

CMRR vs Input Voltage

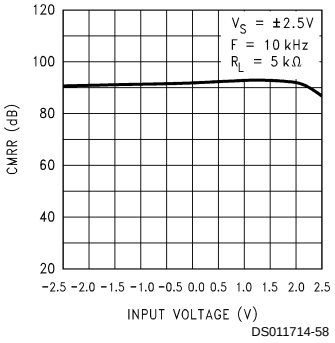

DS011714-58

CMRR vs Input Voltage

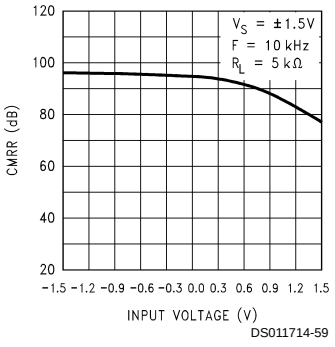

DS011714-59

ΔV_{OS} vs CMR

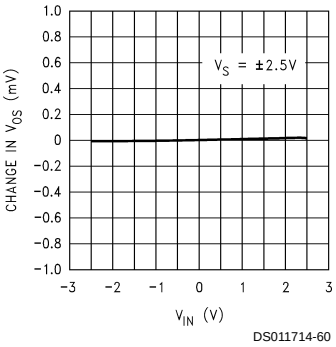

DS011714-60

ΔV_{OS} vs CMR

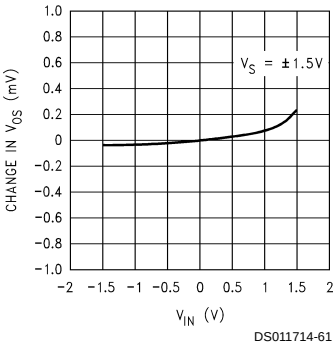

DS011714-61

Typical Performance Characteristics V_S = +15V, Single Supply, T_A = 25˚C unless otherwise specified (Continued)

Input Voltage vs Output Voltage

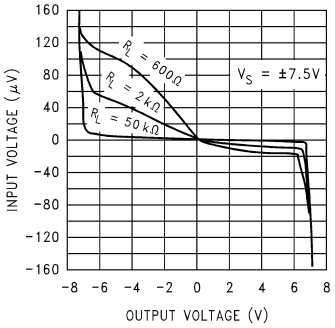

DS011714-62

Input Voltage vs Output Voltage

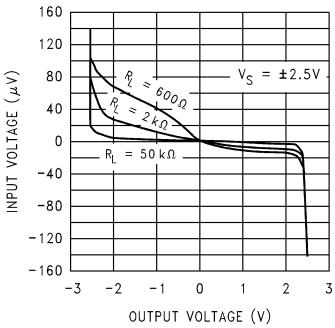

DS011714-63

Open Loop Frequency Response

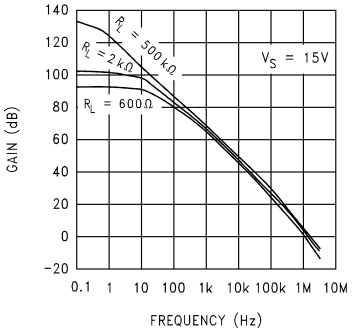

DS011714-64

Open Loop Frequency Response

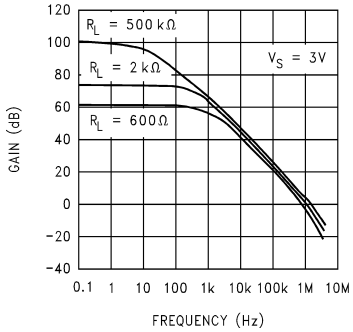

DS011714-65

Open Loop Frequency Response vs Temperature

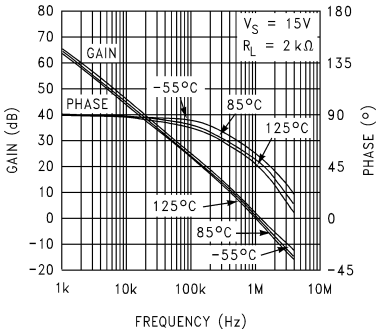

DS011714-66

Maximum Output Swing vs Frequency

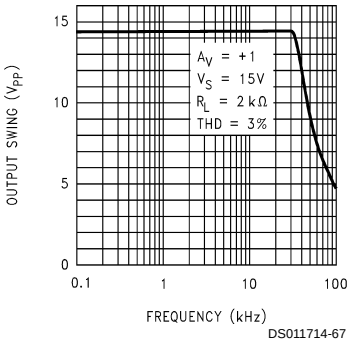

DS011714-67

Gain and Phase vs Capacitive Load

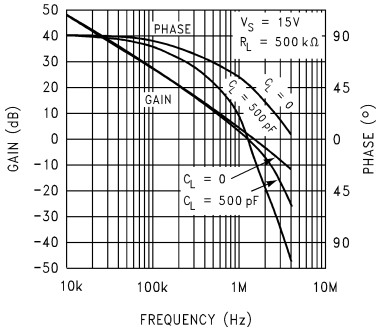

DS011714-68

Gain and Phase vs Capacitive Load

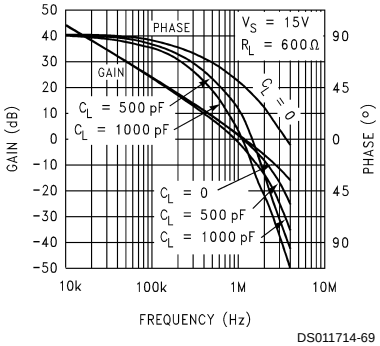

DS011714-69

Open Loop Output Impedance vs Frequency

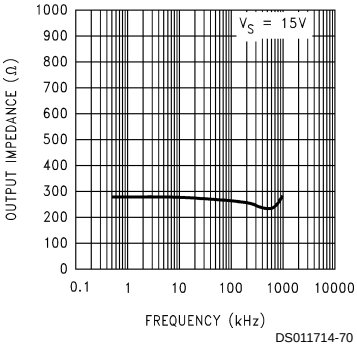

DS011714-70

Typical Performance Characteristics V_S = +15V, Single Supply, T_A = 25˚C unless otherwise specified (Continued)

Open Loop Output Impedance vs Frequency

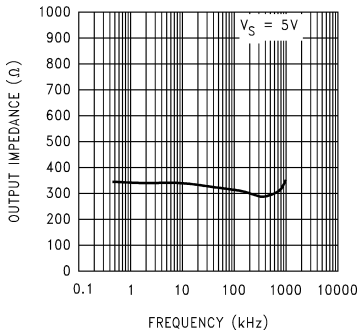

DS011714-71

Slew Rate vs Supply Voltage

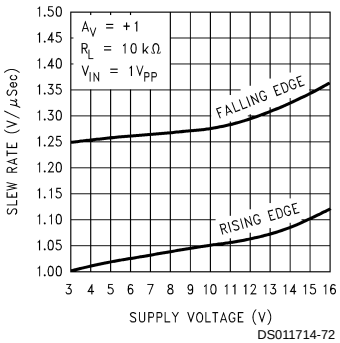

DS011714-72

Non-Inverting Large Signal Pulse Response

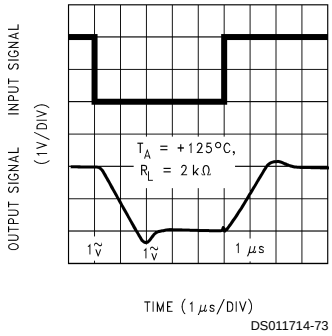

DS011714-73

Non-Inverting Large Signal Pulse Response

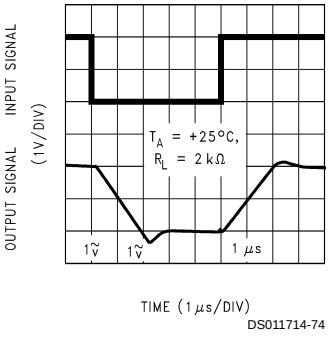

DS011714-74

Non-Inverting Large Signal Pulse Response

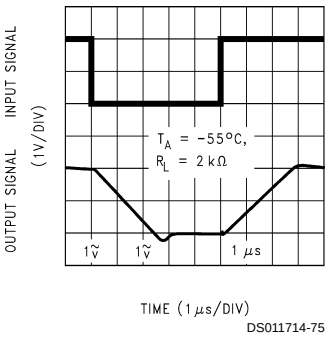

DS011714-75

Non-Inverting Small Signal Pulse Response

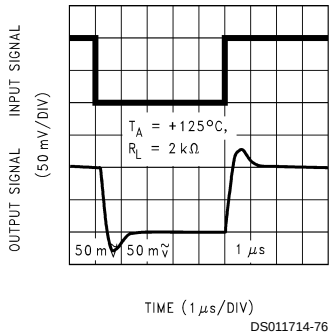

DS011714-76

Non-Inverting Small Signal Pulse Response

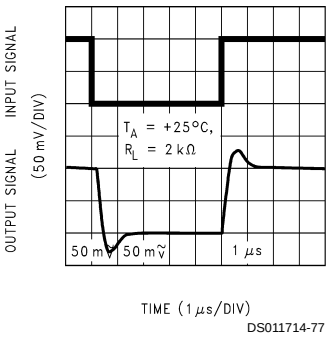

DS011714-77

Non-Inverting Small Signal Pulse Response

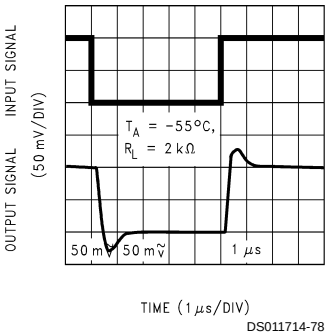

DS011714-78

Inverting Large Signal Pulse Response

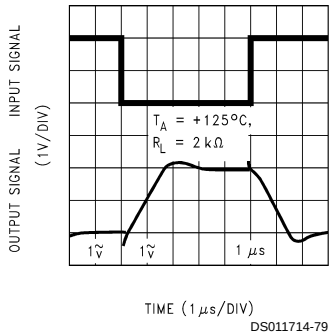

DS011714-79

Typical Performance Characteristics V_S = +15V, Single Supply, T_A = 25˚C unless otherwise specified (Continued)

Inverting Large Signal Pulse Response

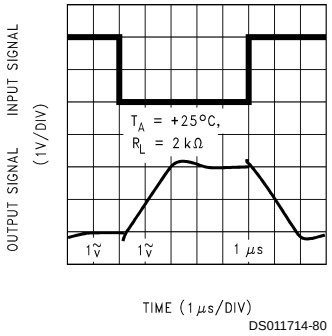

DS011714-80

Inverting Large Signal Pulse Response

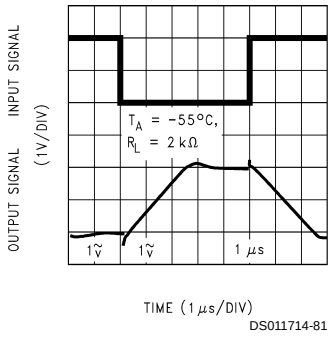

DS011714-81

Inverting Small Signal Pulse Response

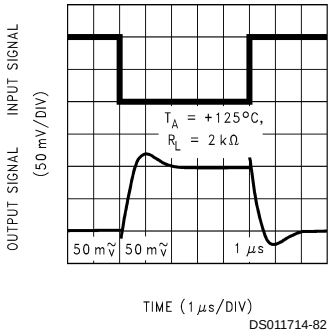

DS011714-82

Inverting Small Signal Pulse Response

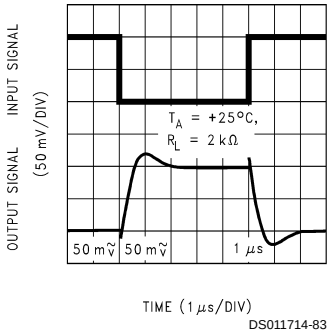

DS011714-83

Inverting Small Signal Pulse Response

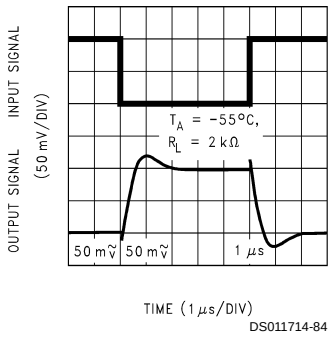

DS011714-84

Stability vs Capacitive Load

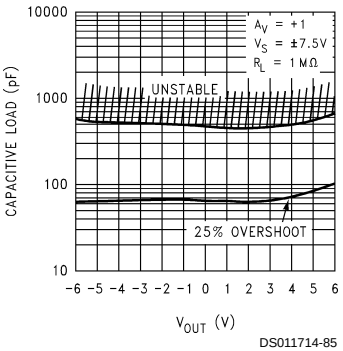

DS011714-85

Stability vs Capacitive Load

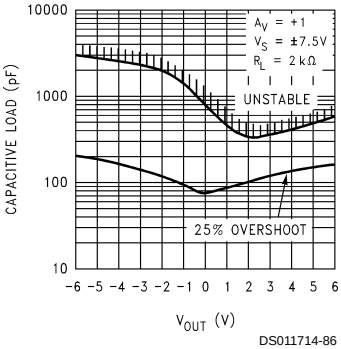

DS011714-86

Stability vs Capacitive Load

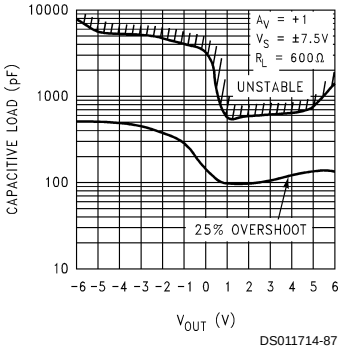

DS011714-87

Stability vs Capacitive Load

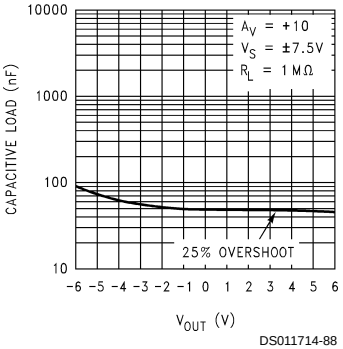

DS011714-88

Typical Performance Characteristics

V_S = +15V, Single Supply, T_A = 25˚C unless otherwise specified (Continued)

Stability vs Capacitive Load

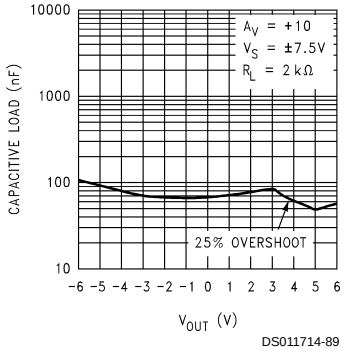

DS011714-89

Stability vs Capacitive Load

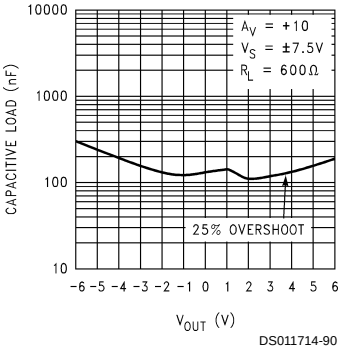

DS011714-90

Application Information

1.0 Amplifier Topology

The LMC6484 incorporates specially designed wide-compliance range current mirrors and the body effect to extend input common mode range to each supply rail. Complementary paralleled differential input stages, like the type used in other CMOS and bipolar rail-to-rail input amplifiers, were not used because of their inherent accuracy problems due to CMRR, cross-over distortion, and open-loop gain variation.

The LMC6484's input stage design is complemented by an output stage capable of rail-to-rail output swing even when driving a large load. Rail-to-rail output swing is obtained by taking the output directly from the internal integrator instead of an output buffer stage.

2.0 Input Common-Mode Voltage Range

Unlike Bi-FET amplifier designs, the LMC6484 does not exhibit phase inversion when an input voltage exceeds the negative supply voltage. *Figure 1* shows an input voltage exceeding both supplies with no resulting phase inversion on the output.

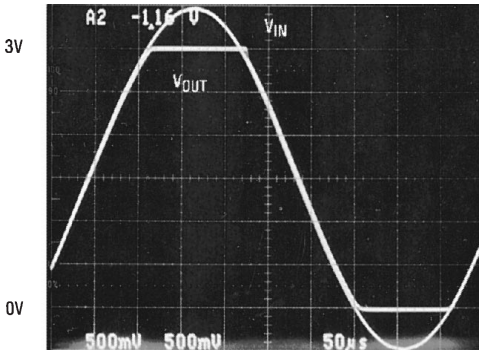

DS011714-10

FIGURE 1. An Input Voltage Signal Exceeds the LMC6484 Power Supply Voltages with No Output Phase Inversion

The absolute maximum input voltage is 300 mV beyond either supply rail at room temperature. Voltages greatly exceeding this absolute maximum rating, as in *Figure 2*, can cause excessive current to flow in or out of the input pins possibly affecting reliability.

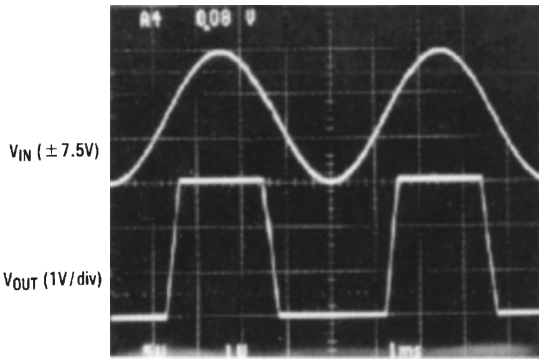

DS011714-12

FIGURE 2. A ±7.5V Input Signal Greatly Exceeds the 3V Supply in *Figure 3* Causing No Phase Inversion Due to R_I

Applications that exceed this rating must externally limit the maximum input current to ±5 mA with an input resistor as shown in *Figure 3*.

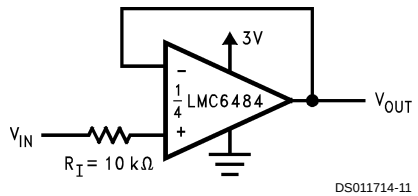

DS011714-11

FIGURE 3. R_I Input Current Protection for Voltages Exceeding the Supply Voltage

3.0 Rail-To-Rail Output

The approximated output resistance of the LMC6484 is 180Ω sourcing and 130Ω sinking at V_S = 3V and 110Ω sourcing and 83Ω sinking at V_S = 5V. Using the calculated output resistance, maximum output voltage swing can be estimated as a function of load.

4.0 Capacitive Load Tolerance

The LMC6484 can typically directly drive a 100 pF load with V_S = 15V at unity gain without oscillating. The unity gain follower is the most sensitive configuration. Direct capacitive

Application Information (Continued)

loading reduces the phase margin of op-amps. The combination of the op-amp's output impedance and the capacitive load induces phase lag. This results in either an underdamped pulse response or oscillation.

Capacitive load compensation can be accomplished using resistive isolation as shown in *Figure 4*. This simple technique is useful for isolating the capacitive input of multiplexers and A/D converters.

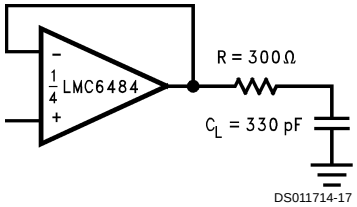

FIGURE 4. Resistive Isolation of a 330 pF Capacitive Load

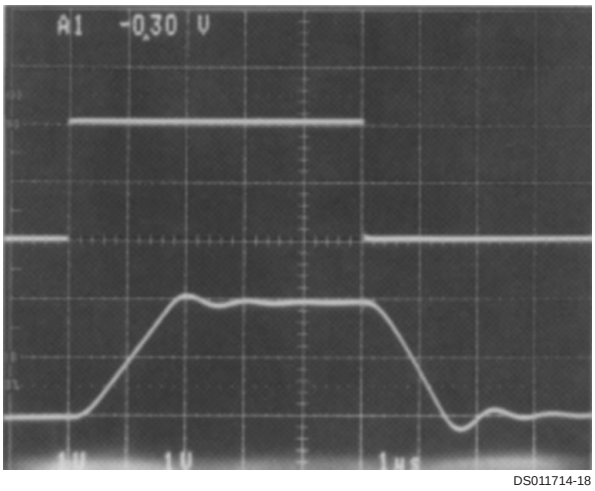

FIGURE 5. Pulse Response of the LMC6484 Circuit in *Figure 4*

Improved frequency response is achieved by indirectly driving capacitive loads as shown in *Figure 6*.

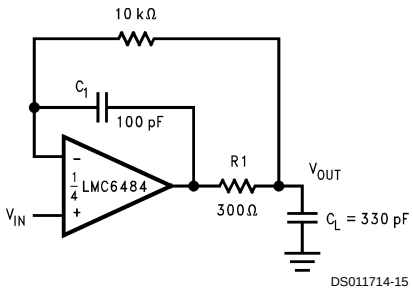

FIGURE 6. LMC6484 Non-Inverting Amplifier, Compensated to Handle a 330 pF Capacitive Load

R1 and C1 serve to counteract the loss of phase margin by feeding forward the high frequency component of the output signal back to the amplifier's inverting input, thereby preserving phase margin in the overall feedback loop. The values of R1 and C1 are experimentally determined for the desired pulse response. The resulting pulse response can be seen in *Figure 7*.

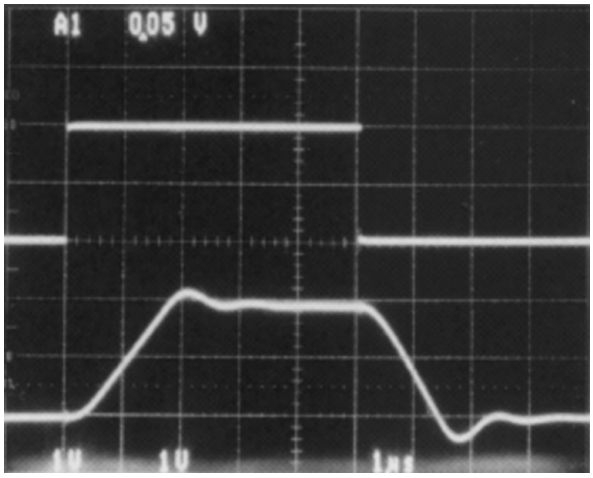

FIGURE 7. Pulse Response of LMC6484 Circuit in *Figure 6*

5.0 Compensating for Input Capacitance

It is quite common to use large values of feedback resistance with amplifiers that have ultra-low input current, like the LMC6484. Large feedback resistors can react with small values of input capacitance due to transducers, photodiodes, and circuit board parasitics to reduce phase margins.

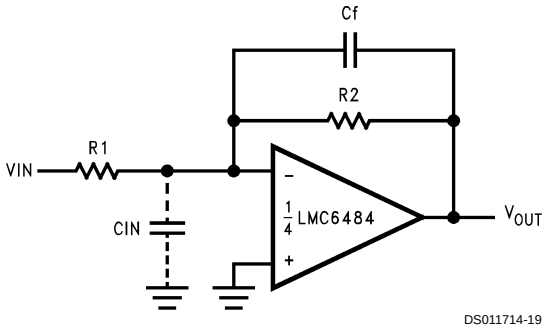

FIGURE 8. Canceling the Effect of Input Capacitance

The effect of input capacitance can be compensated for by adding a feedback capacitor. The feedback capacitor (as in *Figure 8*), C_f, is first estimated by:

$$\frac{1}{2\pi R_1 C_{IN}} \geq \frac{1}{2\pi R_2 C_f}$$

or

$$R_1 C_{IN} \leq R_2 C_f$$

which typically provides significant overcompensation.

Printed circuit board stray capacitance may be larger or smaller than that of a breadboard, so the actual optimum value for C_f may be different. The values of C_f should be checked on the actual circuit. (Refer to the LMC660 quad CMOS amplifier data sheet for a more detailed discussion.)

6.0 Printed-Circuit-Board Layout for High-Impedance Work

It is generally recognized that any circuit which must operate with less than 1000 pA of leakage current requires special layout of the PC board. when one wishes to take advantage

Application Information (Continued)

of the ultra-low input current of the LMC6484, typically less than 20 fA, it is essential to have an excellent layout. Fortunately, the techniques of obtaining low leakages are quite simple. First, the user must not ignore the surface leakage of the PC board, even though it may sometimes appear acceptably low, because under conditions of high humidity or dust or contamination, the surface leakage will be appreciable.

To minimize the effect of any surface leakage, lay out a ring of foil completely surrounding the LMC6484's inputs and the terminals of capacitors, diodes, conductors, resistors, relay terminals, etc. connected to the op-amp's inputs, as in *Figure 9*. To have a significant effect, guard rings should be placed in both the top and bottom of the PC board. This PC foil must then be connected to a voltage which is at the same voltage as the amplifier inputs, since no leakage current can flow between two points at the same potential. For example, a PC board trace-to-pad resistance of $10^{12}\Omega$, which is normally considered a very large resistance, could leak 5 pA if the trace were a 5V bus adjacent to the pad of the input. This would cause a 250 times degradation from the LMC6484's actual performance. However, if a guard ring is held within 5 mV of the inputs, then even a resistance of $10^{11}\Omega$ would cause only 0.05 pA of leakage current. See *Figure 10* for typical connections of guard rings for standard op-amp configurations.

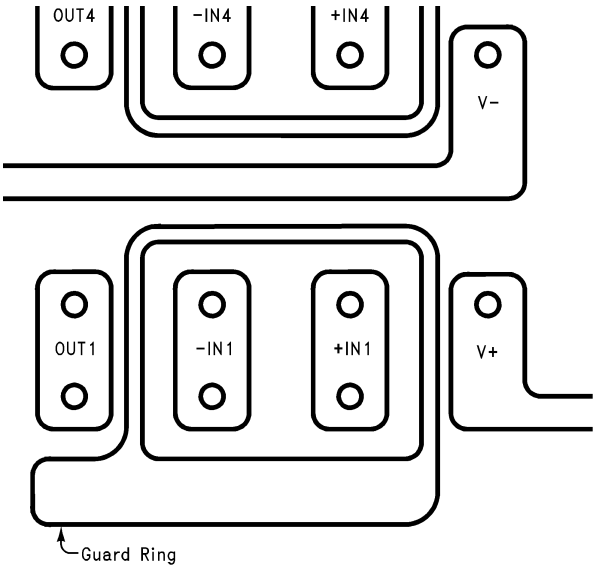

FIGURE 9. Example of Guard Ring in P.C. Board Layout

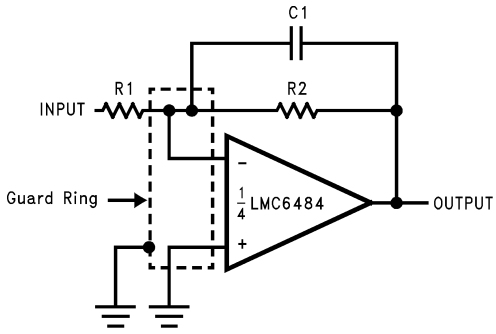

Inverting Amplifier

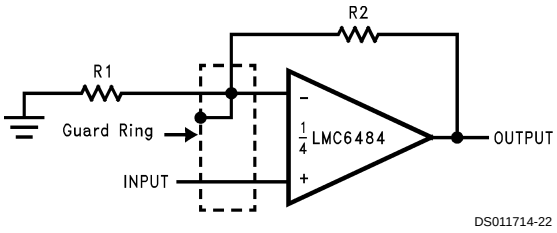

Non-Inverting Amplifier

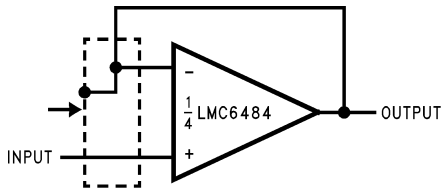

Follower

FIGURE 10. Typical Connections of Guard Rings

The designer should be aware that when it is inappropriate to lay out a PC board for the sake of just a few circuits, there is another technique which is even better than a guard ring on a PC board: Don't insert the amplifier's input pin into the board at all, but bend it up in the air and use only air as an insulator. Air is an excellent insulator. In this case you may have to forego some of the advantages of PC board construction, but the advantages are sometimes well worth the effort of using point-to-point up-in-the-air wiring. See *Figure 11*.

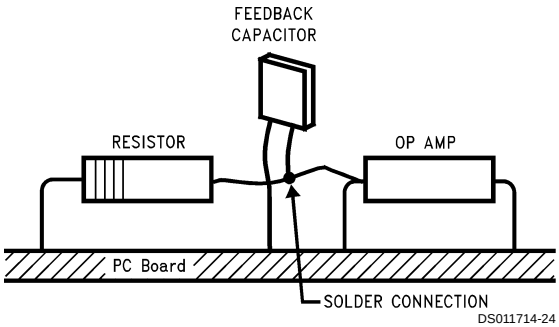

(Input pins are lifted out of PC board and soldered directly to components. All other pins connected to PC board.)

FIGURE 11. Air Wiring

Application Information (Continued)

7.0 Offset Voltage Adjustment

Offset voltage adjustment circuits are illustrated in *Figures 13, 14.* Large value resistances and potentiometers are used to reduce power consumption while providing typically ±2.5 mV of adjustment range, referred to the input, for both configurations with V_S = ±5V.

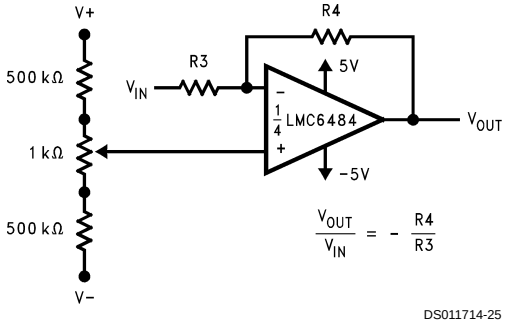

FIGURE 12. Inverting Configuration Offset Voltage Adjustment

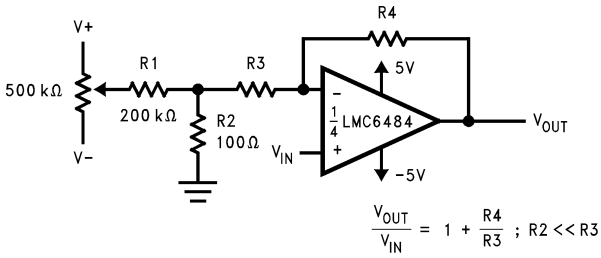

FIGURE 13. Non-Inverting Configuration Offset Voltage Adjustment

8.0 Upgrading Applications

The LMC6484 quads and LMC6482 duals have industry standard pin outs to retrofit existing applications. System performance can be greatly increased by the LMC6484's features. The key benefit of designing in the LMC6484 is increased linear signal range. Most op-amps have limited input common mode ranges. Signals that exceed this range generate a non-linear output response that persists long after the input signal returns to the common mode range.

Linear signal range is vital in applications such as filters where signal peaking can exceed input common mode ranges resulting in output phase inversion or severe distortion.

9.0 Data Acquisition Systems

Low power, single supply data acquisition system solutions are provided by buffering the ADC12038 with the LMC6484 (*Figure 14*). Capable of using the full supply range, the LMC6484 does not require input signals to be scaled down to meet limited common mode voltage ranges. The LMC6484 CMRR of 82 dB maintains integral linearity of a 12-bit data acquisition system to ±0.325 LSB. Other rail-to-rail input amplifiers with only 50 dB of CMRR will degrade the accuracy of the data acquisition system to only 8 bits.

Application Information (Continued)

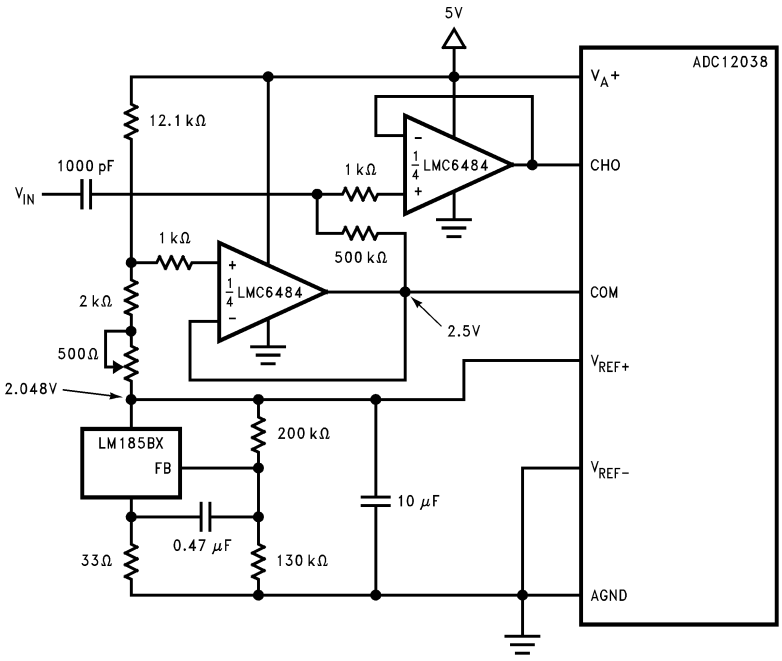

FIGURE 14. Operating from the same Supply Voltage, the LMC6484 buffers the ADC12038 maintaining excellent accuracy

10.0 Instrumentation Circuits

The LMC6484 has the high input impedance, large common-mode range and high CMRR needed for designing instrumentation circuits. Instrumentation circuits designed with the LMC6484 can reject a larger range of common-mode signals than most in-amps. This makes instrumentation circuits designed with the LMC6484 an excellent choice for noisy or industrial environments. Other applications that benefit from these features include analytic medical instruments, magnetic field detectors, gas detectors, and silicon-based transducers.

A small valued potentiometer is used in series with Rg to set the differential gain of the 3 op-amp instrumentation circuit in *Figure 15*. This combination is used instead of one large valued potentiometer to increase gain trim accuracy and reduce error due to vibration.

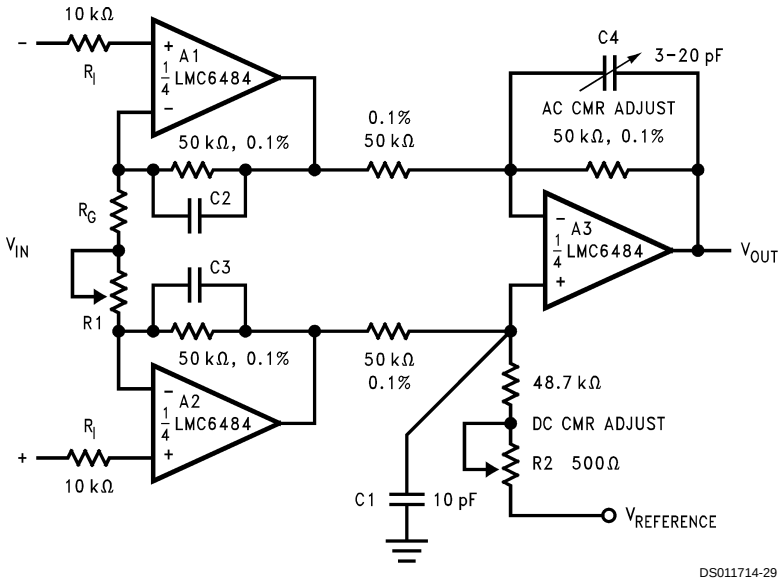

FIGURE 15. Low Power 3 Op-Amp Instrumentation Amplifier

Application Information (Continued)

A 2 op-amp instrumentation amplifier designed for a gain of 100 is shown in *Figure 16*. Low sensitivity trimming is made for offset voltage, CMRR and gain. Low cost and low power consumption are the main advantages of this two op-amp circuit.

Higher frequency and larger common-mode range applications are best facilitated by a three op-amp instrumentation amplifier.

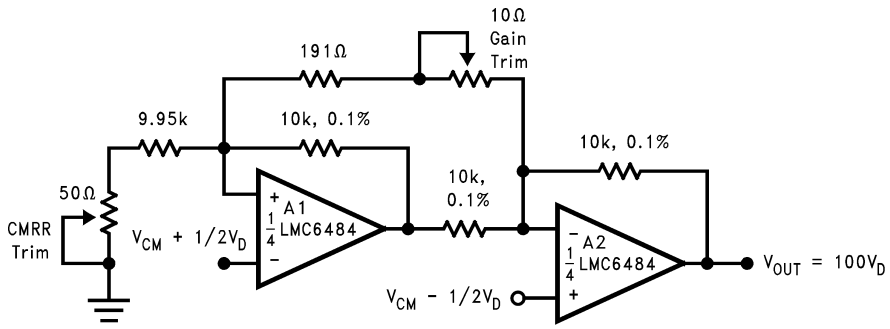

FIGURE 16. Low-Power Two-Op-Amp Instrumentation Amplifier

11.0 Spice Macromodel

A spice macromodel is available for the LMC6484. This model includes accurate simulation of:

- input common-mode voltage range
- frequency and transient response
- GBW dependence on loading conditions
- quiescent and dynamic supply current
- output swing dependence on loading conditions

and many more characteristics as listed on the macromodel disk.

Contact your local National Semiconductor sales office to obtain an operational amplifier spice model library disk.

Typical Single-Supply Applications

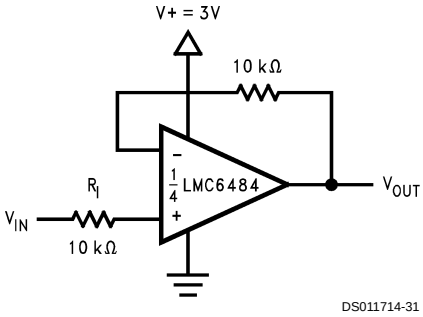

FIGURE 17. Half-Wave Rectifier with Input Current Protection (RI)

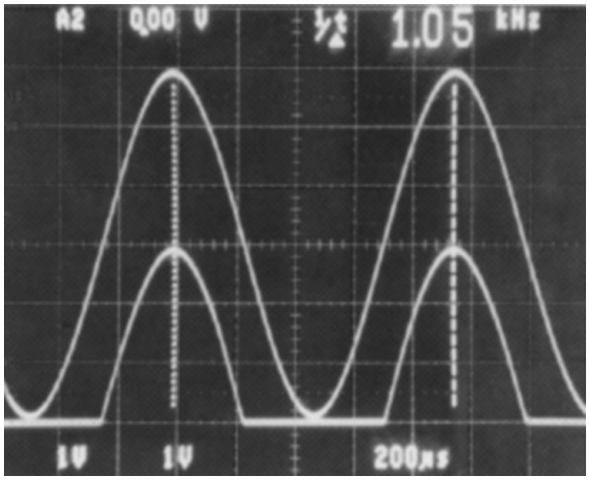

FIGURE 18. Half-Wave Rectifier Waveform

The circuit in *Figure 17* use a single supply to half wave rectify a sinusoid centered about ground. R_I limits current into the amplifier caused by the input voltage exceeding the supply voltage. Full wave rectification is provided by the circuit in *Figure 19*.

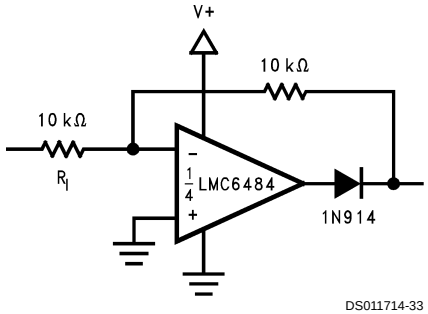

FIGURE 19. Full Wave Rectifier with Input Current Protection (R_I)

Typical Single-Supply Applications (Continued)

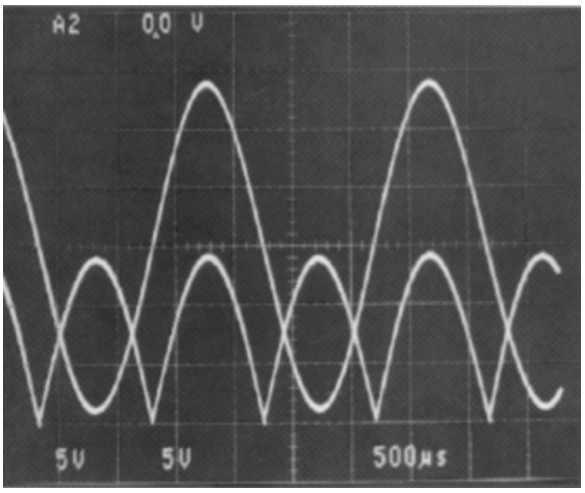

DS011714-34

FIGURE 20. Full Wave Rectifier Waveform

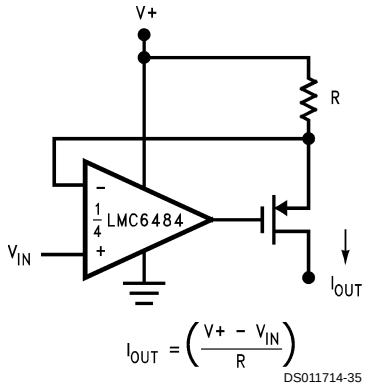

DS011714-35

FIGURE 21. Large Compliance Range Current Source

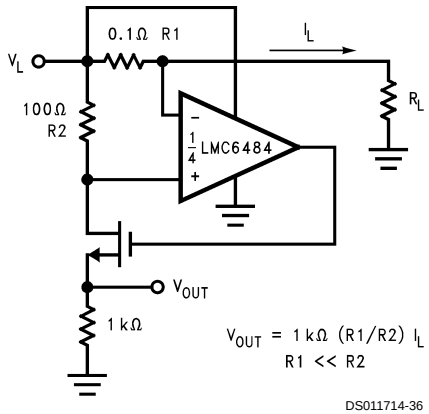

DS011714-36

FIGURE 22. Positive Supply Current Sense

Typical Single-Supply Applications (Continued)

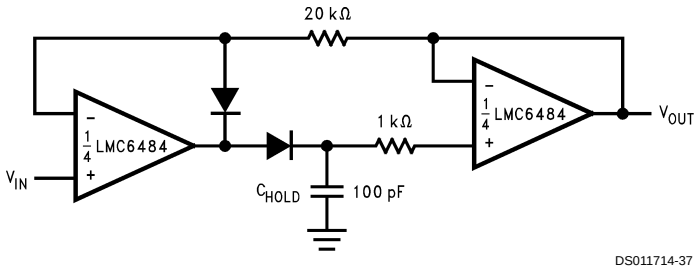

FIGURE 23. Low Voltage Peak Detector with Rail-to-Rail Peak Capture Range

In *Figure 23* dielectric absorption and leakage is minimized by using a polystyrene or polyethylene hold capacitor. The droop rate is primarily determined by the value of C_H and diode leakage current. The ultra-low input current of the LMC6484 has a negligible effect on droop.

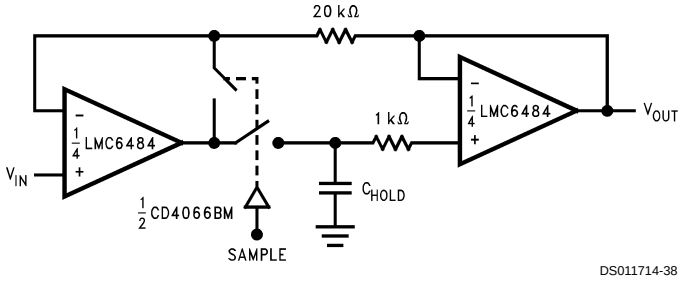

FIGURE 24. Rail-to-Rail Sample and Hold

The LMC6484's high CMRR (85 dB) allows excellent accuracy throughout the circuit's rail-to-rail dynamic capture range.

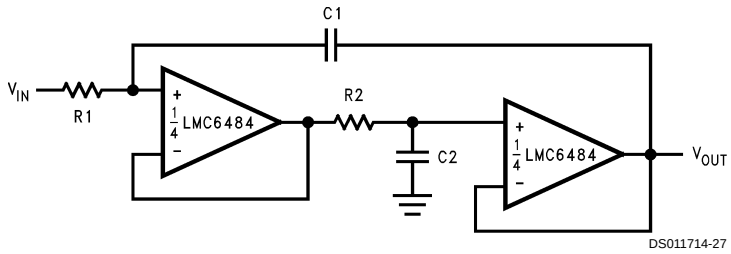

$$R1 = R2,\ C1 = C2;\ f = \frac{1}{2\pi R1C1};\ DF = \frac{1}{2}\sqrt{\frac{C_2}{C_1}}\sqrt{\frac{R_2}{R_1}}$$

FIGURE 25. Rail-to-Rail Single Supply Low Pass Filter

The low pass filter circuit in *Figure 25* can be used as an anti-aliasing filter with the same voltage supply as the A/D converter. Filter designs can also take advantage of the LMC6484 ultra-low input current. The ultra-low input current yields negligible offset error even when large value resistors are used. This in turn allows the use of smaller valued capacitors which take less board space and cost less.

Connection Diagram

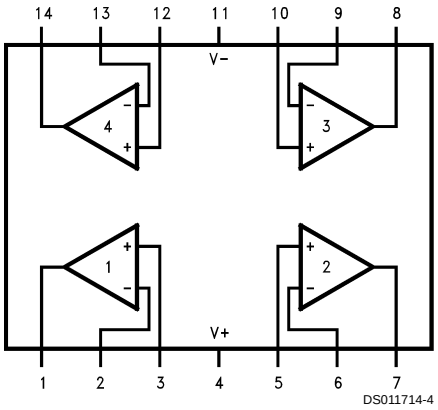

Ordering Information

Package	Temperature Range		NSC Drawing	Transport Media
	Military **−55˚C to +125˚C**	**Industrial** **−40˚C to +85˚C**		
14-pin Molded DIP		LMC6484AIN LMC6484IN	N14A	Rail
14-pin Small Outline		LMC6484AIM, AIMX LMC6484IM, IMX	M14A	Rail Tape and Reel
14-pin Ceramic DIP	LMC6484AMJ/883		J14A	Rail

Physical Dimensions inches (millimeters) unless otherwise noted

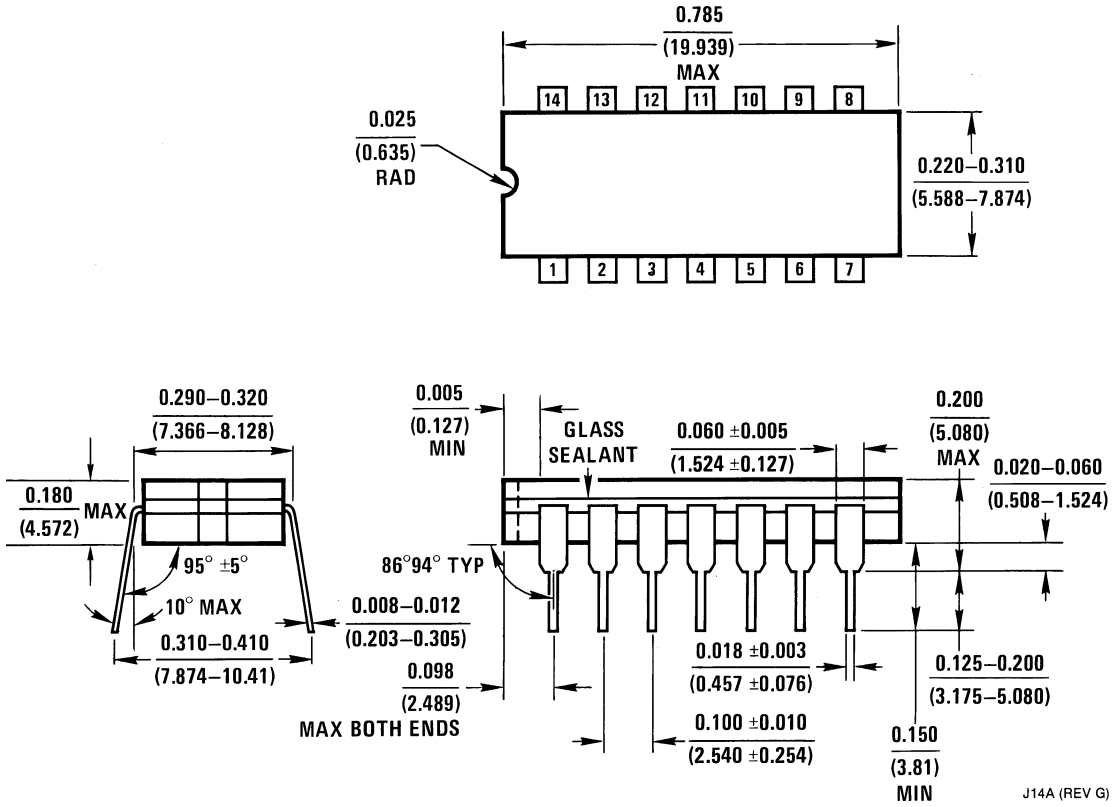

14-Pin Ceramic Dual-In-Line Package
Order Number LMC6484AMJ/883
NS Package Number J14A

Physical Dimensions inches (millimeters) unless otherwise noted (Continued)

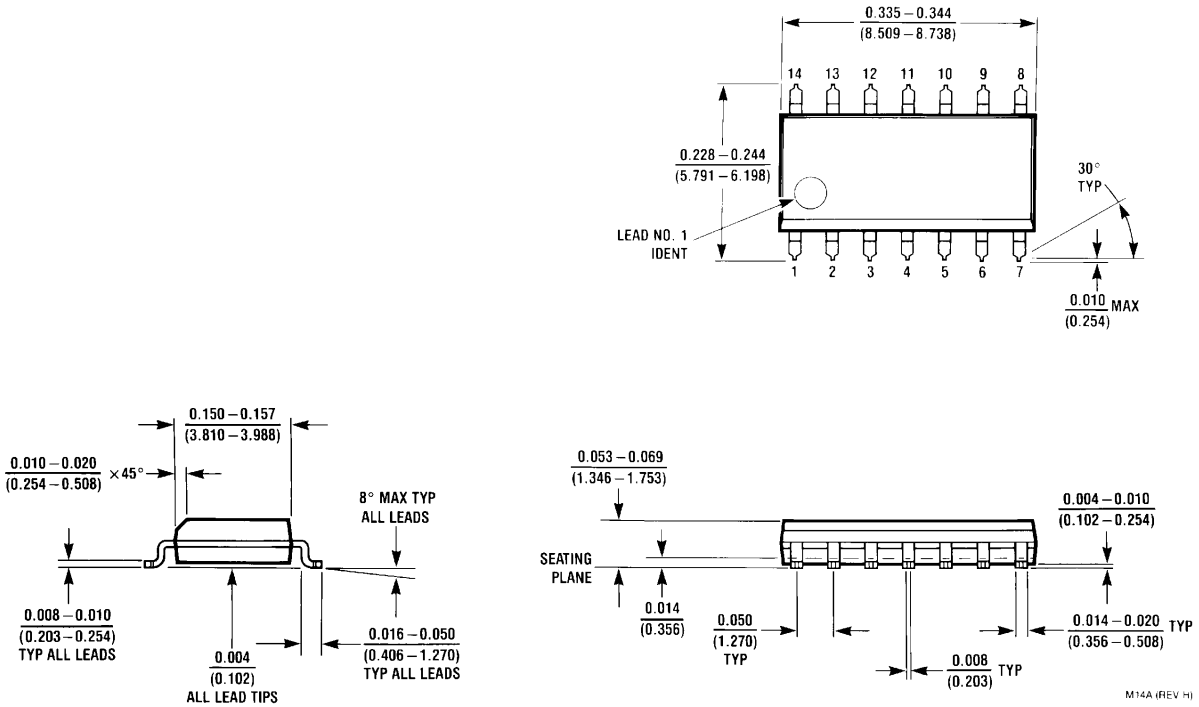

14-Pin Small Outline
Order Package Number LMC6484AIM, LMC6484AIMX, LMC6484IM or LMC6484IMX
NS Package Number M14A

Physical Dimensions inches (millimeters) unless otherwise noted (Continued)

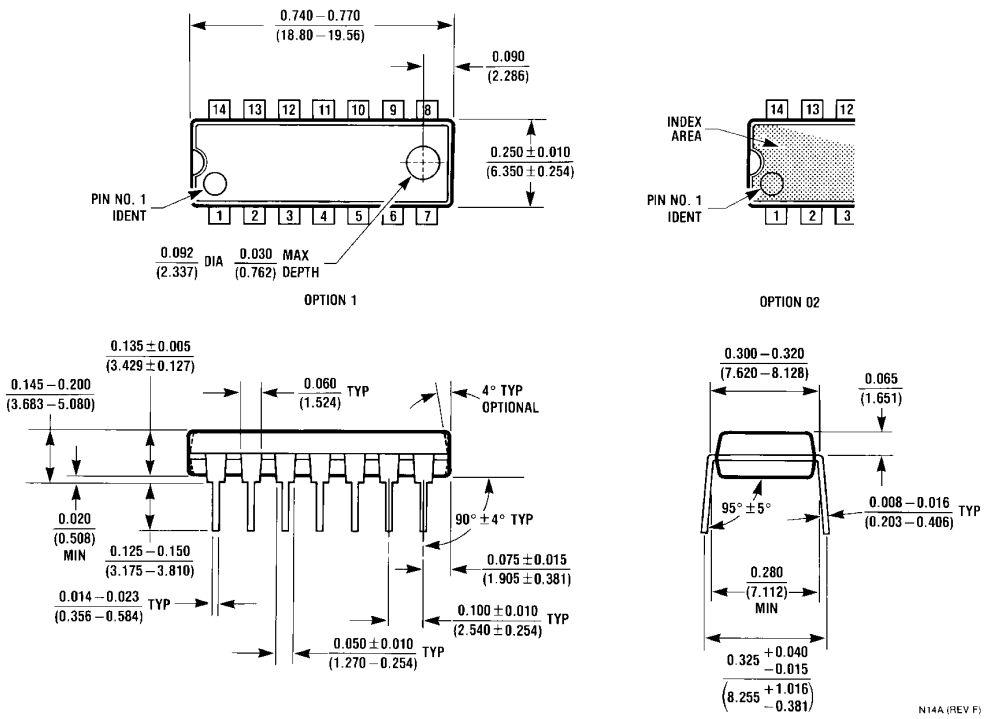

14-Pin Molded DIP
Order Package Number LMC6484AIN, LMC6484IN or LMC6484MN
NS Package Number N14A

LIFE SUPPORT POLICY

NATIONAL'S PRODUCTS ARE NOT AUTHORIZED FOR USE AS CRITICAL COMPONENTS IN LIFE SUPPORT DEVICES OR SYSTEMS WITHOUT THE EXPRESS WRITTEN APPROVAL OF THE PRESIDENT AND GENERAL COUNSEL OF NATIONAL SEMICONDUCTOR CORPORATION. As used herein:

1. Life support devices or systems are devices or systems which, (a) are intended for surgical implant into the body, or (b) support or sustain life, and whose failure to perform when properly used in accordance with instructions for use provided in the labeling, can be reasonably expected to result in a significant injury to the user.
2. A critical component is any component of a life support device or system whose failure to perform can be reasonably expected to cause the failure of the life support device or system, or to affect its safety or effectiveness.

National Semiconductor Corporation
Americas
Tel: 1-800-272-9959
Fax: 1-800-737-7018
Email: support@nsc.com
www.national.com

National Semiconductor Europe
Fax: +49 (0) 180-530 85 86
Email: europe.support@nsc.com
Deutsch Tel: +49 (0) 69 9508 6208
English Tel: +44 (0) 870 24 0 2171
Français Tel: +33 (0) 1 41 91 8790

National Semiconductor Asia Pacific Customer Response Group
Tel: 65-2544466
Fax: 65-2504466
Email: ap.support@nsc.com

National Semiconductor Japan Ltd.
Tel: 81-3-5639-7560
Fax: 81-3-5639-7507